Baryons as Relativistic Bound States of Quark and Diquark

Zusammenfassung

In der vorliegenden Dissertation wird ein Modellrahmen zur Beschreibung von Baryonen als Diquark-Quark-Bindungszustände vorgestellt, der auf eine manifeste Kovarianz der Beschreibung zielt.

Nach einem kurzen Überblick über drei oft verwandte Typen von Baryonmodellen wird das relativistische Problem eines Drei-Quark-Bindungszustandes unter Vernachlässigung von dreiteilchenirreduziblen Wechselwirkungen betrachtet. Diquarks werden als separable Korrelationen in der Zwei-Quark-Korrelationsfunktion eingeführt. Mit diesen hier angenommenen Vereinfachungen gelangt man zu einer Beschreibung der Baryonen mittels einer Bethe-Salpeter-Gleichung für Bindungszustände von Quark und Diquark, wobei die beiden Konstituenten über Quarkaustausch miteinander wechselwirken. Skalare und axialvektorielle Diquarks werden in Analogie zum Massenspektrum der Mesonen als die dominanten Zwei-Quark-Korrelationen in den Baryonen angenommen. Die Struktur der relativistischen Wellenfunktion, die die skalaren und axialvektoriellen Korrelationen beschreibt, wird unter Zuhilfenahme einer Partialwellenzerlegung ausführlich diskutiert.

Die numerischen Lösungen der kovarianten Bethe-Salpeter-Gleichung werden des weiteren zur Berechnung von elektromagnetischen, starken und axialen Nukleon-Formfaktoren herangezogen. Hierbei wird der elektromagnetische Stromoperator in dem Modell so konstruiert, daß er die Eichinvarianz respektiert. Invarianz unter chiralen Symmetrietransformationen ist dagegen leicht verletzt, da Vektordiquarks vernachlässigt wurden. Dies führt zu einer moderaten Verletzung der Goldberger-Treiman-Beziehung.

Weiterhin wird die Möglichkeit, Confinement effektiv über geeignete Modifikationen der Quark- und Diquarkpropagatoren zu parametrisieren, untersucht. Mittels einer solchen Modifikation kann das Massenspektrum der Oktett- und Dekuplettbaryonen berechnet werden. Obwohl diese Vorgehensweise der Confinement-Parametrisierung sich als geeignet für die Berechnung raumartiger Nukleoneigenschaften erweist, versagt sie bei der Behandlung von Prozessen, bei denen große Energien auf das Nukleon übertragen werden, wie z.B. bei ausgewählten Mesonproduktionsprozessen.

In einem weiteren Abschnitt werden die Lösungen für Nukleonwellenfunktionen und -observablen miteinander verglichen, die in der voll relativistischen Behandlung und in einer weitverbreiteten semirelativistischen Näherung gewonnen werden. Die hierbei beobachteten beträchtlichen Abweichungen für die berechneten Observablen, die sich aus der Anwendung der beiden Methoden ergeben, zeigen die Unzulänglichkeiten der semirelativistischen Behandlung auf.

Abstract

In this thesis a model framework for describing baryons as diquark-quark bound states is presented which is formulated in an explicitly covariant manner.

After a short summary of three widely used classes of baryon models the relativistic bound state problem for three quarks is considered, where three-particle irreducible interactions are neglected. Diquarks are introduced as separable correlations in the two-quark correlation function. With these simplifications assumed, baryons are described by a Bethe-Salpeter equation for bound states of quark and diquark which interact by quark exchange. In analogy to the meson spectrum, scalar and axialvector diquarks are considered to be the most important two-quark configurations within baryons. The structure of the relativistic wave function which encompasses the scalar and axialvector correlations is discussed in terms of a partial wave decomposition.

The numerical solutions of the covariant Bethe-Salpeter equation are subsequently employed in the calculation of electromagnetic, strong and axial form factors of the nucleons. The construction of the electromagnetic current operator in the diquark-quark model respects gauge invariance. Invariance under chiral symmetry transformations is slightly violated for vector diquarks have been neglected, leading to a modest violation of the Goldberger-Treiman relation.

The possibility of an effective parametrization of confinement by suitable modifications of the quark and diquark propagators is investigated. Thereby the mass spectrum of octet and decuplet baryons can be calculated. It is shown that the modelling of confinement chosen here is suitable for the calculation of space-like nucleon properties, but its applicability breaks down for processes where large energies are transferred to the nucleon as it is the case in certain meson production processes.

Model solutions for nucleon wave functions and observables are compared between the full relativistic treatment and a widely used semi-relativistic approximation. The considerable deviations between the calculated observables using the two methods illustrate the inadequacy of employing the semi-relativistic treatment.

Contents

Chapter 1

Introduction

1.1 General remarks

Up to now, no convincing solution for the problem of describing baryons and mesons in terms of a few underlying fields has been found, yet it is widely believed that quarks and gluons are the basic entities which build the hadrons. The associated theory is called Quantum Chromodynamics (QCD). The complexity of this theory in the low energy sector is prohibitive for a straightforward deduction of hadronic properties from it. Therefore, models with a simplified dynamics have been employed over the last decades which aim at describing hadrons with degrees of freedom borrowed from QCD (like quarks) or from the observable particle spectrum (like pions) that might be better suited in the treatment of hadrons.

The aim of the present thesis is to study a relativistic framework for the description of baryons employing quark and diquark degrees of freedom. Actual calculations are performed with rather simple assumptions about these, but it is hoped that further progress in knowledge about QCD's quark propagator and the structure of 2-quark correlations will clarify whether the reduction to quarks and diquarks in the treatment of baryons is compatible with QCD.

We refrain from discussing QCD here. The relevance of QCD and its (approximate) symmetries for hadronic physics is discussed in many good textbooks on quantum field theory, see *e.g.* refs. [1, 2].

In the remaining part of this Introduction we will give a short description of the basic ideas underlying three classes of hadronic models which have become popular (and have remained so) over the last years. This brief survey is by no means meant to be exhausting, and serves only as a motivation to consider a fully covariant approach like the diquark-quark model. A short overview about the topics which are covered in the subsequent chapters is given in the last subsection of this chapter.

1.2 Modelling Baryons

1.2.1 Constituent quark models

In the early sixties, it has become recognized that the eight spin-1/2 baryons today referred to as "octet baryons" belong to an eight-dimensional tensor representation of the unitary group $SU(3)$. Obviously this unitary symmetry is broken, as can be seen from the mass differences within the baryon octet, nevertheless a couple of useful relations among *e.g.* the octet masses and magnetic moments could be deduced from unitary symmetry [3] that appeared to be in fair agreement with experiment.

Quarks with their denominations *up*, *down* and *strange* as building blocks of hadrons have been introduced somewhat later as the fundamental representation of the flavor group $SU(3)$. According to this hypothesis, the baryon octet is an irreducible representation which arises from the decomposition of the tensor representation formed by three quarks. Another irreducible representation, the decuplet of spin-3/2 baryons, has been identified in experiments in subsequent years.

To match the baryon quantum numbers, the quarks had to be assigned spin 1/2. Spin and flavor may be combined to the larger group $SU(6)$ and then octet and decuplet baryons can be interpreted as a 56-dimensional representation of this group, with a symmetric spin-flavor wave function. However, the overall wave function needs to be antisymmetric, and if one is not willing to sacrifice the *spatial* symmetry of a baryon ground state wave function, one is led to the hypothesis that all quarks appear in three *colors*. Baryons are then fully antisymmetric *color singlets*.

Still, these group-theoretical considerations do not encompass a dynamical model for baryons in terms of quarks. To explain the plethora of baryon resonances, one of the very first models [4] aims at describing baryons by solutions of a 3-particle Schrödinger equation using the non-relativistic Hamiltonian

$$H \quad = \quad H_{\text{kin}} + H_{\text{conf}} , \tag{1.1}$$

$$H_{\text{kin}} = \sum_{i=1}^{3} \frac{\boldsymbol{p}_i^2}{2m_q} , \qquad H_{\text{conf}} = \frac{1}{2}m_q\omega^2 \sum_{\substack{i,j=1 \\ i<j}}^{3} (\boldsymbol{r}_i - \boldsymbol{r}_j)^2 . \tag{1.2}$$

Massive quarks with $m_q \sim 0.3$ GeV move in a harmonic oscillator potential which (*i*) confines the quarks, (*ii*) allows for the separation of variables easily and (*iii*) leads to a rich spectrum of excitations, even far more than observed. However, the splitting between octet and decuplet has to be provided by some sort of spin-dependent interaction, from the theory of atomic spectra usually known as *hyper-fine* interaction. As meanwhile QCD became favored by many theorists to be the

theory accounting for the strong interactions, a tensorial and a spin-spin interaction term in the Hamiltonian could be motivated by a non-relativistic truncation of one-gluon exchange between quarks [5, 6],

$$
H_{\text{spin}} \;=\; \sum_{\substack{i,j=1 \\ i<j}}^{3} \frac{2\alpha_s}{3m_q^2} \left[\frac{8\pi}{3} \delta^3(\boldsymbol{r}_i - \boldsymbol{r}_j)\, \boldsymbol{S}_i\cdot\boldsymbol{S}_j + \right.
$$
$$
\left. \frac{1}{|\boldsymbol{r}_i - \boldsymbol{r}_j|^3}(3\,\boldsymbol{S}_i\cdot(\boldsymbol{r}_i - \boldsymbol{r}_j)\,\boldsymbol{S}_j\cdot(\boldsymbol{r}_i - \boldsymbol{r}_j) - \boldsymbol{S}_i\cdot\boldsymbol{S}_j) \right] \;. \quad (1.3)
$$

Here, α_s is identified with the QCD fine structure constant and $\boldsymbol{S}_i$ is the spin vector for quark i. Spin-orbit interactions which also result from the non-relativistic expansion of the one-gluon exchange are usually neglected using more or less convincing arguments as they lead to practical complications (*e.g.* three-body interactions) and spoil the calculated hadronic spectrum [6].

We have introduced the basic elements (H_{kin}, H_{conf} and H_{spin}) of nearly all quark potential models that have been devised since the first models have been developed some thirty years ago. The conceptual problems associated with this approach are manifest: lack of covariance and not even an approximate chiral symmetry as the quarks appear with masses of around 0.3 GeV in the Hamiltonian. We shortly discuss approaches that have been taken to remedy this.

In order to include relativistic effects, one certainly has to modify the kinetic energy operator,

$$
H_{\text{kin}} \to \sum_{i=1}^{3} \sqrt{\boldsymbol{p}_i^2 + m_q^2} \;. \quad (1.4)
$$

Fortunately, it is in this case still possible to separate overall bound state variables (total momentum and spin) from relative variables such that the following holds: the hereby constructed mass operator is only a function of the relative variables and the overall and relative variables (considered as operators) fulfill the commutation relations for the Poincaré algebra separately [7]. However, Poincaré invariance does not guarantee a covariant description within Hamiltonian dynamics. Rather, demanding covariance leads to fairly complicated spin-dependent constraints on the Hamiltonian. They have been explicitly formulated for light-cone variables in ref. [8] but are also present for the above discussed conventional use of Galilean time as the Minkowski time variable in relativity. As these constraints are usually overridden in phenomenological applications, covariance is definitely lost in semi-relativistic potential models.

Chiral symmetry and its dynamical breaking lead to massless Goldstone bosons. They are identified with the pseudoscalar mesons which do have mass,

but this being comparatively small. Thus, chiral symmetry appears to be explicitly broken only by small parameters which in QCD are the current quark masses. Within the last years, it has become popular to replace potentials motivated through one-gluon exchange by non-relativistic approximations to one-meson exchange between quarks [9], to pay credit to the importance of pions. This does not render the Hamiltonian chirally symmetric, though, but solves some problems of the level ordering in the baryon spectrum.

To conclude this brief summary of quark potential models, we remark that the practical impossibility of a covariant description limits these models to an effective parametrization of the spectrum and of some static observables. In a non-covariant description, the calculation of dynamical observables, with the simplest being form factors, introduce too much of a frame dependence into the results as that they could be trusted as model predictions.

1.2.2 Soliton models

We now turn to a short discussion about another kind of baryon model which in its original form also predates QCD and even the first quark models. In our exposition, we follow closely ref. [10]. The central idea is to regard baryons as solitons of an effective, non-linear meson theory. To illustrate this, let us start with a chirally symmetric theory describing massless pions and its chiral partner, the σ meson. The so-called σ model is defined by the Lagrangian density

$$\mathcal{L} = \tfrac{1}{2}\left(\partial_\mu\boldsymbol{\pi}\cdot\partial^\mu\boldsymbol{\pi} + \partial_\mu\sigma\partial^\mu\sigma\right) + V(\pi\cdot\pi + \sigma^2)\ . \tag{1.5}$$

The σ field may be regarded as the fourth component of the pion field, and we see that this Lagrangian density is invariant under rotations in the $(\boldsymbol{\pi}, \sigma)$ space leaving $\boldsymbol{\pi}^2 + \sigma^2$ constant. Thus, the Lagrangian is invariant under transformations of the group $O(4)$ which in turn shares the same Lie algebra with the chiral group $SU(2) \times SU(2)$. Depending on the functional form for V, the model may exhibit also the feature of spontaneous symmetry breaking. The non-linear version of this model is defined by demanding

$$\sigma^2 + \boldsymbol{\pi}^2 = c^2 = \mathrm{const}\ . \tag{1.6}$$

Introducing $U = \exp(i\boldsymbol{\tau}\cdot\boldsymbol{\phi})$, the Lagrangian simplifies to

$$\mathcal{L}^{(2)} = \frac{c^2}{4}\mathrm{Tr}\ \partial_\mu U\partial^\mu U^\dagger\ , \tag{1.7}$$

since the potential V reduces to a constant and may be omitted. Now we look for static, finite energy configurations with a finite extension in space which minimize the energy – *solitons*. Due to the constraint in eq. (1.6), $\boldsymbol{\pi}$ is a variable which labels

the points of the three-dimensional unit sphere. A finite energy configuration only exists if U approaches a constant value for $|\boldsymbol{x}| \to \infty$, with $\boldsymbol{x}$ being the position variable. Evidently, all points x on the sphere with radius r may be identified in the limit $r \to \infty$, and a finite energy configuration is determined by the map

$$\boldsymbol{x} \to \boldsymbol{\pi}(\boldsymbol{x}) \; : \; S^3 \to S^3 \,, \tag{1.8}$$

which is labelled by its topological invariants, the *winding numbers*. These considerations can be easily extended to time-dependent fields $\boldsymbol{\pi}(\boldsymbol{x}, t)$ since the same boundary conditions as for the static configurations must hold at infinity. Thus a topological current may be defined,

$$B^\mu = \frac{1}{24\pi^2} \epsilon^{\mu\nu\rho\lambda} \mathrm{Tr} \; \left[(U^\dagger \partial_\nu U)(U^\dagger \partial_\rho U)(U^\dagger \partial_\lambda U) \right] \,, \tag{1.9}$$

which conserves the winding number as the corresponding charge. It has been the conjecture of Skyrme [11] to identify the *topological* current B^μ with the *baryon* current and the winding number with the baryon number. Unfortunately, one finds by scaling $U(\boldsymbol{r}, t) \to U(\lambda \boldsymbol{r}, t)$ that a configuration of minimal energy is only obtained for $\lambda \to \infty$, *i.e.* the soliton is not stable and collapses to size zero. This already indicates the way to resolve the problem, by adding a term to the Lagrangian (1.7) with more derivatives (but no more than two time-derivatives in view of later quantization) which stabilizes the soliton,

$$\mathcal{L}^{(4)} = \frac{1}{32e^2} \mathrm{Tr} \; \left([(U^\dagger \partial_\mu U), (U^\dagger \partial_\nu U)] \; [(U^\dagger \partial^\mu U), (U^\dagger \partial^\nu U)] \right) \,. \tag{1.10}$$

Then a static soliton configuration is given by the ingenious *hedgehog ansatz*,

$$U_0 = \exp(i\boldsymbol{\tau} \cdot \hat{\boldsymbol{x}} \, F(r)) \,. \tag{1.11}$$

We see that the isovector pion field is simply proportional to the position vector. The strength of the pion field is determined by $F(r)$, the *chiral angle*. The boundary conditions for finite energy configuration may be translated into the requirements $F(0) = n\pi$ and $F(\infty) = 0$ for a configuration with baryon number n. Thus we have found a classical description of baryons within the context of a simple non-linear meson theory.

There arises the immediate question of how the baryons obtain their half-integer spin and isospin, since the fundamental pion field possesses spin zero and isospin one. To answer this question, the soliton needs to be quantized and to this end, time-dependent soliton solutions are needed. We do not want to go into detail here and just line out the basic ideas. Full time dependent solutions to the theory described by the Lagrangian $\mathcal{L} = \mathcal{L}^{(2)} + \mathcal{L}^{(4)}$ are hard to come by. Nevertheless

one observes that global rotations in isospace, caused by a time-dependent matrix $A(t) \in SU(2)$,

$$U(\boldsymbol{x}, t) = A(t)\, U_0(\boldsymbol{x})\, A^{\dagger}(t) , \tag{1.12}$$

do not change the "potential" energy of the hedgehog, *i.e.* the part in the Lagrangian depending only on spatial derivatives. Therefore they might be a suitable *ansatz* for a time-dependent soliton solution.[1] The time derivatives in the Lagrangian create terms which represent the rotational energy. Upon using the hedgehog properties and a suitable definition of angular velocities as canonical variables one finds [10]:

- The absolute values of spin and isospin are equal, $\boldsymbol{J}^2 = \boldsymbol{T}^2$.

- The Hamiltonian of the problem reduces to the one of the spherical top, $H = \frac{1}{2\theta}\boldsymbol{J}^2 + M$. Here, θ is a moment of inertia and M is the static energy (the mass) of the soliton.

Thus, upon quantizing the top, J and T as the quantum numbers for spin and isospin may be well assigned half-integer values, though there is no compelling reason to do this.

Alas, one would like to extend the theory to three flavors and to chiral $SU(3) \times SU(3)$ symmetry in order to describe the baryon octet and decuplet. A detailed review on this subject is provided by ref. [12]. Let the Lagrangian $\mathcal{L} = \mathcal{L}^{(2)} + \mathcal{L}^{(4)}$ remain unchanged but define the chiral field as an $SU(3)$ field using the mesons ϕ^a, $a = 1, \ldots, 8$, built by pions, kaons and the octet component of the η,

$$U = \exp\left(i \sum_a \phi^a \lambda^a \right) . \tag{1.13}$$

One may wish to add some flavor symmetry breaking terms to the Lagrangian and can then proceed as described above, *i.e.* by introducing the collective rotations and quantizing the soliton. At some point one would like to relate the effective meson theory to QCD, and one could start by comparing symmetries. It turns out that this model possesses an extra discrete symmetry that is not shared by QCD. Under parity transformations $\mathbf{P}$ the pseudoscalar meson fields as described by QCD should obey

$$\mathbf{P} : \phi^a(\boldsymbol{x}, t) \to -\phi^a(-\boldsymbol{x}, t) . \tag{1.14}$$

---

[1]The static soliton violates isospin or, equivalently, rotational symmetry. Therefore it needs to be projected onto good spin/isospin states. The introduction of the collective rotation in isospace exactly does this job.

In the meson theory, one therefore defines $\mathbf{P}$ as

$$\mathbf{P}: \ \boldsymbol{x} \to -\boldsymbol{x}, \ U \to U^\dagger \ . \tag{1.15}$$

The Lagrangian is however invariant under $\boldsymbol{x} \to -\boldsymbol{x}$ and $U \to U^\dagger$ separately. To break this unwanted symmetry, one needs to add some extra term to the meson action, the famous *Wess-Zumino-Witten (WZW) term* [13]. We state the consequences which come about by adding this term:

- If photons are added in a gauge invariant manner to the meson theory, the WZW term generates a vertex for the anomalous decay $\pi^0 \to \gamma\gamma$. This decay is determined in QCD by the triangle graph which is proportional to the number of colors, N_C. Thus, the strength of the WZW term can be related to N_C.

- If one considers an adiabatic 2π rotation of the soliton during an infinite time interval, the WZW term gives a contribution $N_C\pi$ to the action while all other contributions vanish. Thus the soliton acquires a phase $(-1)^{N_C}$ for such a rotation. For N_C odd, the soliton must therefore be quantized as a fermion, in accordance with $N_C = 3$ in QCD.

We find that incorporating the QCD symmetries (for three flavors) already generates a good argument to identify baryons with solitons.

There is one more connection of the soliton picture to QCD. Witten has shown in ref. [14] that in the limit $N_C \to \infty$ QCD transforms into a theory of weakly interacting mesons and baryons emerge as solitons in this theory. However, an exact mapping has not been found in this limit.

Instead, one can consider a Nambu-Jona-Lasinio (NJL) model involving explicit quark degrees of freedom, defined by the Lagrangian [15]

$$\mathcal{L}_{\mathrm{NJL}} = \bar{q}(i\slashed{\partial} - m^0)q - G\left(\bar{q}\frac{\Lambda_C^a}{2}\gamma_\mu q\right)\left(\bar{q}\frac{\Lambda_C^a}{2}\gamma^\mu q\right) \ . \tag{1.16}$$

Here, quarks (q) are assumed to come in 3 flavors and N_C colors, m^0 denotes a current quark mass matrix which is assumed to contain small diagonal terms and Λ_C^a are the generators of the color group $SU(N)$. The model is an approximation to QCD if one assumes the gluon propagator to be diagonal in color space and $\sim \delta^4(x)$. Additionally, in the limit $m^0 = 0$ it conserves the chiral $SU(3) \times SU(3)$ symmetry of QCD (with massless current quarks) which is of importance for meson and baryon properties. Upon Fierz transforming the NJL Lagrangian into attractive channels, one can show that in the limit $N_C \to \infty$ only the meson channels survive indeed.

Furthermore, this specific model and other quark models of the NJL type admit solitonic solutions which are reviewed in refs. [16, 17]. In contrast to the non-linear σ models discussed before, these solitons are non-topological. In minimizing the energy of a field configuration, one determines the quark energy levels in a background meson field of the hedgehog type, and a unit baryon number is still provided by a configuration of N_C quarks. It is an advantageous feature to retain quark degrees of freedom in the solitonic picture, if one considers phenomenological applications such as calculations of structure functions and parton distributions which have been performed in the last years.

We will stop at this point and summarize some important features of soliton models. They possess a deep conceptual appeal as with the requirement of chiral symmetry imposed onto some effective meson theory the baryons arise as lumps of these without further ado. The possible transformation of QCD in the limit $N_C \to \infty$ into such a nonlinear meson theory creates the link to the fundamental quarks. However, in practical calculations one has to abstract from quarks entirely or must resort to NJL models as crude approximations to QCD. For both strategies it turns out that in leading order of N_C (quasiclassical soliton configuration with quantized collective variables) static baryon observables are only accurate on the $20 \ldots 30$ % level, as known from nearly all hadronic models. Corrections due to the finite number of colors (or, phrased otherwise, due to mesonic fluctuations) yield substantial contributions, and their technically involved calculation tends to hide the original conceptual beauty. Another point of weakness is the non-covariant formulation which will hamper the possible application of this model to hadronic processes in the intermediate energy regime.

1.2.3 Bag models

Soon after QCD surfaced in theory circles, it became popular to associate hadrons with a different phase of the theory as compared to the vacuum phase. This picture motivates the original M.I.T. bag model, where the vacuum phase is assumed to prohibit the propagation of quarks and gluons but creates bubbles of hadronic size in which quarks and gluons may propagate ordinarily. The model is reviewed in ref. [18]. It is formalized by the Lagrangian

$$\mathcal{L}_{\text{bag}} = \left(\mathcal{L}_{\text{QCD}} - B\right)\theta_V - \frac{1}{2}\bar{q}q\Delta_S \ . \tag{1.17}$$

Inside the bag, to be specified, $\theta_V = 1$, and outside, $\theta_V = 0$. The surface function Δ_S is defined by $\frac{\partial \theta_V}{\partial x_\mu} = n^\mu \Delta_S$ and $n^\mu = (n^0, \boldsymbol{n})$ is a normalized unit vector perpendicular to the surface. According to this setup, no quark or gluon current can escape the bag, due to the boundary conditions (for a static bag)

$$\boldsymbol{n} \times \boldsymbol{B}_C = 0 \ , \quad \boldsymbol{n} \cdot \boldsymbol{E}_C = 0 \ , \quad \bar{q}\slashed{n}q = 0 \ , \tag{1.18}$$

where $\boldsymbol{B}_C$ and $\boldsymbol{E}_C$ denote the color magnetic and electric field, respectively. The bag constant B has been introduced to balance the surface pressure of the confined color fields.

The usual procedure in finding the ground state is to assume a spherical, static bag and evaluate the quark wave functions and energy levels perturbatively. To this end, one solves the free Dirac equation with the spherical boundary conditions, and the lowest-lying energy level for a massless quark is approximately 400 MeV for a bag radius of 1 fm, slightly above the constituent quark masses used in the potential models. The splitting between nucleon (spin 1/2) and Δ (spin 3/2) is evaluated by a one-loop gluon correction to the "bare" quark levels. In the end one finds that the bag radius usually comes out too large, above 1 fm, and for the QCD fine structure constant $\alpha_s > 2$ to account for the $N - \Delta$ mass difference. Hence the validity of a perturbative treatment is highly questionable. Furthermore, pionic bags give just the wrong pion mass.

This led to the idea to couple σ mesons and pions to the bag in order to regain chiral invariance. These models come under different guises as

- a "hybrid" bag where quarks and $\sigma - \boldsymbol{\pi}$ couple on the bag surface and the latter are also allowed to propagate inside the bag,

- a "little" bag where in contrast to the hybrid bag pions are excluded from the interior of the bag,

- a "cloudy" bag where the mesons are constrained to the chiral circle and are allowed inside the bag, and

- a "chiral" bag where the constrained mesons are described outside the bag by the Skyrme Lagrangian $\mathcal{L} = \mathcal{L}^{(2)} + \mathcal{L}^{(4)}$ which was discussed in the previous subsection, *cf.* eqs. (1.7,1.10).

All these facets of a softened bag are described on an introductory level in ref. [19]. Usually all these models improve on the shortcomings mentioned above. The bag radius can be chosen considerably smaller and α_S needs not be as large since the $N - \Delta$ splitting arises partially from the pions. Additionally, they support the popular picture of a nucleon as consisting of a valence quark core surrounded by a pionic cloud. As it will be of interest later on, the non-zero electric form factor of the neutron is frequently attributed to "the" pion cloud around the neutron but such a statement has to be interpreted with care as it is only valid in a model context such as a bag model, where valence quarks alone yield zero for the form factor indeed.

Especially the chiral bag mentioned last in the above list aims at combining the soliton picture of baryons with the valence quark picture. At first sight, it is appealing to think of the bag surface as a borderline which indicates where to switch

from a description with quark degrees of freedom to a description with mesons. Then observables should depend very little on the size of the bag *(Cheshire Cat Principle)* and this has been found indeed. Unfortunately the static properties of baryons are not improved as compared to the pure soliton, and come out even worse than for solitons which are formulated with pseudoscalar and vector mesons [12, 20]. Non-covariance of the formulation and possible large modifications of observables by quantum fluctuations also remain present as problems to be solved.

1.2.4 The diquark-quark picture: baryons as relativistic bound states

Hopefully, the short review of the basic principles of three established classes of baryon models has illustrated the conceptual variance that exists among the models. Yet, all of them describe static and a few dynamic observables fairly well on the proverbial twenty-percent-level of accuracy, and their degrees of freedom may be motivated from underlying QCD and its symmetries. Nevertheless we find that none of these is formulated in a manifestly covariant manner, and a model which deliberately cares about covariance might bridge the gap between soft and high-energy physics. Experimental progress in this intermediate energy regime has been considerable within the last years, and therefore understanding the corresponding results within a hadronic model with substructure constitutes a good motivation.

In the next chapter, the framework of a diquark-quark model will be described in detail. In this model, we identify baryons with poles in the 3-quark correlation function. These poles may arise by summing over infinitely many interaction graphs, and it is well known that this summation leads to bound state equations such as the Bethe-Salpeter equation which is usually formulated for two particles but can be extended to n particles as well. We will reduce the 3-quark problem to an effective two-particle problem by introducing quasi-particles (diquarks) as separable 2-quark correlations. The corresponding Bethe-Salpeter equation can be solved *without* any non- or semi-relativistic reduction. For the model calculations, we employ in a first attempt massive constituent quarks with the corresponding free-fermion propagator. It is certainly reasonable to assume that a constituent quark mass is generated in QCD, and this mass generation is reflected in the quark propagator [21], but we acknowledge that the full structure of the quark propagator in QCD is certainly described inadequately by just a free, massive propagator.

In chapter 3, we calculate the nucleon electromagnetic form factors maintaining covariance and gauge invariance which demonstrates the feasibility of a fully relativistic treatment also for dynamic observables. The electric nucleon properties can be described very well, we emphasize here in anticipation of the results

that the behavior of the neutron electric form factor can be understood without any explicit reference to pions. The magnetic moments turn out to be underestimated, at this stage.

The results for the pion-nucleon form factor and the isovector axial form factor, presented in chapter 4, are, for the latter and away from the soft point, in accordance with the available data. For the pion-nucleon form factor, our predictions converge with the predictions of other baryon models. However, the results reveal an overestimate for the pion-nucleon and the weak coupling constant which are obtained in the soft limit. Chiral symmetry demands here a further extension of the model to include another diquark correlation, but this proved to be beyond the scope of this work.

In contrast to the baryon models described above, confinement is not included by construction in the diquark-quark model. In chapter 5 we investigate the possibility of incorporating confinement by a suitable modification of quark and diquark propagators. Thereby we are in the position to calculate the mass spectrum of octet and decuplet baryons, and also the nucleon magnetic moments receive some improvement. The justification of these modifications is discussed thoroughly.

Chapter 6 is concerned with a critical comparison to a semi-relativistic solution of the model which is shown to be inadequate. Finally, we summarize the obtained results in chapter 7 and comment upon further perspectives in the description of baryons within the context of the diquark-quark model.

Most of the results presented here have been published previously, *cf.* refs. [22, 23, 24, 25, 26]. Also, the author of this thesis has benefited a lot from the collaboration with the authors of ref. [27] and ref. [28].

Throughout the text we work in Euclidean space, if not indicated otherwise. The conventions relevant in this connection are summarized in appendix A.1.

Chapter 2

The Covariant Diquark-Quark Model

2.1 Reduction of the relativistic three-quark problem

The three-body problem has attracted a great deal of attention over the last decades and the formal framework presents itself to us as being quite established, for an introduction see refs. [29, 30]. Most work in the field has been restricted to the treatment of quantum mechanical systems, though, where certain theorems about existence and uniqueness of solutions could be proved, see *e.g.* ref. [31] for the case of three-particle scattering with just two-body potentials. For relativistic systems the few-body problem seems to be somehow ill-posed as formal requirements like covariance and locality have led to the formulation of quantum field theories which employ infinitely many degrees of freedom (that come about by the possible creation and annihilation of particles). Nevertheless, the spectrum of mesons and baryons, their static properties and transitions indicate that only the degrees of freedom of a fixed number of (constituent) quarks are relevant. Therefore let us introduce the notion of baryon wave functions as matrix elements of three quark operators that interpolate between the vacuum and a bound state with observable quantum numbers (see below eq. (2.7)). Within QCD, the non-perturbative vacuum is a non-trivial condensate and therefore these wave functions would contain *per definitionem* sea quark and gluonic parts. However, it seems to be justified phenomenologically to regard wave functions which are matrix elements of three effective quark operators between the perturbative vacuum and a bound state as the dominant ones compared to other operator matrix elements that involve an arbitrary number of particle creation and annihilation operators. Then the quantum mechanical formulation of the three-body problem can be taken over

to field theory in the formulation of Green's functions.

2.1.1   Distinguishable quarks

First, let us consider three distinguishable quarks. Later we will generalize the obtained results to indistinguishable particles.

To save on notation, we will drop Dirac, flavor and color indices. They are assumed to be contained in the single particle labels. In our definitions of Green's functions or bound state matrix elements we always take out one δ-function representing conservation of the total momentum, *e.g.* we will denote a (dressed) single quark propagator by S_i with

$$
\begin{aligned}
(2\pi)^4 \delta^4(k_i - p_i)\, S_i(k_i; p_i) \;&=\; \int d^4 x_{k_i} \int d^4 y_{p_i} \exp\left[i(k_i \cdot x_{k_i} - p_i \cdot y_{p_i})\right] \\
&\hspace{2.5em} \times \langle 0 | T q_i(x_{k_i}) \bar{q}_i(y_{p_i}) | 0 \rangle \hspace{3em} (2.1) \\
&=:\; \text{F.T. } \langle 0 | T q_i(x_{k_i}) \bar{q}_i(y_{p_i}) | 0 \rangle \; . \hspace{2em} (2.2)
\end{aligned}
$$

We will use the abbreviation 'F.T. (x)' for the Fourier transform of the subsequent expression (x) in the following. The annihilation operator for a quark of kind i is denoted by q_i. In this way, the disconnected (free) three-quark propagator is found to be

$$
G_0(k_i; p_i) \;=\; \delta^4(k_1 - p_1) \delta^4(k_2 - p_2) \prod S_i(k_i; p_i) \hspace{2em} (2.3)
$$

Sum and product run over $i = 1, 2, 3$. The full quark 6-point function (or the 3-quark correlation function) G is accordingly

$$
(2\pi)^4 \delta^4\left(\sum (k_i - p_i)\right) G(k_i; p_i) \;=\; \text{F.T. } \langle 0 | T \prod q_i(x_{k_i}) \bar{q}_i(y_{p_i}) | 0 \rangle \; . \; (2.4)
$$

It obeys Dyson's equation, symbolically written as

$$
G = G_0 + G_0\, K\, G \; . \hspace{2em} (2.5)
$$

K is the three-quark scattering kernel that contains all two- and three-particle irreducible graphs and the whole equation involving the symbolic products reads explicitly

$$
\begin{aligned}
G(k_i; p_i) \;=\; & G_0(k_i; p_i) + \hspace{10em} (2.6) \\
& \int \frac{d^4 l_1}{(2\pi)^4} \int \frac{d^4 l_2}{(2\pi)^4} \int \frac{d^4 m_1}{(2\pi)^4} \int \frac{d^4 m_2}{(2\pi)^4}\, G_0(k_i; l_i)\, K(l_i; m_i)\, G(m_i; p_i) \; .
\end{aligned}
$$

Besides the four-dimensional integrations, sums over Dirac indices, color and flavor labels are implicitly understood in the symbolic multiplication.

We define a three-particle wave function ψ to be the transition matrix element between the vacuum and a state with an on-shell four-momentum P and appropriate discrete quantum numbers (spin, isospin, ...),

$$(2\pi)^4 \delta^4 \left(\sum p_i - P \right) \psi(p_1, p_2, p_3) = \text{F.T.} \langle 0|q_1(x_1)q_2(x_2)q_3(x_3)|P \rangle . \quad (2.7)$$

A bound state of mass M with wave function ψ will show up as a pole in the 6-point function, *i.e.* in the vicinity of the pole G becomes

$$G \sim \frac{\psi(k_1, k_2, k_3) \; \bar{\psi}(p_1, p_2, p_3)}{P^2 + M^2} , \quad (2.8)$$

where $P = p_1 + p_2 + p_3$. Inserting this into Dyson's equation (2.5) and comparing residues, one finds the homogeneous bound state equation

$$\psi = G_0 \, K \, \psi \quad \leftrightarrow \quad G^{-1} \, \psi = 0 . \quad (2.9)$$

This is our starting point. As it stands, the equation is far too complicated as neither the fully dressed quark propagator nor an expression for all two- and three-particle irreducible graphs are known. One has to resort to some sort of approximation in which the problem is tractable and judge the quality of the chosen approximation by the results for the bound state properties.

The problem is greatly simplified when one discards three-particle irreducible graphs from the interaction kernel K. We will call this approximation the Faddeev (bound state) problem in the following. The kernel then consists of three terms,

$$K = K_1 + K_2 + K_3 . \quad (2.10)$$

The K_i, $i = 1, 2, 3$, describe the interactions of quark pairs (jk), *i.e.* with quark (i) as a spectator. (ijk) is here a cyclic permutation of (123). In figure 2.1, examples for admitted and excluded graphs in the kernel K for the Faddeev problem are shown. The two-quark propagators g_i fulfill their own Dyson's equation with respect to the kernel K_i,

$$g_i = G_0 + G_0 \, K_i \, g_i . \quad (2.11)$$

The objects g_i and K_i are defined in three-quark space. The former contain a factor S_i, the propagator of the spectator quark, and the latter contain a factor of S_i^{-1} (although the spectator quark is not involved in the interactions described by K_i). The matrix $\hat{t}_i$ is defined by amputating all incoming and outgoing quark legs from the connected part of g_i,

$$g_i = G_0 + G_0 \, \hat{t}_i \, G_0 . \quad (2.12)$$
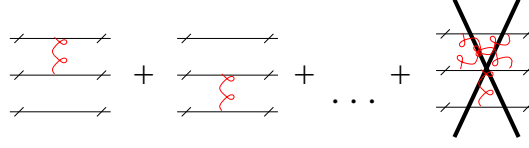
Figure 2.1: Examples for admitted and excluded graphs in the 3-quark interaction kernel K for the Faddeev problem.

Combining the two previous equations yields an integral equation for $\hat{t}_i$,

$$\hat{t}_i = K_i + K_i \, G_0 \, \hat{t}_i \, . \tag{2.13}$$

Still this matrix contains remnants of the spectator quark, this time S_i^{-1}. Therefore the two-quark t matrix of the interacting quarks (jk) is obtained by

$$t_i = \hat{t}_i \, S_i \, , \tag{2.14}$$

and contains just a trivial unit matrix in the subspace of the spectator quark.

We need one more definition before we can tackle the bound state problem. The so-called Faddeev components ψ_i are introduced by

$$\psi_i = G_0 \, K_i \, \psi \, , \tag{2.15}$$

and by virtue of eqs. (2.9,2.10) $\psi = \sum \psi_i$. Solving eq. (2.11) for $G_0 K_i$ and inserting the result into eq. (2.9) yields

$$\psi = g_i \, (K_j + K_k) \, \psi \, . \tag{2.16}$$

Using the definition of $\hat{t}_i$ and t_i in eqs. (2.12,2.14) the equation can be rewritten as

$$\psi_i = G_0 \, \hat{t}_i \, (\psi_j + \psi_k) = (S_j S_k) \, t_i \, (\psi_j + \psi_k) \, . \tag{2.17}$$

These are the famous Faddeev bound state equations relating the Faddeev component ψ_i to ψ_j, ψ_k using the full two-quark correlation function t_i (instead of the kernel K). In turn the t_i would have to be determined in a full solution to the Faddeev problem by solving eq. (2.13) which involves the kernel components K_i. The relativistic Faddeev equations, depicted in figure 2.2, are a set of coupled 4-dimensional integral equations and are thus a considerable simplification of the original 8-dimensional integral equation problem defined in eq. (2.9). Still, the wave function components ψ_i depend on the two relative momenta between the three quarks and expanding these components in Dirac space [32] leads to an enormous number of coupled integral equations.
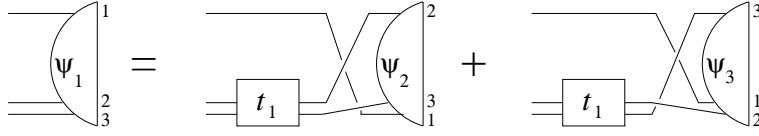
Figure 2.2: The Faddeev bound state equation for the component ψ_1. The equations for ψ_2 and ψ_3 follow by cyclic permutation of the particle indices.

Therefore, we aim at further simplification of the bound state problem. This will be achieved by approximating the two-quark correlation function t_i in terms of a sum over separable correlations,

$$t_i(k_1, k_2; p_1, p_2) = \sum_a \chi_i^a(k_1, k_2) \, D_i^{(a)}(k_1 + k_2) \, \bar{\chi}_i^a(p_1, p_2) \,, \qquad (2.18)$$

pictorially shown in figure 2.3. Separability refers to the assumed property of t_i that it does not depend on any of the scalar products $k_i \cdot p_j$ $(i, j = 1, 2)$. We call these separable correlations "diquarks". The function χ^a is the vertex function of two quarks with a diquark (labelled with a), $\bar{\chi}^a$ correspondingly denotes the conjugate vertex function.[1] Different a's refer to different representations in flavor and Dirac space, and we name $D^{(a)}$ the "diquark propagator" for the respective diquark. The assumption of separability in the two-quark correlations is the starting point in the description of baryons within the diquark-quark model. In the following section we will introduce scalar and axialvector diquarks as the supposedly most important correlations and explore the consequences of quark antisymmetrization for their parametrization.

A suitable *ansatz* for the Faddeev components ψ_i, see figure 2.4, takes the form

$$\psi_i(p_i, p_j, p_k) = \sum_a G_0 \, \chi_i^a(p_j, p_k) \, D_i^{(a)}(p_j + p_k) \, \phi_i^a(p_i, p_j + p_k) \,, \qquad (2.19)$$

where we introduced an effective vertex function of the baryon with quark and diquark, ϕ_i^a. It only depends on the relative momentum between the momentum

---

[1]We refer here to the conjugate of a Bethe-Salpeter vertex function. For the scalar and axialvector diquarks which will be of interest, it is introduced in eqs. (2.48,2.49).
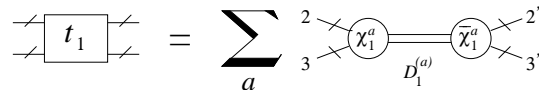
Figure 2.3: The separable matrix t_1.
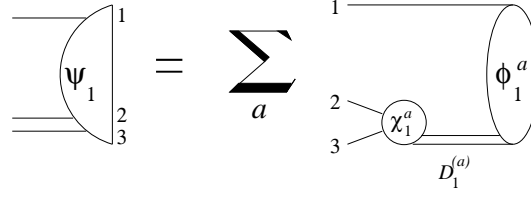
Figure 2.4: The *ansatz* for ψ_1 using effective baryon-quark-diquark vertex functions ϕ_1^a.

of the spectator quark, p_i, and the momentum of the diquark quasiparticle, $p_j + p_k$. A detailed derivation of this property of ϕ_i^a can be found in refs. [29, 33].

Inserting this *ansatz* into the Faddeev equations (2.17) yields coupled integral equations for the effective vertex functions,

$$\phi_i^a = \bar{\chi}_i^a \; (S_j S_k) \; \sum_b (\chi_j^b D_j^{(b)} \phi_j^b + \chi_k^b D_k^{(b)} \phi_k^b) \; . \tag{2.20}$$

We will rewrite these equations into a form that will be familiar from the theory of Bethe-Salpeter equations [34, 35]. To this end we define a relative momentum between quark i and the diquark made of the quarks with label (jk),

$$p_i^{\rm rel} = (1 - \eta)p_i - \eta(p_j + p_k) \; , \tag{2.21}$$

and the total momentum

$$P = p_1 + p_2 + p_3 \; . \tag{2.22}$$

In contrast to the separation of variables in a non-relativistic two-body problem, we have no unique definition of the relative momentum between quark and diquark. Therefore we have introduced the parameter η which distributes relative and total momentum between quark and diquark.[2] Physical observables, like the mass of the bound states, form factors *etc.* should of course not depend on this parameter.

Using the last two definitions for total and relative momentum and taking into account all momentum conservation conditions in eq. (2.20), the bound state equa-

---

[2]Let x_q and x_d be the coordinates of quark and diquark in configuration space. Translational invariance tells us that $\phi_i^a(x_q + h, x_d + h) = \exp(-iP \cdot h)\phi_i^a(x_q, x_d)$. Therefore one introduces a relative coordinate $x^{\rm rel} = x_q - x_d$ and an overall configuration variable $X = \eta x_q + (1 - \eta)x_d$. The momenta $p^{\rm rel}$ and P are the conjugate variables to $x^{\rm rel}$ and X. Then $\phi_i^a(x_q + h, x_d + h) = \phi_i^a(x^{\rm rel}, X + a)$ and, after a Fourier transformation, translational invariance is seen to be fulfilled with this choice of coordinates, leaving the freedom to choose η arbitrarily.

tions read

$$\phi_i^a(p_i^{\mathrm{rel}}, P) = \sum_b \sum_{j=1}^3 \int \frac{d^4 k_j^{\mathrm{rel}}}{(2\pi)^4} \, K_{ij,ab}^{\mathrm{BS}}(p_i^{\mathrm{rel}}, k_j^{\mathrm{rel}}, P) \, G_{0\,(b)}^{\mathrm{q-dq}}(k_j^{\mathrm{rel}}, P) \, \phi_j^b(k_j^{\mathrm{rel}}, P) \, .$$

(2.23)

$G_{0\,(b)}^{\mathrm{q-dq}}$ describes the disconnected ("free") quark-diquark propagator in the diquark channel b,

$$G_{0\,(b)}^{\mathrm{q-dq}}(k_j^{\mathrm{rel}}, P) = S_j(\eta P + k_j^{\mathrm{rel}}) \, D_j^{(b)}((1-\eta)P - k_j^{\mathrm{rel}}) \, ,$$

(2.24)

and $K_{ij,ab}^{\mathrm{BS}}$ is the quark-diquark interaction kernel given by

$$K_{ij,ab}^{\mathrm{BS}}(p_i^{\mathrm{rel}}, k_j^{\mathrm{rel}}, P) \;=\; \sum_{k=1}^3 \bar\delta_{ijk} \, \bar\chi_i^a(k_j, q) \, S_k(q) \, \chi_j^b(q, p_i) \, ,$$

(2.25)

$$k_j \;=\; \eta P + k_j^{\mathrm{rel}} \, ,$$

(2.26)

$$p_i \;=\; \eta P + p_i^{\mathrm{rel}} \, ,$$

(2.27)

$$q \;=\; -p_j^{\mathrm{rel}} - k_i^{\mathrm{rel}} + (1 - 2\eta)P \, .$$

(2.28)

The symbol $\bar\delta_{ijk}$ is equal to 1 if i, j, k are pairwise distinct and 0 otherwise.

Clearly this Bethe-Salpeter interaction kernel $K_{ij,ab}^{\mathrm{BS}}$ describes the quark exchange between the two-particle configurations of quark i/diquark a and quark j/ diquark b. To arrive at an equation for physical baryons, we have to project these configurations onto the respective baryon quantum numbers. This will be done for the nucleons and the Δ resonances in section 2.3. As it will turn out, after the projection of the vertex functions the quark exchange generates the attractive interaction that binds quarks and diquarks to baryons.

2.1.2 Identical quarks

For identical quarks antisymmetrization is required. Nevertheless, the Bethe-Salpeter equation (2.23) will take the same algebraic form regardless of the particle index i. Single particle indices i on the quark propagators S_i and the diquark propagators $D_i^{(a)}$ can be omitted now as well as on the vertices χ_i^a as their functional form does not depend on them. However, some care is needed since the *particle* indices i, j, k in eq. (2.23) specified the *summation order* over color, flavor and Dirac indices. Therefore we will introduce for each term in the Bethe-Salpeter equation for identical quarks small Greek multi-indices $_{\alpha,\beta,...}$ for quarks that contain all of the indices mentioned above. Consequently, antisymmetry demands that the diquark-quark vertices $\chi_{\beta\gamma}^a$ be antisymmetric in their indices $_{\beta,\gamma}$.
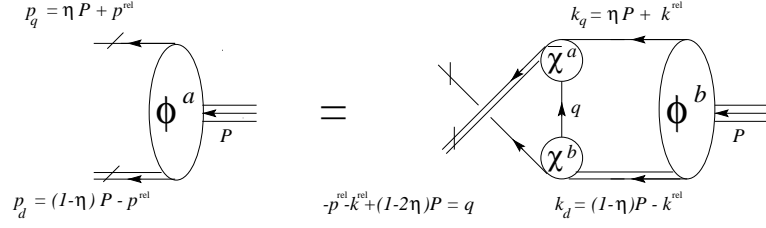
Figure 2.5: The coupled set of Bethe-Salpeter equations for the effective vertex functions ϕ^a.

The Bethe-Salpeter equation for $\phi_i^a \equiv \phi^a$ in the case of identical quarks takes the form

$$
\phi_\alpha^a(p^{\rm rel}, P) = \sum_b \int \frac{d^4 k^{\rm rel}}{(2\pi)^4} K_{\alpha\gamma'}^{\rm BS}(k^{\rm rel}, p^{\rm rel}, P) \times \tag{2.29}
$$
$$
G_{0,\gamma'\gamma}^{\rm q-dq}(k^{\rm rel}, P)\, \phi_\gamma^b(k^{\rm rel}, P)\,,
$$
$$
G_{0,\gamma'\gamma}^{\rm q-dq}(k^{\rm rel}, P) = S_{\gamma'\gamma}(k_q)\, 2D^{(b)}(k_d)\,, \tag{2.30}
$$
$$
K_{\alpha\gamma'}^{\rm BS}(k^{\rm rel}, p^{\rm rel}, P) = \bar\chi_{\beta'\gamma'}^a(k_q, q)\, S_{\beta'\beta}(q)\, \chi_{\alpha\beta}^b(q, p_q)\,. \tag{2.31}
$$

Repeated indices are summed over. Please note that, to save on notation, we neglected the indices for the involved diquark channels in the symbols $G_0^{\rm q-dq}$ and $K^{\rm BS}$. Due to the summation over $\bar\delta_{ijk}$ an overall factor of two emerged that we have to absorb in the definition of the diquark propagator in the case of identical quarks [33]. Spectator quark momenta $k_q[p_q]$, diquark momenta $k_d[p_d]$ and the exchange quark momentum q are given by

$$
k_q[p_q] = \eta P + k^{\rm rel}[p^{\rm rel}]\,, \tag{2.32}
$$
$$
k_d[p_d] = (1-\eta) P - k^{\rm rel}[p^{\rm rel}]\,, \tag{2.33}
$$
$$
q = -k^{\rm rel} - p^{\rm rel} + (1-2\eta)P\,. \tag{2.34}
$$

The set of Bethe-Salpeter equations is pictorially shown in figure 2.5.

To conclude this section, we will write down the completely antisymmetric Faddeev amplitude Γ, obtained by cutting off the three external quark legs from the wave function ψ (*cf.* eq. (2.19)),

$$
\Gamma_{\alpha_1\alpha_2\alpha_3}(p_1, p_2, p_3) = \sum_a \sum_{(ijk)}^{\substack{\rm even \\ \rm perms}} \chi_{\alpha_j\alpha_k}^a(p_j, p_k)\, D^{(a)}\big((1-\eta)-p_i^{\rm rel}\big)\, \phi_{\alpha_i}^a(p_i^{\rm rel})\,.
$$
$$
\tag{2.35}
$$

The relative momentum p_i^{rel} is defined as in eq. (2.21). Due to the antisymmetry of the diquark-quark vertices χ^a the summation over even permutations of (ijk) already generates the fully antisymmetric Faddeev amplitude.

Summarizing the results of this section, we have shown that the determination of a 3-quark wave function defined by eq. (2.7) can be simplified enormously by the following approximations:

1. Neglect all three-particle irreducible contributions to the full three-quark correlation function G.

2. Assume that the truncated, connected two-quark correlations (the t matrices) can be represented as a sum over separable terms that are identified with diquark-quark vertex functions, see eq. (2.18).

The bound state equation (2.9) reduces to a coupled set of Bethe-Salpeter equations for effective baryon-quark-diquark vertex functions ϕ^a, where a labels the diquark types that are summed over in the expression for the separable t matrix, eq. (2.18). These Bethe-Salpeter equations (2.29) are the main result of this section and its only ingredients are

- the quark propagator S,

- the diquark-quark vertices χ^a and

- the diquark propagators $D^{(a)}$.

The aim of this work is to explore the consequences of choosing rather simple forms for S, χ^a and $D^{(a)}$ that in a more elaborate approach should be determined by a suitable effective theory of QCD. In the diquark sectors of Nambu-Jona-Lasinio (NJL) type of models [36], the corresponding bound state equations have been formulated first in ref. [37] and solutions of the full Bethe-Salpeter equation have been obtained in ref. [33]. However, the framework of an NJL model is too tight: quark and diquark are not confined and additionally the diquark is pointlike ($\chi^a \neq \chi^a(p_1, p_2)$ where $p_{1[2]}$ are the quark momenta). Furthermore, the framework presented here is well-suited for the calculation of dynamical observables. In the case of electromagnetic observables, gauge invariance is also maintained in numerical solutions to a high degree of precision. This is somewhat harder to achieve in NJL model calculations employing sharp Euclidean cut-offs. Partly due to this limitation, no dynamical observables of baryons have been calculated in the diquark sector of the NJL model so far, using fully four-dimensional solutions of the Bethe-Salpeter equation.

2.2   Diquark correlations

As explained in the previous section, "diquarks" or "diquark correlations" refer to the use of a separable two-quark correlation function, the t matrix. As the diquark-quark model presented here is inspired by the NJL model, we will describe shortly how separable t matrices arise in it and discuss previous approaches to the diquark-quark picture of baryons. The following main part of this section introduces our parametrization of the t matrix including the explicit form for the diquark-quark vertices and the diquark propagators.

Before we embark upon these points, let us discuss heuristically some properties of diquarks. Any two quarks within a baryon have to be in a color anti-symmetric state as required by the Pauli principle and the assumed color singlet nature of baryons. If we consider for the moment diquarks as asymptotic states (in an unphysical subspace of the whole Hilbert space), their spatial wave functions (assumed to be separated from their Dirac structure) will be dominated by a symmetric ground state. This requires the combination of flavor and Dirac structure to be symmetric. Their mass spectrum and therefore their importance as virtual states in baryons can be guessed by looking at the meson spectrum: pseudoscalar mesons correspond to scalar diquarks, vector mesons to axialvector diquarks since the intrinsic parity of $(q\bar{q})$ is opposite to the intrinsic parity of (qq). Although the pseudoscalar mesons are especially light due to their suspected nature as Goldstone bosons, the scalar diquarks corresponding to them should be still lighter than axialvector diquarks. This point gets support from lattice calculations [38]. In quenched QCD employing Landau gauge the scalar diquark correlation function corresponds to a massive state of around 700 MeV whereas the axialvectors are heavier by around 100 MeV. Vector and pseudoscalar diquark masses are then expected to lie around 1 GeV and therefore assumed to be less important for nucleons. This is indeed the case in a calculation within the Global Color Model [39].

Having motivated the importance of scalar and axialvector diquarks, let us return to their description within the 2-quark correlations. As is well-known, separable t matrices arise from separable 4-quark scattering kernels $K \equiv K_i S_i$ in the following way[3]. Let

$$K^{\text{sep},a}(k_1, k_2; p_1, p_2) = \chi^a(k_i)\, \Lambda^{(a)}(k_1 + k_2)\, \bar{\chi}^a(p_i)\,, \qquad (2.36)$$

be the scattering kernel in the particular channel a. Then the corresponding t matrix in this channel can be inferred from eq. (2.13) which for identical particles

---

[3]The kernels K_i introduced in eq. (2.10) contain a factor S_i^{-1}, the inverse propagator of the spectator quark.

is modified to

$$t = K + \frac{1}{2} \, K \, G_0^{(2)} \, t \, . \tag{2.37}$$

We denote $G_0^{(2)}$ as the free two-quark propagator, as for distinguishable particles it corresponds to just the product of the single propagators. Due to the antisymmetry of K in the labels (jk), t is also antisymmetric in these labels. Its solution for the separable kernel $K^{\mathrm{sep},a}$ reads

$$t^a(k_i; p_i) = \chi^a(k_i) \, D^{(a)}(k_1 + k_2) \, \bar{\chi}^a(p_i) \, . \tag{2.38}$$

The inverse of the propagator $D^{(a)}$ is determined by

$$\left(D^{(a)}\right)^{-1} = \left(\Lambda^{(a)}\right)^{-1} - \frac{1}{2} \, \bar{\chi}^a \, G_0^{(2)} \chi^a \, . \tag{2.39}$$

We use the symbolic product notation as in the previous chapter. The last term in eq. (2.39) describes a quark loop with insertions of the vertex functions χ^a and $\bar{\chi}^a$.

In QCD the simplest term in the perturbative kernel, the gluon exchange, has already a non-separable form. However, when approximating the gluon propagator by a δ-function in configuration space, the resulting model is a Nambu-Jona-Lasinio (NJL) model with pointlike four-quark interactions that can be viewed as color octet–flavor singlet quark current interactions. This local current-current interaction can be rewritten into attractive interactions in color singlet meson and color triplet diquark channels [15]. Let us pick the quark-quark scattering kernel in the scalar channel s which we write in the form

$$
\begin{aligned}
(K^s)_{\alpha\beta,\gamma\delta} &= 4G_s(\chi^s)_{\alpha\beta} \, (\bar{\chi}^s)_{\gamma\delta} \tag{2.40} \\
&= 4G_s \, (\gamma^5 C \, \tau^2 \, \lambda^k)_{\alpha\beta} \, (C^T \gamma^5 \, \tau^2 \, \lambda^k)_{\gamma\delta} \, , \tag{2.41}
\end{aligned}
$$

where we consider just an isospin doublet of two quarks that are in a flavor antisymmetric (τ^2) and a color antitriplet state (λ^k, $k = 2, 5, 7$). The τ^i are Pauli matrices and the λ^k are Gell-Mann matrices [40]. The coupling constant G_s regulates the strength in this interaction channel and C denotes the charge conjugation matrix. The scalar diquark propagator is by virtue of eq. (2.39)

$$\left(D^{(s)}\right)^{-1}(k^2) = \frac{1}{4G_s} - 2 \operatorname{Tr}_D \int \frac{d^4q}{(2\pi)^4} (C^T \gamma^5) \, S(q + k/2) \, (\gamma^5 C) \, S^T(k/2 - q) \, . \tag{2.42}$$

After suitable regularization of the divergent integral it turns out that the inverse propagator has zeros for certain values of k^2, therefore bound scalar diquarks exist

in the NJL model and the propagator can be viewed as a scalar propagator which contains the effect of the dressing quark loop.

In analogy to the meson spectrum where pseudoscalar mesons are the lightest ones, followed by vector mesons, axialvector diquarks are expected to be important in the diquark channel. In fact, the axialvector diquark propagator acquires poles [41], but their appearance depends on the ratio of the coupling constant in the diquark channel to the coupling constant in the pseudoscalar meson channel.

Having obtained separable t matrices for the scalar and the axialvector correlations, the spectrum of spin-1/2 and spin-3/2 baryons is in principle calculable from the Bethe-Salpeter equation (2.29). This was done in refs. [42, 43], however, for the quark exchange kernel a static approximation was used (which amounts to neglecting all momentum dependence in the propagator of the exchange quark). In doing this, covariance is lost, and the rich relativistic structure of the effective nucleon-quark-diquark vertex functions, to be described in section 2.4, has been furthermore approximated by the dominating non-relativistic components, the s waves. The full solution of the Bethe-Salpeter equations, *i.e.* with scalar and axialvector diquarks, for nucleon and Δ was obtained in ref. [33]. Subsequent calculations of static nucleon observables employed unfortunately only the solutions in the scalar diquark sector [44, 45]. Especially the magnetic moments turned out to be deficient, thus calling for including the axialvector diquark channel.

The approximation of the two-quark t matrix by a finite sum of isolated poles at timelike momenta k^2 seems to be supported by these calculations. Solutions for on-shell diquarks were also obtained in the ladder-approximated Global Color model [39]. The Global Color Model employs a non-local current-current interaction, mediated by an effective gluon propagator and therefore avoids the regularization problems present in the NJL model. Parametrizing the t matrix with only the hereby obtained scalar diquark pole the nucleon Bethe-Salpeter equation was solved in ref. [46].

However, when going beyond ladder approximation, *i.e.* including higher order perturbation graphs in the quark-quark scattering kernel, the diquark poles disappear in the NJL model [47] as well as in the Munczek-Nemirowsky model [48]. The latter employs for the gluon propagator a δ-function in momentum space and can be regarded as quite complementary to the NJL model, indicating that in higher-order calculations with a more realistic gluon propagator diquark poles may disappear from the quark-quark scattering amplitude too.

Nevertheless, the phenomenological efficacy of using a diquark correlator to parametrize the 2-quark correlations does not rely on the existence of asymptotic diquark states. Rather, the diquark correlator may be devoid of singularities for timelike momenta, which may be interpreted as one possible realization of diquark confinement. In principle, one may appeal to models employing a general, separable diquark correlator which need not have any simple analytic structure, in which

case no particle interpretation for the diquark would be possible. Indeed, the fact that the interaction mechanism in the quark-diquark picture (the quark exchange) is attractive, turns out to be independent of the details of the employed diquark correlations. It can be traced back to the antisymmetry of the diquark and baryon vertices and arises thus from the color and flavor factors in the Bethe-Salpeter equation, see the next section. Last but not least, the usefulness of this picture and of employing specific diquark correlators has to be judged by comparison to the experiment. Calculations of observables have to go beyond nucleon and Δ mass or the octet and decuplet spectrum as these are rather insensitive to the level of sophistication in the treatment.

As the results for the t matrix have such a strong model dependence, we will not resort to a specific effective quark model for calculating it in the following. Rather, we will employ an admittedly simple *ansatz* for the t matrix, the pole approximation in the scalar and axialvector channel. We will assume an isospin-doublet of u and d quarks as we are mainly interested in nucleon properties. Later on, in chapter 5, we will generalize our treatment to the case of broken $SU(3)$ flavor symmetry. We will use vertex functions with a finite extension in momentum space, first because if strong diquark correlations exist their size is most likely of the order of the proton radius, and secondly, to avoid artificial regularizations in solving the bound state equations. The *ansatz* for the 2-quark t matrix reads,

$$
\begin{aligned}
t(k_\alpha, k_\beta; p_\alpha, p_\beta) \equiv t(k, p, P) \;=\; & \chi^5_{\alpha\beta}(k, P) \, D(P) \, \bar{\chi}^5_{\gamma\delta}(p, P) \;+ \\
& \chi^\mu_{\alpha\beta}(k, P) \, D^{\mu\nu}(P) \, \bar{\chi}^\nu_{\gamma\delta}(p, P) \;.
\end{aligned}
\tag{2.43}
$$

The relative momenta are defined as

$$
k[p] = \sigma \, k_\alpha[p_\alpha] - (1 - \sigma) \, k_\beta[p_\beta], \qquad \sigma \in [0, 1] \;.
\tag{2.44}
$$

The diquark propagators used in the scalar and the axialvector channel are taken to be

$$
D(P) \;=\; -\frac{1}{P^2 + m^2_{sc}} \, C(P^2, m = m_{sc}) \;,
\tag{2.45}
$$

$$
D^{\mu\nu}(P) \;=\; -\frac{1}{P^2 + m^2_{ax}} \left(\delta^{\mu\nu} + (1 - \xi) \frac{P^\mu P^\nu}{m^2_{ax}} \right) C(P^2, m = m_{ax}) \;.
\tag{2.46}
$$

The choice $C(P^2, m) = 1$ and $\xi = 0$ corresponds to free propagators of a spin-0 and a spin-1 particle, to be employed here. Most generally, the dressing function C is not necessarily the same for scalar and axialvector diquarks. However, when investigating nontrivial forms for C (which mimic confinement) in chapter 5 we will assume the same C in both channels for simplicity.

For the trivial form, the diquark-quark vertices χ and χ^μ correspond on-shell $(P^2 = -m_{sc[ax]}^2)$ to diquark Bethe-Salpeter vertex functions. With quark legs attached, they are Fourier transforms of the transition matrix element

$$S(\sigma P + p) \, \chi_{\alpha\beta}^{5[\mu]}(p, P) \, S^T((1 - \sigma)P - p) = \qquad (2.47)$$

$$\int d^4X \int d^4x \, \exp(iP\cdot X + ip\cdot x)\langle 0|Tq_\alpha(x_\alpha)q_\beta(x_\beta)|P, \text{sc [ax]}\rangle \, ,$$

with the relative coordinate $x = x_\alpha - x_\beta$ and $X = (1 - \sigma)x_\alpha + \sigma x_\beta$. The Dirac part of the conjugate vertex functions is obtained by charge conjugation,

$$\bar\chi^5(p, P) \;=\; C \, \left(\chi^5(-p, -P)\right)^T \, C^T \, , \qquad (2.48)$$

$$\bar\chi^\mu(p, P) \;=\; -C \, \left(\chi^\mu(-p, -P)\right)^T \, C^T \, . \qquad (2.49)$$

They have to be antisymmetric with respect to the interchange of the two quarks and this entails

$$\chi_{\alpha\beta}^{5[\mu]}(p, P) = -\chi_{\beta\alpha}^{5[\mu]}(-p, P)\Big|_{\sigma\leftrightarrow(1-\sigma)} \, . \qquad (2.50)$$

As any two quarks in a baryon have to belong to the color antitriplet representation, the diquark-quark vertices are proportional to the antisymmetric tensor ϵ_{ABD} with color indices A, B for the quarks, and with D labelling the color of the diquark. Furthermore, the scalar diquark is an antisymmetric flavor singlet $|0\rangle$ represented by $(\tau_2)_{ab}$, and the axialvector diquark is a symmetric flavor triplet $|1, k\rangle$ which can be represented by $(\tau_2\tau_k)_{ab}$. Here, a and b label the quark flavors and k the flavor of the axialvector diquark. For their structure in Dirac space, we maintain only the dominant components, the antisymmetric matrix $(\gamma^5 C)$ for the scalar diquark and the symmetric matrices $(\gamma^\mu C)$ for the axialvector diquark. Thus, with all these indices made explicit, the vertices read[4]

$$\chi_{\alpha\beta}^5(p) \;=\; g_s(\gamma^5 C)_{\alpha\beta} \, V(p^2, p\cdot P) \, \frac{(\tau_2)_{ab}}{\sqrt{2}} \, \frac{\epsilon_{ABD}}{\sqrt{2}} \, , \qquad (2.51)$$

$$\chi_{\alpha\beta}^\mu(p) \;=\; g_a(\gamma^\mu C)_{\alpha\beta} \, V(p^2, p\cdot P) \, \frac{(\tau_2\tau_k)_{ab}}{\sqrt{2}} \, \frac{\epsilon_{ABD}}{\sqrt{2}} \, . \qquad (2.52)$$

Normalizations of the flavor and color part have been chosen such that for the matrix elements in the respective spaces the following holds,

$$\langle \bar{3}, I|\bar{3}, J\rangle_{\text{color}} \;=\; \tfrac{1}{2}\epsilon_{IMN}\epsilon_{JMN} = \delta^{IJ} \, , \qquad (2.53)$$

$$\langle 0|0\rangle_{\text{flavor}} \;=\; \tfrac{1}{2}\text{Tr} \, \tau_2^\dagger\tau_2 = 1 \, , \qquad (2.54)$$

$$\langle 1, i|1, j\rangle_{\text{flavor}} \;=\; \tfrac{1}{2}\text{Tr} \, (\tau_2\tau_i)^\dagger(\tau_2\tau_j) = \delta^{ij} \, . \qquad (2.55)$$

---

[4]Symbolically denoting the totality of quark indices by the same Greek letters that are used as their Dirac indices should not cause confusion. The particular flavor structures are tied to the Dirac decomposition of the diquarks, color-$\bar{3}$ is fixed.

The antisymmetry condition (2.50) translates into a symmetry condition for the scalar function V,

$$V(p^2, p \cdot P) = V(p^2, -p \cdot P)\big|_{\sigma \leftrightarrow (1-\sigma)} \quad . \tag{2.56}$$

For $\sigma \neq 1/2$ and thus for $\bar{p} := p\big|_{\sigma \leftrightarrow (1-\sigma)} \neq p$, it is not possible to neglect the $p \cdot P$ dependence in the vertex without violating the quark-exchange antisymmetry. To maintain the correct quark-exchange antisymmetry, we assume instead that the vertex depends on both scalars, p^2 and $p \cdot P$ in a specific way. In particular, we assume the diquark-quark vertex is given by a function that depends only on the scalar

$$x := (1 - 2\sigma)p \cdot P + p^2 = -(1 - 2\sigma)\bar{p} \cdot P + \bar{p}^2 \tag{2.57}$$

with $\bar{p} = (1 - \sigma)p_\alpha - \sigma p_\beta$ and $p_{\{\alpha,\beta\}}$ as given above. The two scalars that may be constructed from the available momenta p and P which have definite symmetries under quark exchange are given by the two independent combinations $p_\alpha \cdot p_\beta$ (which is essentially the same as above x) and $p_\alpha^2 - p_\beta^2$. The latter may only appear in odd powers which are associated with higher moments of the Bethe-Salpeter vertex in a polynomial expansion in $p_\alpha^2 - p_\beta^2$. Hence, these are neglected by setting

$$V(p^2, p \cdot P) \to V(x) \tag{2.58}$$

which obviously satisfies the symmetry constraint given by eq. (2.56) $\forall \sigma \in [0, 1]$. For the actual calculations we will restrict ourselves to equal momentum partitioning between the quarks in the diquark correlation, $\sigma = 1/2$. The scalar x then reduces to the square of the relative momentum, $x = p^2$.

The overall strength of the diquark correlations given in eqs. (2.51, 2.52) is hidden in the "diquark-quark coupling constants" g_s and g_a. To estimate their values, we can resort to the canonical normalization condition for Bethe-Salpeter vertex functions [34] which reads in our context,

$$\frac{1}{2} \int \frac{d^4 p}{(2\pi)^4} \, \bar{\chi}^5_{\alpha\beta} \, P^\mu \frac{\partial}{\partial P^\mu}(G_0^{(2)})_{\alpha\gamma,\beta\delta} \, \chi^5_{\gamma\delta} \, \overset{!}{=} \, 2m_{sc}^2, \tag{2.59}$$

$$\frac{1}{2} \int \frac{d^4 p}{(2\pi)^4} \, (\bar{\chi}^\nu_{\alpha\beta})_T \, P^\mu \frac{\partial}{\partial P^\mu}(G_0^{(2)})_{\alpha\gamma,\beta\delta} \, (\chi^\nu_{\gamma\delta})_T \, \overset{!}{=} \, 6m_{ax}^2. \tag{2.60}$$

Here, $(\chi^\nu)_T = \chi^\nu - \hat{P}^\nu(\hat{P}^\mu \chi^\mu)$ is the transverse part of the vertex χ^ν. Note that the pole contribution of the axialvector diquark is transverse to its total momentum, and the sum over the three polarization states provides an extra factor of 3 on the r.h.s. of eq. (2.60) as compared to eq. (2.59). With normalizations as chosen

in eqs. (2.51,2.52) the traces over the color and flavor parts yield no additional factors, see eqs. (2.53–2.55).

In the following, we will solve the baryon bound state problem with the coupling constants g_s and g_a fixed in the indicated manner, keeping in mind that the Bethe-Salpeter normalization condition determines these values only on-shell. When calculating diquark contributions to the nucleon electric form factors, we will see that the Ward identity provides for an indirect off-shell constraint on g_s and g_a. However, the ratio between the constants fixed either on- or off-shell will be of the order of unity.

In the model sector with scalar diquarks only, we will explore the ramifications of several *ansätze* for the scalar functions $V(x)$,

$$V_{n-\text{pole}} = \left(\frac{\lambda_n^2}{\lambda_n^2 + x} \right)^n , \tag{2.61}$$

$$V_{\text{exp}} = \exp(-x/\lambda_{\text{exp}}^2) , \tag{2.62}$$

$$V_{\text{gau}} = \exp(-(x - x_0)^2/\lambda_{\text{gau}}^4) . \tag{2.63}$$

The last form, the Gaussian form for the diquark vertices, was suggested as a result of a variational calculation of an approximate diquark Bethe-Salpeter equation in ref. [49]. The nucleon calculations of ref. [46] used this form *without* fixing the strength g_s by a condition such as eq. (2.59). It turns out that the necessary value for λ_{gau} to obtain a reasonable nucleon mass is about an order of magnitude smaller than the value given in ref. [46]. Furthermore, we will show in sect. 2.5.2 that the results for the electric form factors in the scalar diquark sector clearly rule out the Gaussian and the exponential form of the diquark vertices and favor the dipole *ansatz*.

2.3 The diquark-quark Bethe-Salpeter equation

Equipped with the separable form of the two-quark correlations, eq. (2.43), and the functional form of the scalar and axialvector diquark correlations in eqs. (2.51,2.52), we will have a closer look on the effective Bethe-Salpeter equation derived in section 2.1 and set it up for the nucleon and the Δ in turn.[5] To complete the model definition, we have to specify the functional form of the quark propagator. We take it to be a free fermion propagator with a constituent mass m_q,

$$S(p) = \frac{i\not{p} - m_q}{p^2 + m_q^2} \, C(p^2, m = m_q) \qquad \text{with} \ \ C(p^2, m = m_q) = 1. \tag{2.64}$$

---

[5]We will sum up the four nearly mass-degenerate states $\Delta^{++}, \Delta^+, \Delta^0, \Delta^-$ under the label Δ in the following.

This incorporates from the beginning an effective quark mass in the order of magnitude of several hundred MeV which is believed to be dynamically generated in QCD. The property of confinement is neither manifest in eq. (2.64) nor in the form of the diquark propagators, eqs. (2.45,2.46). Effective parametrizations of confinement in the model propagators and its influence on results will be investigated in chapter 5.

2.3.1 Nucleon

The Faddeev amplitude of eq. (2.35) takes the following form,

$$\Gamma_{\alpha\beta\gamma} = \chi^5_{\beta\gamma} \, D \, \left(\Phi^5 u\right)_\alpha + \chi^\mu_{\beta\gamma} \, D^{\mu\nu} \, \left(\Phi^\nu u\right)_\alpha \, . \tag{2.65}$$

The necessary antisymmetrization of $\Gamma_{\alpha\beta\gamma}$, provided by the summation over even permutations of the multi-indices $\alpha\beta\gamma$ as in eq. (2.35), will be understood implicitly from now on. The spinorial quantities

$$\Phi(p, P) \, u(P) := \begin{pmatrix} \Phi^5(p, P) \\ \Phi^\mu(p, P) \end{pmatrix} \, u(P) \tag{2.66}$$

describe the effective nucleon-quark-diquark vertex functions. The quantity $u(P)$ is a positive-energy spinor for a spin-1/2 particle with momentum P.

We define Bethe-Salpeter wave functions by attaching quark and diquark legs to the vertex functions,

$$\tilde{D}(p_d) \;\; := \;\; \begin{pmatrix} D(p_d) & 0 \\ 0 & D^{\mu\nu}(p_d) \end{pmatrix} \, , \tag{2.67}$$

$$\Psi(p, P) \;\; := \;\; \begin{pmatrix} \Psi^5 \\ \Psi^\mu \end{pmatrix} (p, P) = S(p_q) \, \tilde{D}(p_d) \begin{pmatrix} \Phi^5 \\ \Phi^\nu \end{pmatrix} (p, P) \, . \tag{2.68}$$

Vertex and wave function Φ and Ψ are Dirac matrices to be constructed from the quark-diquark relative momentum p, the nucleon momentum P and the set of γ matrices. The task of their decomposition will be taken up in the next section, showing that there are altogether eight components that encompass all possible spin-orbit couplings of quark and diquark to the nucleon spin.

Inserting all these definitions into the Bethe-Salpeter equation (2.29), we find the equation

$$\int \frac{d^4k}{(2\pi)^4} \left(G^{\mathrm{q-dq}}\right)^{-1} (p, k, P) \begin{pmatrix} \Psi^5 \\ \Psi^{\mu'} \end{pmatrix} (k, P) = 0 \, , \tag{2.69}$$

in which $\left(G^{\mathrm{q-dq}}\right)^{-1}(p, k, P)$ is the inverse of the full quark-diquark 4-point function. It is the sum of the disconnected part and the interaction kernel,

$$
\left(G^{\mathrm{q-dq}}\right)^{-1}(p, k, P) = (G_0^{\mathrm{q-dq}})^{-1}(p, k, P) - K^{\mathrm{BS}} , \tag{2.70}
$$

$$
(G_0^{\mathrm{q-dq}})^{-1}(p, k, P) = (2\pi)^4 \, \delta^4(p - k) \, S^{-1}(p_q) \, \tilde{D}^{-1}(p_d) , \tag{2.71}
$$

$$
K^{\mathrm{BS}} = \frac{1}{2} \begin{pmatrix} -\chi^5(p_1^2) \, S^T(q) \, \bar{\chi}^5(p_2^2) & \sqrt{3} \, \chi^{\mu'}(p_1^2) \, S^T(q) \, \bar{\chi}^5(p_2^2) \\ \sqrt{3} \, \chi^5(p_1^2) \, S^T(q) \, \bar{\chi}^\mu(p_2^2) & \chi^{\mu'}(p_1^2) \, S^T(q) \, \bar{\chi}^\mu(p_2^2) \end{pmatrix} . \tag{2.72}
$$

For completeness we list the definitions of quark, diquark and exchange quark momentum, see eqs. (2.32–2.34),

$$
p_q = \eta P + p , \tag{2.73}
$$

$$
p_d = (1 - \eta)P - p , \tag{2.74}
$$

$$
q = -p - k + (1 - 2\eta)P . \tag{2.75}
$$

The diquark vertices and their conjugates depend on the relative momenta between a spectator quark and the exchange quark,

$$
p_1 = p + k/2 - (1 - 3\eta)P/2 , \tag{2.76}
$$

$$
p_2 = -k - p/2 + (1 - 3\eta)P/2 . \tag{2.77}
$$

Physical quantities should not depend on the momentum partitioning parameter η which expresses just the invariance under reparametrizations of the relative momentum. As we explained earlier, this follows from relativistic translation invariance for the solutions of the Bethe-Salpeter equation. This implies that for every solution $\Psi(p, P; \eta_1)$ of the Bethe-Salpeter equation there exists a family of solutions of the form $\Psi(p + (\eta_2 - \eta_1)P, P; \eta_2)$. The manifestation of this invariance in actual numerical calculations will be investigated in section 2.5.2.

Color and flavor factors have already been worked out in eqs. (2.69,2.70). Their derivation has been relocated to appendix A.2.1.

2.3.2   Delta

The $\Delta(1232)$ resonance is a spin-3/2, isospin-3/2 state. Therefore only axialvector diquark correlations can be present in the 2-quark t matrix since the flavor state of the Δ has to be fully symmetric. Accordingly its Faddeev amplitude reads

$$
\Gamma^\Delta_{\alpha\beta\gamma} = \chi^\mu_{\beta\gamma} \, D^{\mu\nu} \, (\Phi^{\nu\rho} u^\rho)_\alpha . \tag{2.78}
$$

The effective Δ-quark-diquark vertices are now quantities which transform as vector-spinors: $\Phi^{\mu\nu}(p, P)u^\nu(P)$, where $u^\nu(P)$ is a Rarita-Schwinger spinor describing a free spin-3/2 particle with momentum P. We may construct Bethe-Salpeter wave functions by attaching legs,

$$\Psi^{\mu\nu}(p, P) = S(p_q)\, D^{\mu\mu'}(p_d)\, \Phi^{\mu'\nu}(p, P)\,. \tag{2.79}$$

Both vertex and wave function $\Phi^{\mu\nu}$ and $\Psi^{\mu\nu}$ are Dirac matrices with two uncontracted Lorentz indices, respectively. Their complete decomposition in Dirac space will be shown in the next section.

The Bethe-Salpeter equation for the Δ is in compact notation

$$\int \frac{d^4k}{(2\pi)^4} \left(G_\Delta^{\mathrm{q-dq}}\right)^{-1}(p, k, P)\Psi_\Delta^{\mu'\nu}(k, P) = 0\,, \tag{2.80}$$

where the inverse quark-diquark propagator G_Δ^{-1} in the Δ-channel is given by

$$\begin{aligned}
\left(G_\Delta^{\mathrm{q-dq}}\right)^{-1}(p, k, P) &= (2\pi)^4\delta^4(p-k)\, S^{-1}(p_q)\, (D^{\mu\mu'})^{-1}(p_d) + \\
&\quad \chi^{\mu'}(p_1^2)\, S^T(q)\, \bar\chi^\mu(p_2^2)\,.
\end{aligned} \tag{2.81}$$

The necessary color algebra that enters the explicit form of $(G_\Delta^{\mathrm{q-dq}})^{-1}$ does not differ from the nucleon case as all diquarks are in a color antitriplet state. The computation of the flavor factor is given in appendix A.2.2.

2.4 Decomposition of the Faddeev amplitudes

At this point we will solve the problem of the Dirac space decomposition of nucleon and Δ vertex functions with quark and diquark. The exercise seems to be clearly straightforward in the sense that, using a finite basis of Dirac matrices, tensorial (Δ) or vector and scalar matrices (nucleon) have to be found that yield proper spin and describe positive parity and energy solutions. We will go a step further, however, and show that representations can be found which correspond to a partial wave decomposition in the baryon rest frame, *i.e.* a decomposition into eigenfunctions of spin and angular momentum. Thereby we recover all non-relativistic basis elements that would survive a corresponding reduction. In addition, virtual components due to the off-shell axialvector diquark and relativistic "lower components" will be found. The results obtained in this section are thus an explicit illustration of the difference between relativistic and non-relativistic baryon wave functions.

Nucleon

In eq. (2.65) we have defined the nucleon Faddeev amplitudes in terms of the effective spinors $\Phi^5(p, P)\, u(P)$ and $\Phi^\mu(p, P)\, u(P)$ that describe the scalar and the axialvector correlations in the nucleon. In the following we will describe the complete decomposition of the vertex function Φ in Dirac space such that the Faddeev amplitudes describe a spin-1/2 particle with positive energy and have positive parity.

First let us define the projectors onto positive energy, Λ^+, and for negative energy, Λ^-, by

$$\Lambda^+(P) = \frac{1}{2}\left(1 + \frac{\not{P}}{iM_n}\right)\ , \quad \Lambda^-(P) = \frac{1}{2}\left(1 - \frac{\not{P}}{iM_n}\right)\ . \tag{2.82}$$

The nucleon bound state mass is denoted by M_n, and in the rest frame the nucleon momentum is given by $P = (\mathbf{0}, iM_n)$. The projectors defined above form a complete set ($\Lambda^+ + \Lambda^- = 1$) and thus the effective spinors can be written as

$$\Phi\, u(P) = \Phi(\Lambda^+ + \Lambda^-)\, u(P) = \Phi\, \Lambda^+\, u(P). \tag{2.83}$$

In the following, we will substitute the projected vertex function for the vertex function itself, $\Phi\Lambda^+ \to \Phi$. Clearly it is then an eigenfunction of the positive-energy projector,

$$\Phi\Lambda^+ = \Phi\ . \tag{2.84}$$

Next we consider the transformation properties of the Faddeev amplitudes under parity. To describe nucleons with positive parity the Faddeev amplitude must fulfill

$$
\begin{aligned}
\mathbf{P}\Gamma_{\alpha\beta\gamma}(q, p, P) &= (\gamma^4\chi^5(\tilde{q})\gamma^4)_{\beta\gamma}\, D(\tilde{p}, \tilde{P})\, (\gamma^4\Phi^5(\tilde{p}, \tilde{P})u(\tilde{P}))_\alpha + \\
&\quad\ (\gamma^4\chi^\nu(\tilde{q})\gamma^4)_{\beta\gamma}\, D^{\nu\mu}(\tilde{p}, \tilde{P})\, (\gamma^4\Phi^\mu(\tilde{p}, \tilde{P})u(\tilde{P}))_\alpha \\
&\overset{!}{=}\ \Gamma_{\alpha\beta\gamma}(q, p, P)\ ,
\end{aligned}
\tag{2.85}
$$

with $\tilde{p} = \Lambda_\mathbf{P} p$, $\tilde{P} = \Lambda_\mathbf{P} P$ and

$$\Lambda_\mathbf{P}^{\mu\nu} = \mathrm{diag}_4\{-1, -1, -1, 1\}\ . \tag{2.86}$$

Using the transformation properties of the diquark-quark vertices and a Dirac spinor,

$$
\begin{aligned}
\gamma^4\chi^5\gamma^4 &= \chi^5\ , & \tag{2.87} \\
\gamma^4\chi^\mu\gamma^4 &= -\Lambda_\mathbf{P}^{\mu\nu}\chi^\nu\ , & \tag{2.88} \\
\gamma^4 u(P) &= u(\tilde{P})\ , & \tag{2.89}
\end{aligned}
$$

one can deduce from eq. (2.85) a condition for the vertex function Φ:

$$\mathbf{P} \begin{pmatrix} \Phi^5(p, P) \\ \Phi^\mu(p, P) \end{pmatrix} = \begin{pmatrix} \gamma^4 \Phi^5(\tilde{p}, \tilde{P}) \gamma^4 \\ \gamma^4 (\Lambda_{\mathbf{P}}^{\mu\nu} \Phi^\nu(\tilde{p}, \tilde{P})) \gamma^4 \end{pmatrix} \overset{!}{=} \begin{pmatrix} \Phi^5(p, P) \\ -\Phi^\nu(p, P) \end{pmatrix} . \quad (2.90)$$

We see that apart from the Dirac indices Φ^5 transforms like a scalar and Φ^μ like a pseudovector.

The conditions (2.84) and (2.90) greatly restrict the number of independent components in the vertex function. The scalar correlations Φ^5 are described by two components and the axialvector correlations by six components,

$$\begin{pmatrix} \Phi^5(p, P) \\ \Phi^\mu(p, P) \end{pmatrix} = \begin{pmatrix} \sum_{i=1}^{2} S_i(p^2, p \cdot P) \, \mathcal{S}_i(p, P) \\ \sum_{i=1}^{6} A_i(p^2, p \cdot P) \, \gamma_5 \mathcal{A}_i^\mu(p, P) \end{pmatrix} . \quad (2.91)$$

The scalar functions S_i and A_i depend on the two possible scalars (p^2 and $p \cdot P$) that can be formed out of the relative momentum p and the nucleon momentum P. The Dirac components describing the scalar correlations may be built out of Λ^+ and $\not{p}\Lambda^+$ and the Dirac part of the axialvector correlations can be constructed using the matrices $P^\mu \Lambda^+$, $P^\mu \not{p} \Lambda^+$, $\gamma^\mu \Lambda^+$, $\gamma^\mu \not{p} \Lambda^+$, $p^\mu \Lambda^+$ and $p^\mu \not{p} \Lambda^+$.

In table 2.1 the Dirac components $\mathcal{S}_i$ and $\mathcal{A}_i^\mu$ are given as certain linear combinations of these matrices. First, they obey a useful trace orthogonality condition. Defining the adjoint vertex function in terms of conjugate Dirac components,

$$\begin{pmatrix} \bar{\Phi}^5(p, P) \\ \bar{\Phi}^\mu(p, P) \end{pmatrix} := \begin{pmatrix} \sum_{i=1}^{2} \bar{\mathcal{S}}_i(p, P) \, S_i(p^2, p \cdot P) \\ \sum_{i=1}^{6} \bar{\mathcal{A}}_i^\mu(p, P) \gamma_5 \, A_i(p^2, p \cdot P) \end{pmatrix} , \quad (2.92)$$

we find for them

$$\begin{pmatrix} \bar{\mathcal{S}}_i(p, P) \\ \bar{\mathcal{A}}_i^\mu(p, P) \end{pmatrix} = \begin{pmatrix} C \, (\mathcal{S}_i(-p, -P))^T \, C^{-1} \\ -C \, (\mathcal{A}_i^\mu(-p, -P))^T \, C^{-1} \end{pmatrix} . \quad (2.93)$$

This identification of the conjugated components follows by charge-conjugating the Faddeev amplitude and using the definition of the conjugate diquark-quark vertices in eqs. (2.48,2.49). The trace orthogonality property takes the following form,

$$\mathrm{Tr} \, \bar{\mathcal{S}}_i \mathcal{S}_j = 2(-1)^{j+1} \delta_{ij} \quad (2.94)$$

$$\mathrm{Tr} \, \bar{\mathcal{A}}_i^\mu \mathcal{A}_j^\mu = 2(-1)^{j+1} \delta_{ij} \quad (2.95)$$

$$\mathrm{Tr} \, \bar{\mathcal{S}}_i \gamma_5 \mathcal{A}_j^\mu = \mathrm{Tr} \, \bar{\mathcal{A}}_j^\mu \gamma_5 \mathcal{S}_i = 0 \quad (2.96)$$

$\mathcal{S}_1$	Λ^+
$\mathcal{S}_2$	$-i\,\hat{p}_T\,\Lambda^+$
$\mathcal{A}_1^\mu$	$\hat{P}^\mu\,\Lambda^+$
$\mathcal{A}_2^\mu$	$-i\,\hat{P}^\mu\,\hat{p}_T\,\Lambda^+$
$\mathcal{A}_3^\mu$	$\frac{1}{\sqrt{3}}\,\gamma_T^\mu\,\Lambda^+$
$\mathcal{A}_4^\mu$	$\frac{i}{\sqrt{3}}\,\gamma_T^\mu\,\hat{p}_T\,\Lambda^+$
$\mathcal{A}_5^\mu$	$\sqrt{\frac{3}{2}}\left(\hat{p}_T^\mu\,\hat{p}_T - \frac{1}{3}\,\gamma_T^\mu\right)\Lambda^+$
$\mathcal{A}_6^\mu$	$i\sqrt{\frac{3}{2}}\left(\hat{p}_T^\mu - \frac{1}{3}\,\gamma_T^\mu\,\hat{p}_T\right)\Lambda^+$

Table 2.1: Basic Dirac components of the nucleon vertex function. With a hat we denote normalized 4-vectors, $\hat{p} = \frac{p}{|p|}$. In the case of the complex on-shell nucleon momentum, we define $\hat{P} = \frac{P}{iM}$. The subscript $_T$ denotes the transversal component of a vector with respect to the nucleon momentum P, *e.g.* $p_T = p - (p\cdot\hat{P})\hat{P}$.

As a second attribute, the Faddeev amplitude written with these Dirac components is given as a complete decomposition into partial waves, *i.e.* into components that are eigenstates of the spin as well as of the angular momentum operator in the nucleon rest frame. This will be shown in section 2.4.1.

Delta

The Faddeev amplitudes for the Δ are described by an effective Rarita-Schwinger spinor $\Phi^{\mu\nu}u^\nu$, see eq. (2.78). As in the nucleon case we only need to consider the projected tensor vertex function $\Phi^{\mu\rho}\mathbb{P}^{\rho\nu} \to \Phi^{\mu\nu}$. $\mathbb{P}^{\rho\nu}$ is the Rarita-Schwinger projector [50] onto positive-energy, spin-3/2 spinors,

$$\mathbb{P}^{\mu\nu} := \Lambda^+ \left(\delta^{\mu\nu} - \frac{1}{3}\gamma^\mu\gamma^\nu + \frac{2}{3}\frac{P^\mu P^\nu}{M_\Delta^2} - \frac{i}{3}\frac{P^\mu\gamma^\nu - P^\nu\gamma^\mu}{M_\Delta} \right) =: \Lambda^+ \Lambda^{\mu\nu} \;. \quad (2.97)$$

It obeys the constraints

$$P^\mu\,\mathbb{P}^{\mu\nu} = \gamma^\mu\,\mathbb{P}^{\mu\nu} = 0 \;. \quad (2.98)$$

The tensor vertex function must be an eigenfunction of the projector, therefore

$$\Phi^{\mu\nu} = T^{\mu\rho}\,\mathbb{P}^{\rho\nu} \;. \quad (2.99)$$

Due to the constraints (2.98), $T^{\mu\rho}$ must be either proportional to $\delta^{\mu\rho}$ or the transverse relative momentum $p_T = p - \hat{P}(p \cdot \hat{P})$ may contract with one index of the Rarita-Schwinger projector and therefore

$$T^{\mu\rho} = \mathcal{D}'\delta^{\mu\rho} + \mathcal{E}'^\mu \hat{p}_T^\rho \ , \qquad (2.100)$$

with $\mathcal{D}'$ and $\mathcal{E}'^\mu$ being Dirac matrices yet to be determined.

To further constrain the vertex function, let us consider the effect of the parity transformation onto the Faddeev amplitude,

$$
\begin{aligned}
\mathbf{P}\Gamma^\Delta_{\alpha\beta\gamma}(q, p, P) &= (\gamma^4 \chi^\rho(\tilde{q})\gamma^4)_{\beta\gamma} \ D^{\rho\mu}(\tilde{p}, \tilde{P}) \ (\gamma^4 \Phi^{\mu\nu}(\tilde{p}, \tilde{P})u^\nu(\tilde{P}))_\alpha \\
&\overset{!}{=} \Gamma^\Delta_{\alpha\beta\gamma}(q, p, P) \ .
\end{aligned}
\qquad (2.101)
$$

We need to evaluate the effect of a parity transformation on the Rarita-Schwinger spinor. The latter may be built as follows [51],

$$u^\mu(P, s) = \sum_{m, s'} C^{\frac{3}{2}s}_{1m, \frac{1}{2}s'} \ \epsilon^\mu_m(P) \ u(P, s') \ . \qquad (2.102)$$

The ϵ^μ_m are spin-1 polarization vectors $(m = 0, \pm 1)$ that can be written in terms of a 3-dimensional spin-1 polarization vector basis $\hat{\boldsymbol{\epsilon}}_m$ as

$$\epsilon^\mu_m(P) = \begin{pmatrix} \hat{\boldsymbol{\epsilon}}_m + \dfrac{\hat{\boldsymbol{\epsilon}}_m \cdot \boldsymbol{P}}{M_\Delta} \dfrac{\boldsymbol{P}}{|P^4| + M_\Delta} \\ i\dfrac{\hat{\boldsymbol{\epsilon}}_m \cdot \boldsymbol{P}}{M_\Delta} \end{pmatrix} \ . \qquad (2.103)$$

In eq. (2.102), these covariant polarization vectors are combined with a Dirac spinor $u(P)$ of helicity s' and appropriate Clebsch-Gordan coefficients $C^{\frac{3}{2}s}_{1m, \frac{1}{2}s'}$ to give a spin-3/2 object with helicity s. From these definitions it can be seen that under parity the u^μ transform as follows,

$$\gamma^4 \Lambda^{\mu\nu}_{\mathbf{P}} u^\nu(\tilde{P}) = -u^\mu(P) \ , \qquad (2.104)$$

and therefore the vertex function must obey

$$\mathbf{P}\Phi^{\mu\nu}(p, P) = \gamma^4 \ (\Lambda^{\mu\rho}_{\mathbf{P}} \Phi^{\rho\lambda}(\tilde{p}, \tilde{P})\Lambda^{\lambda\nu}_{\mathbf{P}}) \ \gamma^4 = \Phi^{\mu\nu}(p, P) \qquad (2.105)$$

which translates into conditions for the unknown Dirac matrices appearing in eq. (2.100),

$$\gamma^4 \begin{pmatrix} \mathcal{D}'(\tilde{p}, \tilde{P}) \\ \Lambda^{\mu\nu}_{\mathbf{P}} \mathcal{E}'^\nu(\tilde{p}, \tilde{P}) \end{pmatrix} \gamma^4 = \begin{pmatrix} \mathcal{D}'(p, P) \\ \mathcal{E}'^\mu(p, P) \end{pmatrix} \ . \qquad (2.106)$$

$\mathcal{D}_1^{\mu\nu}$	$\delta^{\mu\rho}\,\mathbb{P}^{\rho\nu}$
$\mathcal{D}_2^{\mu\nu}$	$-i\,\frac{3}{5}\sqrt{5}\left(\hat{p}_T\,\delta^{\mu\rho}-i\,\frac{2}{3}\,\gamma_T^\mu\,\hat{p}_T^\rho\right)\mathbb{P}^{\rho\nu}$
$\mathcal{D}_3^{\mu\nu}$	$\sqrt{3}\,\hat{p}_T\,\hat{P}^\mu\,\hat{p}_T^\rho\,\mathbb{P}^{\rho\nu}$
$\mathcal{D}_4^{\mu\nu}$	$i\sqrt{3}\,\hat{P}^\mu\,\hat{p}_T^\rho\,\mathbb{P}^{\rho\nu}$
$\mathcal{D}_5^{\mu\nu}$	$\gamma_T^\mu\,\hat{p}_T\,p_T^\rho\,\mathbb{P}^{\rho\nu}$
$\mathcal{D}_6^{\mu\nu}$	$-i\,\gamma_T^\mu\,p_T^\rho\,\mathbb{P}^{\rho\nu}$
$\mathcal{D}_7^{\mu\nu}$	$3\left(p_T^\mu\,p_T^\rho-\frac{1}{3}\left[\delta^{\mu\rho}+\gamma_T^\mu\,\hat{p}_T\,p_T^\rho\right]\right)\mathbb{P}^{\rho\nu}$
$\mathcal{D}_8^{\mu\nu}$	$-i\sqrt{5}\left(\hat{p}_T\,p_T^\mu\,p_T^\rho-\frac{1}{5}\left[\hat{p}_T\,\delta^{\mu\rho}+\gamma_T^\mu\,p_T^\rho\right]\right)\mathbb{P}^{\rho\nu}$

Table 2.2: Basic Dirac components of the Δ vertex function.

These transformation properties suggest that $\mathcal{D}'$ is a linear combination of the $\mathcal{S}_i$ and $\mathcal{E}'^\mu$ can be composed using the $\mathcal{A}_i^\mu$ that were found for the nucleon. Again we will reshuffle the matrices to find a decomposition that is orthogonal and yields partial wave components:

$$\Phi^{\mu\nu}(p,P)=\sum_{i=1}^{8} D_i(p^2,p\cdot P)\,\mathcal{D}_i^{\mu\nu}(p,P)\ . \tag{2.107}$$

The eight components $\mathcal{D}_i^{\mu\nu}$ are given in table 2.2. To state the orthogonality condition we write the adjoint vertex function as

$$\bar{\Phi}^{\mu\nu}(p,P)=\sum_{i=1}^{8}\bar{\mathcal{D}}_i^{\mu\nu}(p,P)D_i(p^2,p\cdot P)\ . \tag{2.108}$$

The definition of the adjoint Dirac components is inferred from the charge-conjugated Faddeev amplitude and the corresponding relations for the axialvector diquark vertex and the Rarita-Schwinger spinor,

$$\bar{\mathcal{D}}_i^{\mu\nu}(p,P)=C\,\left(\mathcal{D}_i^{\nu\mu}(-p,-P)\right)^T\,C^{-1}\ . \tag{2.109}$$

Orthogonality of the basic components can now be expressed as

$$\mathrm{Tr}\,\bar{\mathcal{D}}_i^{\mu\rho}\mathcal{D}_j^{\rho\mu}=4(-1)^{j+1}\delta^{ij}\ . \tag{2.110}$$

2.4.1 Partial wave decomposition

In a general moving frame, all the components of the Faddeev amplitude $\Gamma^{[\Delta]}_{\alpha\beta\gamma}$ possess just the total angular momentum, 1/2 for the nucleon and 3/2 for the Δ, as a good quantum number. A further interpretation of the components is not obvious. In the rest frame of the bound state, however, the trispinor $\Gamma^{[\Delta]}_{\alpha\beta\gamma}$ can be written as a sum of trispinor components each possessing definite orbital angular momentum and spin, thus allowing a direct interpretation in terms of partial waves.

First we set up the general formalism and apply it to nucleon and Δ in turn. In the rest frame the Pauli-Lubanski operator for an arbitrary tri-spinor $\psi_{\alpha\beta\gamma}$ is given by

$$W^i = \frac{1}{2}\epsilon_{ijk}\mathcal{L}^{jk} , \qquad (2.111)$$

whose square characterizes the total angular momentum,

$$\mathbf{W}^2\psi_{\alpha\beta\gamma} = J(J+1)\psi_{\alpha\beta\gamma} . \qquad (2.112)$$

The tensor $\mathcal{L}$ is the sum of an orbital part, L, and a spin part, S, which read

$$L^{jk} = \sum_{a=1}^{3}(-i)\left(p_a^j\frac{\partial}{\partial p_a^k} - p_a^k\frac{\partial}{\partial p_a^j}\right) , \qquad (2.113)$$

$$2(S^{jk})_{\alpha\alpha',\beta\beta',\gamma\gamma'} = (\sigma^{jk})_{\alpha\alpha'}\otimes\delta_{\beta\beta'}\otimes\delta_{\gamma\gamma'} + \delta_{\alpha\alpha'}\otimes(\sigma^{jk})_{\beta\beta'}\otimes\delta_{\gamma\gamma'} +$$
$$\delta_{\alpha\alpha'}\otimes\delta_{\beta\beta'}\otimes(\sigma^{jk})_{\gamma\gamma'} , \qquad (2.114)$$

such that $\mathcal{L} = L+S$. The tensor L is proportional to the unit matrix in Dirac space. The definition $\sigma^{\mu\nu} := -\frac{i}{2}[\gamma^\mu, \gamma^\nu]$ differs by a minus sign from its Minkowski counterpart. The tensors L and S are written as a sum over the respective tensors for each of the three constituent quarks which are labelled $a = 1, 2, 3$ and with respective Dirac indices $\alpha\alpha',\beta\beta',\gamma\gamma'$.

With the definition of the spin matrix $\Sigma^i = \frac{1}{2}\epsilon_{ijk}\sigma^{jk}$ the Pauli-Lubanski operator reads

$$(W^i)_{\alpha\alpha',\beta\beta',\gamma\gamma'} = L^i\,\delta_{\alpha\alpha'}\otimes\delta_{\beta\beta'}\otimes\delta_{\gamma\gamma'} + (S^i)_{\alpha\alpha',\beta\beta',\gamma\gamma'} , \qquad (2.115)$$

$$L^i = (-i)\epsilon_{ijk}\left[p^j\frac{\partial}{\partial p^k} + q^j\frac{\partial}{\partial q^k}\right] , \qquad (2.116)$$

$$(S^i)_{\alpha\alpha',\beta\beta',\gamma\gamma'} = \frac{1}{2}\left((\Sigma^i)_{\alpha\alpha'}\otimes\delta_{\beta\beta'}\otimes\delta_{\gamma\gamma'} + \delta_{\alpha\alpha'}\otimes(\Sigma^i)_{\beta\beta'}\otimes\delta_{\gamma\gamma'} + \right.$$
$$\left.\delta_{\alpha\alpha'}\otimes\delta_{\beta\beta'}\otimes(\Sigma^i)_{\gamma\gamma'}\right) , \qquad (2.117)$$

where we have already introduced the relative momentum p between quark and diquark and the relative momentum q within the diquark via a canonical transformation:

$$P = p^1 + p^2 + p^3, \quad p = \eta(p^1 + p^2) - (1 - \eta)p^3, \quad q = \frac{1}{2}(p^1 - p^2) \ . \quad (2.118)$$

In the diquark-quark model, the quark (α) and diquark ($\beta\gamma$) Dirac indices of $\psi_{\alpha\beta\gamma}$ do separate. In the parametrization of the diquark-quark vertices $\chi^5_{\beta\gamma}(q)$ and $\chi^\mu_{\beta\gamma}(q)$, *cf.* eqs. (2.51,2.52), we retained only the dominant Dirac component along with a scalar function of q. Therefore no orbital angular momentum is carried by the diquarks,

$$\mathbf{L}^2 \chi^5_{\beta\gamma}(q) = \mathbf{L}^2 \chi^\mu_{\beta\gamma}(q) = 0 \ , \quad (2.119)$$

and the second term in the definition of L^i in eq. (2.116) depending on q may safely be dropped. The operator $\mathbf{W}^2$ now takes the form

$$\mathbf{W}^2 \ = \ \mathbf{L}^2 + 2\boldsymbol{L}\cdot\boldsymbol{S} + \mathbf{S}^2 \ , \quad (2.120)$$

$$\mathbf{L}^2 \ = \ \left(2p^i \frac{\partial}{\partial p^i} - \boldsymbol{p}^2 \Delta_p + p^i p^j \frac{\partial}{\partial p^i} \frac{\partial}{\partial p^j} \right) \ , \quad (2.121)$$

$$2(\mathbf{L}\cdot\mathbf{S})_{\alpha\alpha',\beta\beta',\gamma\gamma'} \ = \ -\epsilon_{ijk} p^j \frac{\partial}{\partial p^k} \left((\Sigma^i)_{\alpha\alpha'} \otimes \delta_{\beta\beta'} \otimes \delta_{\gamma\gamma'} + \right.$$
$$\left. \delta_{\alpha\alpha'} \otimes \left[(\Sigma^i)_{\beta\beta'} \otimes \delta_{\gamma\gamma'} + \delta_{\beta\beta'} \otimes (\Sigma^i)_{\gamma\gamma'} \right] \right) \ , \quad (2.122)$$

$$(\mathbf{S}^2)_{\alpha\alpha',\beta\beta',\gamma\gamma'} \ = \ \tfrac{1}{4} \left(9\,\delta_{\alpha\alpha'} \otimes \delta_{\beta\beta'} \otimes \delta_{\gamma\gamma'} + \right.$$
$$2\,\Sigma^i{}_{\alpha\alpha'} \otimes \left[(\Sigma^i)_{\beta\beta'} \otimes \delta_{\gamma\gamma'} + \delta_{\beta\beta'} \otimes (\Sigma^i)_{\gamma\gamma'} \right] + $$
$$\left. 2\,\delta_{\alpha\alpha'} \otimes (\Sigma^i)_{\beta\beta'} \otimes (\Sigma^i)_{\gamma\gamma'} \right) \ . \quad (2.123)$$

For evaluating the action of the spin operator Σ^i on the diquark-quark vertices χ^5 and χ^μ the following identities proved to be useful,

$$\Sigma^j(\gamma^5 C) + (\gamma^5 C)(\Sigma^j)^T \ = \ 0 \ , \quad (2.124)$$

$$\Sigma^j \begin{pmatrix} (\gamma^4 C) \\ (\gamma^i C) \end{pmatrix} + \begin{pmatrix} (\gamma^4 C) \\ (\gamma^i C) \end{pmatrix} (\Sigma^j)^T \ = \ \begin{pmatrix} 0 \\ 2i\epsilon_{mji}(\gamma^m C) \end{pmatrix} \ , \quad (2.125)$$

$$\Sigma^j(\gamma^5 C)(\Sigma^j)^T \ = \ -3(\gamma^5 C) \ , \quad (2.126)$$

$$\Sigma^j \begin{pmatrix} (\gamma^4 C) \\ (\gamma^i C) \end{pmatrix} (\Sigma^j)^T \ = \ \begin{pmatrix} -3(\gamma^4 C) \\ (\gamma^i C) \end{pmatrix} \ . \quad (2.127)$$

Dirac component	Faddeev amplitude component	EV $l(l+1)$ of $\mathbf{L}^2$	EV $s(s+1)$ of $\mathbf{S}^2$
$\mathcal{S}_1$	$\begin{pmatrix} \varsigma \\ 0 \end{pmatrix}_\alpha (\gamma_5 C)_{\beta\gamma}$	0	$\frac{3}{4}$
$\mathcal{S}_2$	$\begin{pmatrix} 0 \\ (\boldsymbol{\sigma}\hat{\boldsymbol{p}})\varsigma \end{pmatrix}_\alpha (\gamma_5 C)_{\beta\gamma}$	2	$\frac{3}{4}$
$\mathcal{A}_1^\mu$	$\hat{P}^4 \begin{pmatrix} 0 \\ \varsigma \end{pmatrix}_\alpha (\gamma^4 C)_{\beta\gamma}$	0	$\frac{3}{4}$
$\mathcal{A}_2^\mu$	$\hat{P}^4 \begin{pmatrix} (\boldsymbol{\sigma}\hat{\boldsymbol{p}})\varsigma \\ 0 \end{pmatrix}_\alpha (\gamma^4 C)_{\beta\gamma}$	2	$\frac{3}{4}$
$\mathcal{A}_3^\mu$	$\sqrt{\frac{1}{3}} \begin{pmatrix} i\sigma^i\varsigma \\ 0 \end{pmatrix}_\alpha (\gamma^i C)_{\beta\gamma}$	0	$\frac{3}{4}$
$\mathcal{A}_4^\mu$	$\sqrt{\frac{1}{3}} \begin{pmatrix} 0 \\ \sigma^i(\boldsymbol{\sigma}\hat{\boldsymbol{p}})\varsigma \end{pmatrix}_\alpha (\gamma^i C)_{\beta\gamma}$	2	$\frac{3}{4}$
$\mathcal{A}_5^\mu$	$\sqrt{\frac{3}{2}} \begin{pmatrix} i\left(\hat{p}^i(\boldsymbol{\sigma}\hat{\boldsymbol{p}}) - \frac{1}{3}\sigma^i\right)\varsigma \\ 0 \end{pmatrix}_\alpha (\gamma^i C)_{\beta\gamma}$	6	$\frac{15}{4}$
$\mathcal{A}_6^\mu$	$\sqrt{\frac{3}{2}} \begin{pmatrix} 0 \\ i\left(\hat{p}^i - \frac{1}{3}\sigma^i(\boldsymbol{\sigma}\hat{\boldsymbol{p}})\right)\varsigma \end{pmatrix}_\alpha (\gamma^i C)_{\beta\gamma}$	2	$\frac{15}{4}$

Table 2.3: Classification of the components of the nucleon Faddeev amplitude in terms of eigenfunctions of $\mathbf{L}^2$ and $\mathbf{S}^2$ in the rest frame of the bound state. 'EV' abbreviates 'eigenvalue' and ς denotes an arbitrary Pauli two-component spinor. Each Faddeev component is to be multiplied with the diquark width function $V(x = q^2)$. Normalized 4-vectors are $\hat{p} = p/|p|$ and normalized 3-vectors are correspondingly $\hat{\boldsymbol{p}} = \boldsymbol{p}/|\boldsymbol{p}|$.

Nucleon

We will make use of the Bethe-Salpeter wave function Ψ defined in eq. (2.68). The Faddeev takes the following form, if the wave function instead of the vertex function is used,

$$
\begin{aligned}
S_{\alpha\alpha'}(\eta P + p)\Gamma_{\alpha'\beta\gamma}(q, p, P) &= (\Psi^5(p, P)u(P))_\alpha \, \chi^5(q)_{\beta\gamma} + \\
&\quad (\Psi^\mu(p, P)u(P))_\alpha \, \chi^\mu(q)_{\beta\gamma} \, . \quad (2.128)
\end{aligned}
$$

We will seek eigenfunctions of the spin and orbital angular momentum operators $\mathbf{L}^2$ and $\mathbf{S}^2$, where the eigenfunctions shall be of the general form as indicated above. Thus they represent components of the Faddeev amplitude with the spectator quark leg attached, $(S\Gamma)_{\alpha\beta\gamma}$. We note that for the wave function Ψ an analogous decomposition as for the vertex function holds, see eq. (2.91),

$$
\begin{pmatrix} \Psi^5(p, P) \\ \Psi^\mu(p, P) \end{pmatrix} = \begin{pmatrix} \sum_{i=1}^{2} \hat{S}_i(p^2, p\cdot P) \, \mathcal{S}_i(p, P) \\ \sum_{i=1}^{6} \hat{A}_i(p^2, p\cdot P) \, \gamma_5 \mathcal{A}_i^\mu(p, P) \end{pmatrix} \, . \quad (2.129)
$$

A new set of scalar functions, $\hat{S}_i$ and $\hat{A}_i$, has been introduced whereas the basic Dirac components are the ones from table 2.1. The reason why we choose the wave function for further treatment is that the Faddeev amplitude written with the vertex function depends explicitly on the axialvector diquark propagator $D^{\mu\nu}$ which for the Proca form induces mixing between space components of the vertex function and the (virtual) time component of the axialvector diquark (and *vice versa*) in which case no partial wave decomposition can be found. This can be circumvented by using the wave function as in virtue of its definition the diquark propagator has become absorbed in Ψ.

In table 2.3 we have listed all eight components together with the respective eigenvalues of $\mathbf{L}^2$ and $\mathbf{S}^2$. The Faddeev components that are given in the rest frame of the nucleon have been built using the basic Dirac components for the wave function shown in table 2.1.

There is one s wave associated with the scalar diquark, described by $\mathcal{S}_1$, and two s waves associated with the axialvector diquark, one connected with its virtual time component, $\mathcal{A}_1$, and the other described by $\mathcal{A}_3$. In a non-relativistic limit where diquark off-shell components are neglected, only the s waves $\mathcal{S}_1$, $\mathcal{A}_3$ and the d wave $\mathcal{A}_5$ would survive. It is remarkable that the relativistic description leads to accompanying four p waves, the "lower components", which are expected to give substantial contributions to the fraction of the nucleon spin carried by orbital angular momentum. These p waves would not be present in a non-relativistic model.

Delta

The Faddeev amplitude written in terms of the tensor wave function $\Psi^{\mu\nu}$ defined in eq. (2.79) reads

$$S_{\alpha\alpha'}(\eta P + p)\Gamma^{\Delta}_{\alpha'\beta\gamma}(q, p, P) = (\Psi^{\mu\nu}(p, P)u^{\nu}(P))_{\alpha}\,\chi^{\mu}(q)_{\beta\gamma}\,. \qquad (2.130)$$

Again, the wave function decomposition proceeds in the same manner as done for the Δ vertex function

$$\Psi^{\mu\nu}(p, P) = \sum_{i=1}^{8}\hat{D}_{i}(p^{2}, p\cdot P)\,\mathcal{D}^{\mu\nu}_{i}(p, P)\,. \qquad (2.131)$$

Applying the operators $\mathbf{L}^{2}$ and $\mathbf{S}^{2}$, eqs. (2.121,2.123), to the Faddeev amplitude $(S\Gamma^{\Delta})_{\alpha\beta\gamma}$, this decomposition is seen to yield eigenfunctions of the spin and orbital angular momentum operators. Their explicit form in the rest frame is shown in table 2.4. The strength of the partial waves is determined by the scalar functions $\hat{D}_{i}(p^{2}, p\cdot P)$.

In contrast to the nucleon, only one s wave (described by $\mathcal{D}_{1}$) is found. Two d waves that survive the non-relativistic limit are given by $\mathcal{D}_{5}$ and $\mathcal{D}_{7}$, and one d wave can be attributed to the virtual time component of the axialvector diquark, $\mathcal{D}_{3}$. All even partial waves are accompanied by relativistic "lower" components that could be even more important as in the nucleon case for only one dominant s wave is present compared to three within the nucleon.

To summarize, the relativistic decomposition of nucleon and Δ quark-diquark wave functions yields a rich structure in terms of partial waves. Well-known problems from certain non-relativistic quark model descriptions are avoided from the beginning in a relativistic treatment. First, photoinduced $N-\Delta$ transitions that are impossible in spherically symmetric non-relativistic nucleon ground states (described by only one s wave) will occur in our model through overlaps in the axialvector part of the respective wave functions. Additionally, photoinduced transitions from scalar to axialvector diquarks can take place, thus creating an overlap of the nucleon scalar diquark correlations with the Δ axialvector diquark correlations. Secondly, although the total baryon spin will be mainly made of the quark spin in the s waves, the orbital momentum of the relativistic p waves contributes as well which could not happen in a non-relativistic description since the p waves are absent there.

Dirac component	Faddeev amplitude component	EV $l(l+1)$ of $\mathbf{L}^2$	EV $s(s+1)$ of $\mathbf{S}^2$
$\mathcal{D}_1^{\mu\nu}$	$\begin{pmatrix} \varsigma^i \\ 0 \end{pmatrix}_\alpha (\gamma^i C)_{\beta\gamma}$	0	$\frac{15}{4}$
$\mathcal{D}_2^{\mu\nu}$	$\frac{3}{5}\sqrt{5}\begin{pmatrix} 0 \\ ((\boldsymbol{\sigma}\hat{\boldsymbol{p}})\varsigma^i - \frac{2}{3}\sigma^i(\hat{\boldsymbol{p}}\boldsymbol{\varsigma})) \end{pmatrix}_\alpha (\gamma^i C)_{\beta\gamma}$	2	$\frac{15}{4}$
$\mathcal{D}_3^{\mu\nu}$	$i\sqrt{3}\hat{P}^4\begin{pmatrix} 0 \\ (\boldsymbol{\sigma}\hat{\boldsymbol{p}})(\hat{\boldsymbol{p}}\boldsymbol{\varsigma}) \end{pmatrix}_\alpha (\gamma^4 C)_{\beta\gamma}$	6	$\frac{3}{4}$
$\mathcal{D}_4^{\mu\nu}$	$i\sqrt{3}\hat{P}^4\begin{pmatrix} (\hat{\boldsymbol{p}}\boldsymbol{\varsigma}) \\ 0 \end{pmatrix}_\alpha (\gamma^4 C)_{\beta\gamma}$	2	$\frac{3}{4}$
$\mathcal{D}_5^{\mu\nu}$	$\begin{pmatrix} \sigma^i(\boldsymbol{\sigma}\hat{\boldsymbol{p}})(\hat{\boldsymbol{p}}\boldsymbol{\varsigma}) \\ 0 \end{pmatrix}_\alpha (\gamma^i C)_{\beta\gamma}$	6	$\frac{3}{4}$
$\mathcal{D}_6^{\mu\nu}$	$\begin{pmatrix} 0 \\ \sigma^i(\hat{\boldsymbol{p}}\boldsymbol{\varsigma}) \end{pmatrix}_\alpha (\gamma^i C)_{\beta\gamma}$	2	$\frac{3}{4}$
$\mathcal{D}_7^{\mu\nu}$	$3\begin{pmatrix} \hat{p}^i(\hat{\boldsymbol{p}}\boldsymbol{\varsigma}) - \frac{1}{3}[\varsigma^i + \sigma^i(\boldsymbol{\sigma}\hat{\boldsymbol{p}})(\hat{\boldsymbol{p}}\boldsymbol{\varsigma})] \\ 0 \end{pmatrix}_\alpha (\gamma^i C)_{\beta\gamma}$	6	$\frac{15}{4}$
$\mathcal{D}_8^{\mu\nu}$	$\sqrt{5}\begin{pmatrix} 0 \\ (\hat{p}^i(\boldsymbol{\sigma}\hat{\boldsymbol{p}})(\hat{\boldsymbol{p}}\boldsymbol{\varsigma}) - \frac{1}{5}[\sigma^i(\hat{\boldsymbol{p}}\boldsymbol{\varsigma}) + (\boldsymbol{\sigma}\hat{\boldsymbol{p}})\varsigma^i]) \end{pmatrix}_\alpha (\gamma^i C)_{\beta\gamma}$	12	$\frac{15}{4}$

Table 2.4: Classification of the components of the Δ Faddeev amplitude in terms of eigenfunctions of $\mathbf{L}^2$ and $\mathbf{S}^2$ in the rest frame of the bound state. ς^i denotes an arbitrary $2_{\text{Pauli}} \times 3_{\text{vector}}$-component spinor that represents the non-vanishing components of u^μ in the Δ rest frame. Each Faddeev component is to be multiplied with the diquark width function $V(x = q^2)$.

2.5 Numerical solutions

After having described the numerical algorithm that solves the Bethe-Salpeter equations for nucleon and Δ, we will first present solutions for the nucleon with scalar diquark correlations only. These results, published in ref. [23], will provide us with constraints on the scalar functions which enter the diquark-quark vertices. Especially results on the neutron electric charge radius and the proton electric form factor signal the superiority of using a dipole form for the scalar function P appearing in eqs. (2.51,2.52). Although presenting form factors at this point is an early anticipation of results which are not derived until chapter 3, it motivates the choice of the specific diquark-quark vertex in the full scalar-axialvector calculations of section 2.5.3.

2.5.1 Numerical method

We will solve the Bethe-Salpeter equations for nucleons, eq. (2.69), and for the Δ, eq. (2.80), in the baryon rest frame as a system of equations for vertex and wave function. In a concise notation the system of equations reads

$$\psi(p, P) = G_0^{\mathrm{q-dq}}(p, P)\, \phi(p, P) \tag{2.132}$$

$$\phi(p, P) = \int \frac{d^4 k}{(2\pi)^4}\, K^{\mathrm{BS}}\, \psi(k, P)\,. \tag{2.133}$$

The product of quark and diquark propagators is given by $G_0^{\mathrm{q-dq}}$ and K^{BS} is the quark exchange kernel.

The procedure to solve the equations can be divided into the following steps:

- We will project out the unknown scalar functions describing the partial waves from the expansions for wave and vertex function by contraction with appropriate Dirac components.

- As the scalar functions depend on *two* Lorentz scalars, p^2 and $p \cdot P = iM|p|\,\hat{p}\cdot\hat{P}$, we shift the dependence on $\hat{p}\cdot\hat{P}$ into an expansion in Chebyshev polynomials and project the equations onto the expansion coefficients, the Chebyshev moments. We will see that this expansion is close to a hyperspherical expansion.

- The interaction kernel can be *approximated* by a finite number of Chebyshev polynomials. Employing appropriate orthogonality relations, the equations are reduced to a coupled system of one-dimensional integral equations

for the Chebyshev moments. The numerical effort will be considerably re-
duced compared to the brute force method which puts wave and vertex func-
tion on a two-dimensional grid, since only a few Chebyshev polynomials
will be needed.

These steps are described in more detail in the following.

The wave function ψ and the vertex function ϕ have been expanded in Dirac
space according to eqs. (2.91,2.129) in the nucleon case and for the Δ according
to eqs. (2.107,2.131). We will use the generic labels Y_i ($i = 1, \ldots, 8$) for the
scalar functions describing the partial waves in the vertex function and likewise
$\hat{Y}_i$ for the wave function. The scalar functions depend in turn on the scalars p^2,
$\hat{p} \cdot \hat{P}$, and the latter scalar reduces in the baryon rest frame to $z = \cos \Theta$ where
Θ is the angle between p and the 4-axis, see appendix A.1 for our conventions
for hyperspherical coordinates. For numerical convenience, we redefine the scalar
functions associated with the "lower" components,

$$Y_i[\hat{Y}_i] \rightarrow \frac{1}{\sqrt{1 - z^2}} \, Y_i[\hat{Y}_i], \qquad (i \ \text{odd}) \,. \tag{2.134}$$

The set of scalar functions is now expanded into Chebyshev polynomials of the
first kind [52],

$$Y_i(p^2, z) = \sum_{n=0}^{\infty} i^n Y_i^n(p^2) \, T_n(z) \,, \tag{2.135}$$

$$\hat{Y}_i(p^2, z) = \sum_{n=0}^{\infty} i^n \hat{Y}_i^n(p^2) \, T_n(z) \,, \tag{2.136}$$

thereby defining the Chebyshev moments Y_i^n and $\hat{Y}_i^n$. Here, we employ a con-
venient (albeit non-standard) normalization for the zeroth Chebyshev moment by
setting $T_0 = 1/\sqrt{2}$.

In the first step, we project the left hand sides of eqs. (2.132,2.133) onto
the scalar functions Y_i and $\hat{Y}_i$ using the orthogonality relations (2.94–2.96) and
(2.110),

$$\hat{Y}_i(p^2, z) = (g'_0)^{ij}(p^2, z) \, Y_j(p^2, z) \tag{2.137}$$

$$Y_i(p^2, z) = \int \frac{d^4 k}{(2\pi)^4} \, (H')^{ij}(p^2, k^2, y', z, z') \, \hat{Y}_i(k^2, z') \,. \tag{2.138}$$

The new propagator matrix $(g'_0)^{ij}$ and the modified kernel $(H')^{ij}$ are the result of
taking Dirac traces after multiplication with the respective adjoint Dirac compo-
nents. As a consequence, the kernel $(H')^{ij}$ depends on the possible scalar products

between the vectors k, p, P which are can be expressed as $k^2, p^2, z' = \hat{k}\hat{P}, z = \hat{p}\hat{P}$ and $y' = \hat{\boldsymbol{k}} \cdot \hat{\boldsymbol{p}}$.

Using the orthogonality relation of the Chebyshev polynomials,

$$\int_{-1}^{1} \frac{T_n(z)T_m(z)}{\sqrt{1-z^2}}\, dz = \frac{\pi}{2}\delta_{nm}\,, \tag{2.139}$$

the system of equations for the scalar quantities Y_i and $\hat{Y}_i$ is projected onto their Chebyshev moments,

$$\hat{Y}_i^n(p^2) = \int_{-1}^{1} dz\, \frac{2}{\pi} (g_0')^{ij}(p^2, z) \sum_{m=0}^{m_{\max}} i^{m-n} Y_j^m(p^2) \frac{T_m(z)T_n(z)}{\sqrt{1-z^2}} \tag{2.140}$$

$$Y_i^m(p^2) = \int_{-1}^{1} dz\, \frac{2}{\pi} \int \frac{d^4k}{(2\pi)^4}\, (H')^{ij}(p^2, k^2, z, z', y') \times$$
$$\sum_{n=0}^{n_{\max}} i^{n-m} \hat{Y}_j^n(k^2) \frac{T_n(z')T_m(z)}{\sqrt{1-z^2}}\,. \tag{2.141}$$

Of course, in the practical calculation the Chebyshev expansion can be taken into account only up to a $m_{\max}^{th}$ moment for the Y_i^m and up to a $n_{\max}^{th}$ moment for the $\hat{Y}_i^n$. The propagator matrix $(g_0')^{ij}$ can be expanded into Chebyshev polynomials as well and thereby results an expression from eq. (2.140) that involves an integral over three Chebyshev polynomials. The addition theorem

$$T_n(z)\, T_m(z) = \tfrac{1}{2}(T_{|n-m|}(z) + T_{n+m}(z)) \quad (n, m \neq 0)\,, \tag{2.142}$$
$$T_0(z)\, T_m(z) = \tfrac{1}{\sqrt{2}} T_m(z) \tag{2.143}$$

simplifies this expression to a form where a subsequent application of the orthogonality relation (2.139) reduces it to a matrix equation,

$$\hat{Y}_i^n(p^2) = (g_0)^{ij,nm}(p^2)\, Y_i^m(p^2)\,. \tag{2.144}$$

The elements of the propagator matrix $(g_0)^{ij,nm}$ are all real due to the explicit phase factor i^n in the Chebyshev expansions.

Let us now focus attention on eq. (2.141), the 4-dimensional integral over the Bethe-Salpeter kernel,

$$Y_i^m(p^2) = \int_0^{\infty} \frac{k^3}{4\pi^4} d|k| \int_{-1}^{1} \sqrt{1-z'^2}\, dz' \int_{-1}^{1} dz \int_{-1}^{1} dy'\, (H')^{ij}(p^2, k^2, y', z, z')$$
$$\times \sum_{n=0}^{n_{\max}} i^{n-m} \hat{Y}_j^n(k^2) \frac{T_n(z')T_m(z)}{\sqrt{1-z^2}}\,. \tag{2.145}$$

We will take care of the angular integrations over z and z' next. To this end we *approximate* the Bethe-Salpeter kernel with Chebyshev polynomials in the following manner,

$$(H'')^{ij} = (1 - z'^2)(H')^{ij} = \sum_{s=1}^{m_{\max}+1} \sum_{t=1}^{n_{\max}+1} c^{ij,st} \, T_{s-1}(z) T_{t-1}(z') \; . \qquad (2.146)$$

The coefficients $c^{ij,st}$ are *not* the Chebyshev moments of $(H'')^{ij}$ but rather

$$
\begin{aligned}
c^{ij,st} \;=\;& \frac{2}{(m_{\max}+1)} \frac{2}{(n_{\max}+1)} \sum_{u=1}^{m_{\max}+1} \sum_{v=1}^{n_{\max}+1} T_{s-1}(z_u) T_{t-1}(z'_v) \\
& \times (H'')^{ij}(p^2, k^2, y', z_u, z'_v) \; .
\end{aligned}
\qquad (2.147)
$$

The $z_u \, [z'_v]$ are the *zeros* of the Chebyshev polynomial $T_{m_{\max}+1}(z) \; [T_{n_{\max}+1}(z')]$. Eqs. (2.146,2.147) are an example of the so-called Chebyshev approximation of a function which we have applied to both the arguments z and z'. As is known from the literature [53], the Chebyshev approximation of a function is very close to the approximation by the *minimax polynomial*, which (among all polynomials of the same degree) has the smallest maximum deviation from the true function.

When inserting the kernel approximation back into eq. (2.145), we see that the orthogonality relation (2.139) will take care of the integrations over z and z'. We find

$$
\begin{aligned}
Y_i^m(p^2) \;=\;& \frac{1}{(m_{\max}+1)(n_{\max}+1)} \int_0^\infty \frac{k^3}{4\pi^2} d|k| \int_{-1}^1 dy' \sum_{u=1}^{m_{\max}+1} \sum_{v=1}^{n_{\max}+1} i^{n-m} \\
& \times T_m(z_u) T_n(z'_v) \, (H'')^{ij}(p^2, k^2, y', z_u, z'_v) \, \hat{Y}_j^n(k^2) \; .
\end{aligned}
\qquad (2.148)
$$

Here the sum runs also over the label j and the Chebyshev moment label n.

Finally we have succeeded to transform the original 4-dimensional integral equation into a system of coupled one-dimensional equations. In summary, the system reads,

$$\hat{Y}_i^n(p^2) \;=\; (g_0)^{ij,nm}(p^2) \, Y_i^m(p^2) \; , \qquad (2.149)$$

$$Y_i^m(p^2) \;=\; \int_0^\infty d|k| \, H^{ij,mn}(k^2, p^2) \, \hat{Y}_i^n(k^2) \; , \qquad (2.150)$$

with the definition

$$
\begin{aligned}
H^{ij,mn}(k^2, p^2) \;=\;& \frac{1}{(m_{\max}+1)(n_{\max}+1)} \frac{k^3}{4\pi^2} \int_{-1}^1 dy' \sum_{u=1}^{m_{\max}+1} \sum_{v=1}^{n_{\max}+1} i^{n-m} \\
& \times T_m(z_u) T_n(z'_v) \, (H'')^{ij}(p^2, k^2, y', z_u, z'_v) \; .
\end{aligned}
\qquad (2.151)
$$

The momentum k is discretized on a mesh with $n_{|k|}$ points, with typically $n_{|k|} = 20, \ldots, 50$, and the integration is performed as a Gaussian quadrature. Then the problem is equivalent to tuning the lowest eigenvalue of a matrix equation to one by readjusting the parameters of the model.

We have introduced the numerical method from a merely technical point of view. Combining the Chebyshev expansion of the scalar functions describing the partial waves with the Chebyshev approximation of the quark exchange kernel replaces the angular integrations over $z = \cos\Theta$ and $z' = \cos\Theta'$ by sums that are truncated by m_{max} and n_{max}, the highest Chebyshev moments of the vertex and wave function partial waves, respectively. The question is whether there is another, more intuitive argument that supports a quick convergence of the solution with increasing $m_{\mathrm{max}}[n_{\mathrm{max}}]$.

There exists a motivation using this kind of expansion that is related to symmetries in a simpler dynamical system. The numerical solution of the ladder approximated Bethe-Salpeter equation in the massless and massive Wick-Cutkosky model has been studied extensively in the literature, for a review see [54]. In this model, two massive mesons interact by exchanging a third (massless or massive) meson. In the case of a massless exchange meson, the Bethe-Salpeter equation exhibits an $O(4)$ symmetry [55]. By expanding the wave functions into hyperspherical harmonics $\mathcal{Y}_{nlm}$ (*cf.* appendix A.1), the solutions can be classified using the quantum numbers n (four-dimensional angular momentum) and l, m (three-dimensional orbital angular momentum and its third component). The zero orbital angular momentum states of the Wick-Cutkosky model ($l = 0$) are essentially given by

$$\psi_{l=0}^{\mathrm{Wick}} \sim Y_n^{\mathrm{Wick}}(p^2)\, U_n(z) \;, \tag{2.152}$$

with the $U_n(z)$ being Chebyshev polynomials of the *second* kind. They are related to the $T_n(z)$ by

$$T_n(z) = U_n(z) - z U_{n-1}(z) \;, \qquad (n > 0) \;. \tag{2.153}$$

Thus an expansion of wave functions into the T_n's is closely related to the expansion into hyperspherical harmonics. Furthermore, the authors of ref. [56] have shown that in the case of a massive exchange meson, where the $O(4)$ symmetry is broken, the expansion into hyperspherical harmonics converges amazingly quickly although n ceases to be a good quantum number. Typically $n_{\mathrm{max}} < 6$ was sufficient to obtain stable solutions, except for the very weak binding regime.

After this short digression let us return to the Bethe-Salpeter equations in the diquark-quark model. The Bethe-Salpeter equations treated here are ladder equations as well, though complicated by the mixing of components with differing

angular momentum. Nevertheless, the expansion into *spinor* hyperspherical harmonics in the model sector with pointlike scalar diquarks only has been shown to work well in ref. [57]. This finding has been confirmed and extended to pointlike axialvector diquarks in refs. [58, 22]. Thus we can conclude that the $O(4)$ symmetry is also in the diquark-quark model approximately valid.

Let us point out the kinematical situations in which there might arise problems. Due to the singularities in the propagator denominators of $G_0^{\text{q}-\text{dq}}$, the allowed range of the momentum partitioning parameter η in the nucleon Bethe-Salpeter equation is restricted to

$$\eta \in [1 - m_{sc}/M_n, \; m_q/M_n] \,, \tag{2.154}$$

if $m_{ax} \geq m_{sc} > m_q$ is assumed. Singularities in the exchange quark propagator and the diquark vertices employing n-pole scalar functions V, see eq. (2.61), impose the additional bounds

$$\eta \; \in \; \left[\tfrac{1}{2}(1 - m_q/M_n), \tfrac{1}{2}(1 + m_q/M_n)\right] \,, \tag{2.155}$$
$$\eta \; \in \; \left[\tfrac{1}{3}(1 - 2\lambda_n/M_n), \tfrac{1}{3}(1 + 2\lambda_n/M_n)\right] \,. \tag{2.156}$$

Note that these bounds on the value of η arise in the practical calculations when performed as outlined above. In principle, η could be chosen arbitrarily between 0 and 1, but beyond these bounds the connection of the respective Bethe-Salpeter equation in Minkowski space and the present one in Euclidean space is no longer given by a simple Wick rotation, but the Euclidean space equation picks up additional residue terms.[6]

If η is chosen to be close to one of the boundaries given in eqs. (2.154–2.156) then the propagators vary strongly due to the vicinity of the poles and their Chebyshev expansion, employed to derive eq. (2.144), will converge slowly. Thus, the number of Chebyshev moments for the partial waves in the wave function ψ, $n_{\max}$, needs to be increased in order to achieve sufficient accuracy for the vertex function. We will also see in the numerical solutions that the wave function expansion itself will converge more slowly under these circumstances.

2.5.2 Solutions I: The scalar diquark sector

In this subsection, we will present results in the model sector with scalar diquarks only, summarizing the work described in ref. [23]. We recall the Faddeev amplitude for the nucleon, *cf.* eq. (2.128) and table 2.3, that has been decomposed into

---

[6]We will encounter the problem of relating Minkowski and Euclidean vertex and wave functions again in section 3.2.1 when calculating current matrix elements.

Fixed width $S_1(p^2)|_{|p|=0.2M_n} = 1/2$

$V(x)$	$m_s\ [M_n]$	$m_q\ [M_n]$	$\lambda\ [M_n]$	g_s
$n = 1$	0.7	0.685	0.162	117.1
$n = 2$	0.7	0.620	0.294	91.79
$n = 4$	0.7	0.605	0.458	85.47
$n = 6$	0.7	0.600	0.574	84.37
$n = 8$	0.7	0.598	0.671	83.76
exp	0.7	0.593	0.246	82.16
gau	0.7	0.572	0.238	71.47

Fixed masses

$n = 1$	0.7	0.62	0.113	155.8
$n = 2$	0.7	0.62	0.294	91.79
$n = 4$	0.7	0.62	0.495	81.08
$n = 6$	0.7	0.62	0.637	78.61
exp	0.7	0.62	0.283	74.71

Table 2.5: Summary of parameters used for the various scalar functions $V(x)$ in the diquark-quark vertices, *cf.* eqs. (2.61–2.63).

partial waves. Using scalar diquarks only, it reads in the rest frame

$$(S\Gamma)_{\alpha\beta\gamma} = \begin{pmatrix} \hat{S}_1\,\varsigma \\ \hat{S}_2(\boldsymbol{\sigma}\hat{\boldsymbol{p}})\,\varsigma \end{pmatrix}_\alpha (g_s V)\,(\gamma_5 C)_{\beta\gamma}\,. \tag{2.157}$$

The two scalar functions $\hat{S}_1$ and $\hat{S}_2$ (related to the wave function) describe upper and lower component of the effective nucleon spinor. Likewise only the two functions S_1 and S_2 enter the decomposition of the vertex function.

We will start out with investigations of the various forms of the scalar function $V(x)$ that parametrizes the diquark-quark vertex, see eqs. (2.61–2.63). Furthermore we pick $\sigma = 1/2$ for the momentum distributing parameter in the diquark-quark vertex.

We have chosen to consider two cases: First we fix the the ratios of quark and scalar diquark mass to the nucleon mass (m_q/M_n and m_{sc}/M_n) and tune the width parameter λ in the scalar function $V(x)$ until the normalization g_s, calculated using eq. (2.59), provides enough binding to reach the physical nucleon mass. This corresponds to the constraint that iterating the system of equations

	$n_{\max}$	0	2	4	6	8
				$\eta = 0.4$		
$m_{\max}$						
0		0.7005	0.9551	0.9731	0.9738	
2		0.7806	0.9797	0.9967	0.9979	
4		0.7844	0.9922	0.9993	0.9999	
6		0.7846	0.9928	0.9999	1.0000	
				$\eta = 0.31$		
0		0.6517	0.8379	0.9285	0.9431	0.9449
2		0.8755	0.8988	0.9743	0.9940	0.9965
4		0.9326	0.9614	0.9904	0.9977	0.9996
6		0.9406	0.9714	0.9978	0.9992	0.9998
8		0.9416	0.9726	0.9992	0.9998	0.9999

Table 2.6: Convergence of the ground state eigenvalue of the Bethe-Salpeter equation in terms of $m_{\max}$ and $n_{\max}$, shown for two values of the momentum distributing parameter η. For the kernel integration the Gauss quadrature with $n_{y'} = 20$ grid points was used, *cf.* eq. (2.151). The momentum integration in the iteration was performed with $n_{|k|} = 20$ grid points, *cf.* eq. (2.150). Higher accuracy in these integrations does not affect the eigenvalue in the precision given here.

(2.149,2.150) yields an eigenvalue 1. The results for the ratios $m_q/M_n = 0.62$ and $m_{sc}/M_n = 0.7$ are given in the upper half of table 2.5. With this choice and the choice of a dipole form for $V(x)$ we find a good description of the nucleon electric form factors, see below. In the second case, we have kept fixed the diquark mass ($m_{sc}/M_n = 0.7$ as before) and vary the quark mass and the width parameter λ until a solution of the Bethe-Salpeter equation was found with the property

$$S_1^0(p^2)|_{|p|=0.2M_n} = 1/2 . \tag{2.158}$$

This condition fixes the width of the zeroth Chebyshev moment of the s wave amplitude S_1 which we normalize by setting $S_1^0(0) = 1$. We can regard this as a condition on the extension of the whole nucleon-quark-diquark vertex in momentum space since the zeroth moment of S_1 dominates in the expansion of the nucleon vertex function. The resulting parameter sets that solve the Bethe-Salpeter equation are displayed in the lower half of table 2.5.

All of the parameter sets suffer from a general defect that results from the
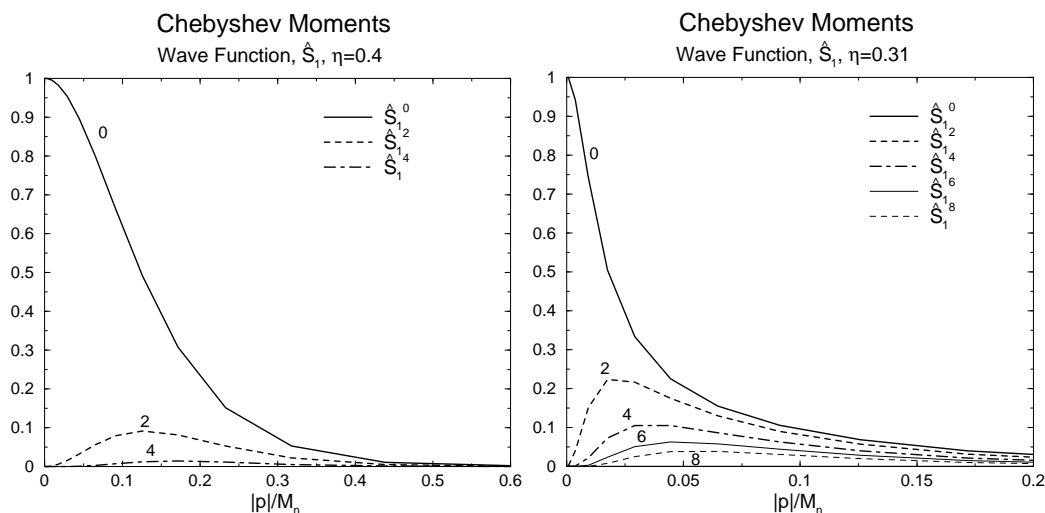
Figure 2.6: The Chebyshev moments of the dominating scalar function $\hat{S}_1$ in the expansion of the wave function. In the left panel, the moments for the choice $\eta = 0.4$ are shown. For the respective moments depicted in the right panel, the employed value of $\eta = 0.31$ is close to the diquark propagator poles.

restriction to scalar diquarks only. The constituent quark mass m_q has to be chosen rather large (corresponding to a strongly bound scalar diquark) such that the diquark normalization g_s provides enough binding energy for the nucleon. Furthermore, the diquark-quark vertices are rather narrow in momentum space as can be seen from the values for λ. In configuration space[7], the extension of the scalar diquark (measured by the FWHM value for the scalar function V) is roughly 1 fm and thus the diquark is as broad as the nucleon appears to be when probed with electrons or pions [59]! The inclusion of the axialvector diquark provides another attractive channel, therefore the scalar diquark normalization g_s could be adjusted to smaller values and consequently the constituent quark mass will drop. The results to be shown in section 2.5.3 indeed confirm this argument.

We turn now to the convergence properties of the Chebyshev expansion, picking as an example the set of parameters employing a dipole form ($n = 2$) for the scalar function $V(x)$. Here the pole in the diquark propagator and the poles appearing in $V(x)$ put the restriction $\eta \in [0.3, 0.52]$, *cf.* eqs. (2.154,2.156). We exemplify our results with the choice $\eta = 0.4$ (far away from any poles) and $\eta = 0.31$ (close to the diquark propagator pole). First we investigate the convergence of the eigenvalue (that is obtained in the numerical iteration of the Bethe-

---

[7]We refer here to the Fourier transform of the relative momentum between the quarks within the diquark that corresponds to the distance between the two quarks.

Salpeter equation) in terms of the highest Chebyshev moment m_{max} employed in the expansion of the vertex function and n_{max} for the wave function. The results of table 2.6 show that for the "safe" value of $\eta = 0.4$ seven Chebyshev moments for both wave and vertex function are sufficient to determine the eigenvalue to a precision below 10^{-4}. For the choice of η near the diquark propagator pole two more Chebyshev moments are needed to arrive at the same precision. Furthermore the results demonstrate that in order to obtain an η-independent eigenvalue, the *full* dependence of the scalar functions S_i, $\hat{S}_i$ on the angle $z = \cos\Theta$ has to be taken into account, *i.e.* η-invariance is not guaranteed for an arbitrary truncation in the Chebyshev expansion.

In the determination of observables the explicit solutions for wave or vertex function enter. We will therefore have a look at their convergence properties as well. The Chebyshev moments of the scalar functions S_1 and S_2 building the *vertex function* show a very similar convergence pattern for the different choices of η. Each subsequent moment drops in its magnitude by a factor of 7 ... 10 as compared to the magnitude of the previous one. The situation is completely different for the Chebyshev moments of $\hat{S}_1$ and $\hat{S}_2$, making up the *wave function*. This is depicted in figure 2.6. Whereas the convergence for the choice of $\eta = 0.4$ is still reasonably rapid (a factor of 10 between the subsequent even Chebyshev momenta), the moments of $\hat{S}_1$ for the choice $\eta = 0.31$ become squeezed in momentum space and only converge slowly with increasing Chebyshev order.

In the calculation of form factors we will need *both* wave and vertex function, depending on the diagrams to compute. The slow convergence of the wave function expansion will put certain restrictions on the numerical accuracy whenever the respective scalar functions are employed.

Electromagnetic Properties

In the following we will quote from ref. [23] some results for electric form factors, electric radii and magnetic moments which have been obtained with the parameter sets of table 2.5. The definitions for the current operator, the form factors and radii are collected in chapter 3. The necessary formalism for calculating the appropriate current matrix elements is also presented there, along with the proof of current conservation. Presenting the results at this point will exhibit the shortcomings of the scalar diquark sector and furthermore motivates the choice of the dipole form for $V(x)$ in the calculations with scalar and axialvector diquarks.

In table 2.7 we have compiled the results for the proton and neutron charge radii as well as for the nucleon magnetic moments. A first glance at the proton charge radius confirms that fixing the width of the dominant scalar function S_1^0 of the nucleon-quark-diquark vertex function fixes roughly this radius as well. But whereas all parameter sets show for the proton charge radius a maximal deviation of about 15 % to the experimental value, the results for the neutron charge radius

	Form of diquark vertex $V(x)$	r_p (fm)	r_n^2 (fm^2)	μ_p	μ_n
fixed $S_{1,0}$-width :	$n = 1$	0.78	-0.17	0.95	-0.80
	$n = 2$	0.82	-0.14	1.09	-0.93
	$n = 4$	0.84	-0.12	1.13	-0.97
	exp	0.83	-0.04	1.16	-1.00
	gauss	0.92	0.01	1.22	-1.07
fixed masses:	$n = 1$	0.97	-0.24	0.98	-0.86
	$n = 2$	0.82	-0.14	1.09	-0.93
	$n = 4$	0.75	-0.03	1.12	-0.95
	exp	0.73	-0.01	1.13	-0.96
experiment		0.84	-0.11	2.79	-1.91

Table 2.7: Electric radii of proton/neutron and the nucleon magnetic moments for the parameter sets having either the S_1^0-width or the quark mass fixed.

differ drastically. The dipole and the quadrupole form for $V(x)$ are here closest to the observed radius.

We have plotted the nucleon electric form factors up to a momentum transfer of $Q^2 = 2.25$ GeV^2 in figure 2.7. The proton form factor (left panel) has been normalized to the phenomenological dipole fit

$$G_E^{\text{phen}} = \frac{1}{\left(1 + Q^2/(0.71 \text{ GeV}^2)\right)^2} \, , \qquad (2.159)$$

which represents for momentum transfer below 1 GeV^2 a quite accurate description of the experimentally measured G_E [60]. Here the results for the parameter set employing the dipole shape for $V(x)$ follows the phenomenological dipole closest as compared to the other curves. Therefore we employ the dipole in the diquark vertex for further calculations. Regarding the overall shape of the neutron form factor, only the Gaussian parametrization for $V(x)$ produces results grossly deviating from the scarce experimental information one has about this quantity. A discussion of the available experimental results is postponed until section 3.2.2.

Returning to the discussion of the results in table 2.7, we see that the proton and neutron magnetic moments are (i) much too small and (ii) their ratio is far from the experimentally measured value. Both defects are known from exploratory studies within other forms of quark-scalar diquark models [62] and can
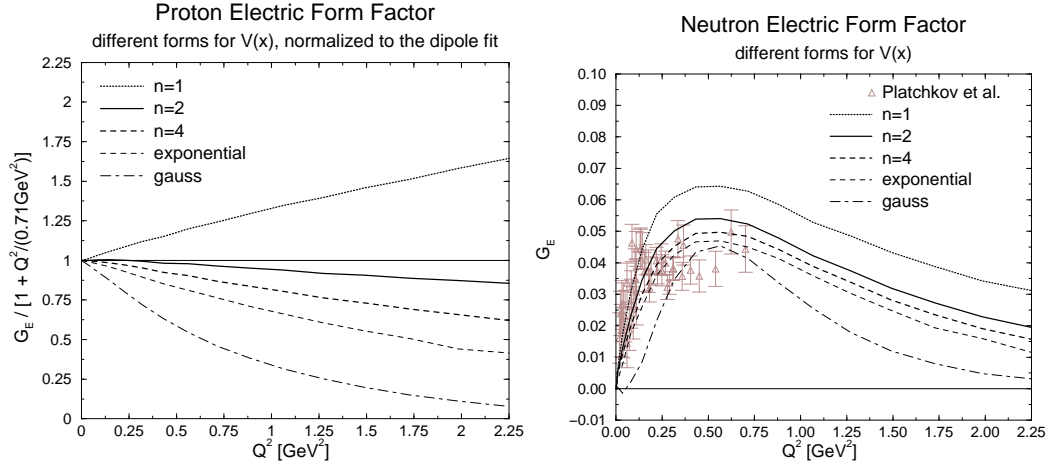
Figure 2.7: Proton (left panel) and neutron (right panel) electric form factors for the various parameter sets with fixed width of the zeroth Chebyshev moment S_1. The experimental data for the neutron is taken form ref. [61].

be attributed to the oversimplification of the two-quark correlations to just the propagation of a spinless scalar diquark that cannot exhibit a spin flip when struck by a photon. The problem is furthermore enhanced by the comparatively large values of the constituent quark mass in all parameter sets. Remember that the main indication for a quark mass scale of around 0.3 GeV comes from a non-relativistic estimate of the nucleon magnetic moments. According to this argument, the nucleon magnetic moments are proportional to M_n/m_q and thus quark masses being larger than 0.5 GeV are expected to yield magnetic moments that are far too small.

Although the results on the electromagnetic properties have been reported at this stage without derivation, we regard the previously unspecified form of the diquark vertex as being fixed now by the dipole form. With the ingredients of the model being complete, we present in the next subsection solutions for nucleon and Δ using the scalar and the axialvector diquark channel.

2.5.3 Solutions II: Scalar and axialvector diquarks

Including axialvector diquarks, the Bethe-Salpeter equations can now be solved for nucleon and Δ. The full decomposition of wave and vertex functions, shown in table 2.3 for the nucleon and in table 2.4 for the Δ, has to be taken into account and the equations are solved for the eight scalar functions that describe vertex and wave function respectively. Altogether there are four parameters: the quark mass m_q, the diquark masses m_{sc} and m_{ax}, and the width λ of the dipole-shaped

Set	m_q [GeV]	m_{sc} [GeV]	m_{ax} [GeV]	λ [GeV]	g_s	g_a	M_Δ [GeV]	M_n [GeV]
I	0.36	0.625	0.684	0.95	9.29	6.97	1.007	0.939
II	0.425	0.598	0.831	0.53	22.10	6.37	1.232	0.939

Table 2.8: The two parameter sets of the full model together with the values of diquark normalizations (couplings) and the bound masses M_n, M_Δ that arise for these sets.

diquark-quark vertex.

The solutions in the scalar diquark sector suffered from the large constituent quark masses that set a wrong scale within the nucleon, as seen by the results for the magnetic moments. The inclusion of the attractive axialvector diquark channel now allows for solutions with smaller quark masses and smaller binding energy for the scalar diquark. The diquark normalization (or coupling) constant g_s drops for this reason and therefore the nucleon binding energy becomes smaller in the scalar channel, but the additional binding provided by the axialvector diquark compensates this effect to yield the physical nucleon mass.

In the calculations presented here and in the following chapters we shall illustrate the consequences of the model assumptions with two different parameter sets which emphasize slightly different aspects. For Set I, we employ a constituent quark mass of $m_q = 0.36$ GeV which is close to the values commonly used by non- or semi-relativistic constituent quark models. Due to the free-particle poles in the bare quark and diquark propagators, the axialvector diquark mass is below 0.72 GeV and the delta mass below 1.08 GeV. On the other hand, nucleon *and* delta masses are fitted by Set II, *i.e.* the parameter space is constrained by these two masses. In particular, this implies $m_q > 0.41$ GeV. Both parameter sets together with the corresponding values resulting for the effective diquark couplings and baryon masses are given in table 2.8.

Two differences between the two sets are important in the following: The strength of the axialvector correlations within the nucleon is rather weak for Set II, as the ratio of axialvector to scalar diquark normalization (coupling), $g_a/g_s = 0.29$, is much smaller than for Set I where $g_a/g_s = 0.75$. We will quantify the correlation strength more precisely when assessing the contributions of scalar and axialvector correlations to the normalization of the nucleon, *cf.* section 3.2.2. Secondly, the 15 % difference between the constituent quark masses of the two sets will have an influence on the results for magnetic moments that is even stronger than could be expected from the non-relativistic argument.
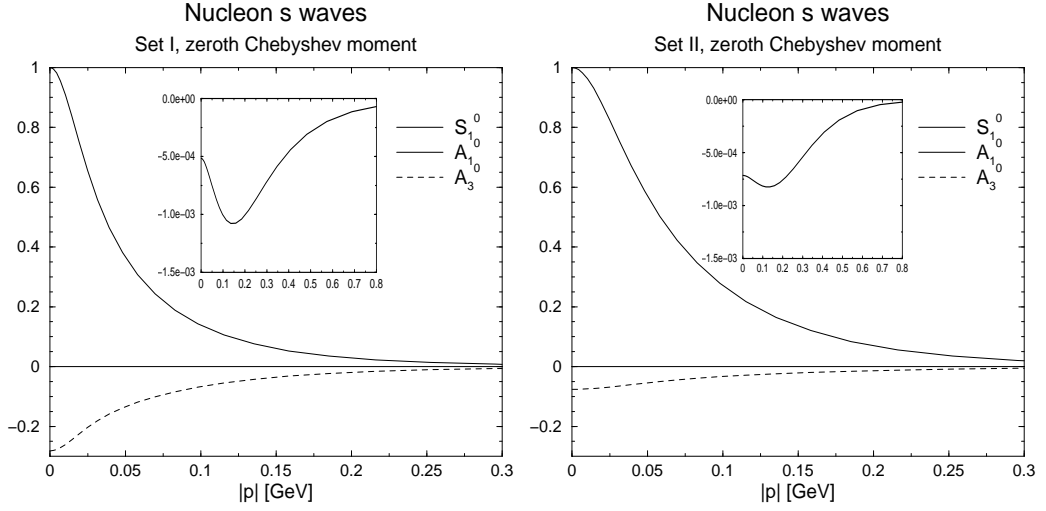
Figure 2.8: The leading Chebyshev moments of the functions $\hat{S}_1$, $\hat{A}_1$ and $\hat{A}_3$ related to the nucleon s waves. All functions are normalized by the condition $\hat{S}_1^0 = 1$.

Although the wave and the vertex function are no physical observables they do enter observable matrix elements via Mandelstam's formalism [63] (to be described in the next chapter) and therefore the strengths of the single components give a hint on their effect on observables. We have plotted the leading Chebyshev moments of the scalar functions describing the nucleon s waves in figure 2.8. These are $\hat{S}_1^0$ and $\hat{A}_3^0$, describing the s waves for scalar and axialvector diquark and $\hat{A}_1^0$ that is connected with the virtual time component of the latter. We see for both sets that the functions $\hat{A}_1^0$ are suppressed by a factor of 10^3 compared to the dominating $\hat{S}_1^0$. The strength of the other s wave associated with the axialvector diquark is roughly proportional to the ratio g_a/g_s for the respective parameter set.

In appendix A.3 the nucleon partial waves for Set I and the Δ partial waves for Set II (here the Δ bound state mass corresponds to the physical one) are shown and discussed. In summary, all the remarks from the previous subsection on the numerical accuracy and the convergence properties for wave and vertex functions apply also in the case of the full model. Especially for Set II, the Δ is an extremely weakly bound state and thus the Chebyshev expansion for the wave function converges quite slowly.

Before we turn to the detailed discussion of the nucleon electromagnetic properties we will sum up the results obtained so far. From a physical point of view, the parameters of the model could be chosen more intuitively after having included the axialvector diquark sector of the model. This especially applies to the value of the constituent quark mass which appeared to be rather large in the scalar di-

quark sector. Still, the inclusion of the Δ resonance leads to rather large quark and axialvector diquark masses and consequently small axialvector correlations in the nucleon. This is an artefact of employing free quark and diquark propagators, therefore we will discuss appropriate modifications which mimic confinement later in chapter 5.

From a technical point of view, we have succeeded to transform the full 4-dimensional problem into a manageable form. The chosen expansion in Dirac space into partial waves has been done covariantly and the results for the partial wave strengths identify the leading and subleading components. The Chebyshev expansion for the scalar functions which describe the partial wave strengths has proved to be quite efficient and accurate, furthermore the expansion has been done for a Lorentz invariant variable, $z = \hat{p} \cdot \hat{P}$, with the consequence that the boost of the wave and vertex function solutions is rendered feasible. A similar method for treating mesons in a Bethe-Salpeter approach has been put forward in refs. [64, 65] where the efficacy of this technique has been demonstrated for the solution of the Bethe-Salpeter equations as well as in calculations of mesonic observables.

As a conclusion, there is no technical reason why one should stick to some kind of non-relativistic approximation in solving a ladder Bethe-Salpeter equation. Such an approximation could only be justified in a *very* weak binding situation and results for physical observables should depend in a controlled manner on the non-relativistic truncation. We investigate this issue in chapter 6 for the case of the diquark-quark model where we compare results for vertex function solutions and observables obtained (i) with the exact treatment and (ii) in the Salpeter approximation [66], a popular semi-relativistic approximation of the Bethe-Salpeter equation. We find that the Salpeter approximation strongly violates the approximate $O(4)$ symmetry present in the solutions of the full Bethe-Salpeter equation and observables obtained with both methods deviate in a rather unpredictable manner.

Chapter 3

Electromagnetic Form Factors

Electromagnetic form factors describe one of the most basic dynamic observables of a composite system: the elastic scattering of an electron on the composite target. Electron and target interact with each other by exchanging quanta of the electromagnetic field. For the target being a nucleon, the scattering is from a classical point of view a function of the charge and magnetization distributions within the target which interact with charge and spin of the electron, respectively. The Sachs form factors G_E and G_M, to be introduced in eqs. (3.4,3.5), describe in the Breit system exactly the Fourier transforms of these distributions [67]. In the usual field theoretical treatment it is justified to assume that the scattering is mediated by one virtual photon (due to the smallness of the coupling constant in quantum electrodynamics), thereby the information on the electromagnetic structure of the probe is contained in the following matrix element, defined in momentum space,

$$\langle J^\mu \rangle (Q) = \langle \text{target}; \, P_f | \, J^\mu \, | \text{target}; \, P_i \rangle (Q) \,, \tag{3.1}$$

where initial and final target state possess on-shell four-momenta $P_i = P - Q/2$ and $P_f = P + Q/2$, respectively. The current operator J^μ is obtained from a suitable model Lagrangian where it is the coefficient of the linear term in A^μ, the electromagnetic vector potential. For nucleon targets the matrix element is written in the most general form as

$$\langle J^\mu \rangle = \bar{u}_{\sigma_f}(P_f) \left[-i\gamma^\mu \mathcal{F}_1 + \frac{i\kappa \mathcal{F}_2}{2M_n} \sigma^{\mu\nu} Q^\nu \right] u_{\sigma_i}(P_i) \,. \tag{3.2}$$

Here, $\mathcal{F}_1$ and $\mathcal{F}_2$ are the Dirac charge and the Pauli anomalous magnetic form factor, respectively. The constant κ describes the anomalous magnetic moment. No further independent structures exist if the current is assumed to transform like a vector under parity transformations and if current conservation,

$$Q^\mu \langle J^\mu \rangle = 0 \,, \tag{3.3}$$

is to hold [68]. The Sachs form factors G_E and G_M are introduced as

$$G_E = \mathcal{F}_1 - \frac{Q^2}{4M^2}\kappa\mathcal{F}_2 \,, \tag{3.4}$$

$$G_M = \mathcal{F}_1 + \kappa\mathcal{F}_2 \,. \tag{3.5}$$

By definition, the values of G_E and G_M at zero momentum transfer are the nucleon charge and magnetic moments.

It is convenient in the following to introduce matrix elements which are themselves matrix valued due to summations over initial and final spin,

$$\langle P_f| \, J^\mu \, |P_i\rangle := \sum_{\sigma_f,\sigma_i} u_{\sigma_f}(P_f) \, \langle J^\mu\rangle \, \bar{u}_{\sigma_i}(P_i) \,, \tag{3.6}$$

to remove the nucleon spinors in the parametrization of $\langle J^\mu\rangle$. Using the Gordon identities [68], this matrix element is written in terms of G_E and G_M as

$$\langle P_f| \, J^\mu \, |P_i\rangle = -i\Lambda^+(P_f) \left[\gamma^\mu G_M + iM\frac{P^\mu}{P^2}(G_E - G_M)\right]\Lambda^+(P_i) \,. \tag{3.7}$$

The form factors can be extracted from this expression by taking traces as follows,

$$G_E(Q^2) = \frac{M_n}{2P^2}\,\mathrm{Tr}\,\langle P_f| \, J^\mu \, |P_i\rangle P^\mu \,, \tag{3.8}$$

$$G_M(Q^2) = \frac{iM_n^2}{Q^2}\,\mathrm{Tr}\,\langle P_f| \, J^\mu \, |P_i\rangle(\gamma^\mu)_T \,, \qquad \left((\gamma^\mu)_T = \gamma^\mu - \hat{P}^\mu\hat{P}\!\!\!/\right) \,. \tag{3.9}$$

This little introductory exercise provided us with the necessary formulae to obtain the form factors from the nucleon current matrix element. The more formidable task is to construct a suitable current operator for the diquark-quark model and to give a prescription how to obtain nucleon matrix elements from the current operator and the solutions of the Bethe-Salpeter equation. The current operator should respect gauge invariance and consequently the condition (3.3), *i.e.* current conservation, should hold.

The following section aims at constructing the current operator. This amounts to clarify how the photon couples to the full quark-diquark propagator $G^{\mathrm{q-dq}}$ given in eq. (2.70), the 4-point function for quark and diquark in the channel with nucleon quantum numbers. The resulting 5-point function has to fulfill a Ward-Takahashi identity which in turn guarantees that for the current matrix elements current conservation holds. Thereby we find non-trivial irreducible couplings of the photon to the diquark-quark vertices χ^5 and χ^μ, the *seagull vertices*, besides the expected photon couplings to quark and diquark. In total we will find that the nucleon current operator consists of

- the photon coupling to quark and diquark (*impulse approximation*),

- the photon-mediated transitions from scalar to axialvector diquarks and the reverse transition (*extended impulse approximation*) and

- contributions from the quark exchange kernel which contains the couplings to the exchange quark and the seagull couplings to the diquark-quark vertices.

Unknown constants like the anomalous magnetic moment of the axialvector diquark and the strength of the scalar-axialvector transitions will be calculated by taking into account the diquark substructure in a first approximation which does not violate gauge invariance for the nucleon current.

The construction of the current operator by using Ward-Takahashi identities provides us furthermore with a proof of the equivalence of the canonical normalization condition for Bethe-Salpeter wave function with the normalization to correct bound state charge. The canonical normalization amounts to fixing the residue of the bound state pole in the full propagator $G^{\mathrm{q-dq}}$.

Equipped with the explicit form of the current operator we will then proceed by calculating the form factors for the two parameter sets introduced in section 2.5.3. We find that current conservation is reflected in the numerical solutions very accurately. The electric form factors of proton and neutron are described very well by our solutions whereas the magnetic form factors fall short by some 15 %, due to our simplified assumptions for the quark and diquark propagators. An interesting point is that the recent experimental data on the ratio G_E/G_M for the proton [69] strongly constrains the axialvector correlations in the nucleon to be rather moderate. We will conclude this chapter by discussing possible further improvements.

3.1 The nucleon current operator in the diquark-quark model

We shall make use of the "gauging of equations" formalism outlined in refs. [70, 71, 72]. To simplify the treatment, we will derive the current operator by assuming that the diquark quasiparticle could in principle be represented by a diquark creation operator $d^{\dagger} = \left(d_s^{\dagger}, d_a^{\mu\dagger}\right)$ which creates scalar and axialvector diquarks. The resulting expressions are equivalent to the results when constructing the current operator by starting from the 3-quark problem, provided a Ward identity for the diquark propagator holds (*cf.* refs. [72, 73]).

We employ a notation for Green's functions as in section 2.1. We remind that their multiplication is to be understood symbolically and involves summation over

Dirac indices and integration over the relative momenta as in eq. (2.6). We assume that, in contrast to eq. (2.70), the quark-diquark propagator in the nucleon channel

$$(2\pi)^4\delta^4(k_q + k_d - p_q - p_d)\, G^{\mathrm{q-dq}}(k_q, k_d; p_q, p_d) = \qquad (3.10)$$
$$\mathrm{F.T.}\ \langle 0|\, Tq(x_{k_q})d(y_{k_d})\, \bar{q}(x_{p_q})d^\dagger(y_{p_d})\, |0\rangle$$

is given as a matrix that describes the propagation of charge eigenstate combinations of quarks u, d and scalar diquark (ud) / axialvector diquarks $[uu]$, $[ud]$, $[dd]$, *cf.* appendix A.2.1. The part described by the free quark and diquark propagators is of course diagonal in the charge eigenstates whereas the possible (multiple) quark exchange describes transitions between them. Likewise the 5-point function is defined to be

$$G^\mu(k_q, k_d; p_q, p_d) = \mathrm{F.T.}\ \langle 0|\, Tq(x_{k_q})d(y_{k_d})\, \bar{q}(x_{p_q})d^\dagger(y_{p_d})\, J^\mu(0)\, |0\rangle\ . \quad (3.11)$$

We fix momentum conservation by $k_q + k_d = p_q + p_d + Q$, where Q denotes the photon momentum. It is evident from the application of Wick's theorem to this equation that G^μ contains (at least) all diagrams that can be constructed from G by attaching a photon to all propagators (like $\langle 0|\, Tq\bar{q}\, |0\rangle$) and vertices (like the diquark-quark vertices $\langle 0|\, Td\,\bar{q}\bar{q}\, |0\rangle$). An equivalent definition of G^μ expresses the procedure of attaching photons on propagators and vertices by a functional derivative,

$$G^\mu(k_q, k_d; p_q, p_d) = -\frac{\delta}{\delta A^\mu(0)}$$
$$\mathrm{F.T.}\ \langle 0|\, Tq(x_{k_q})d(y_{k_d})\, \bar{q}(x_{p_q})d^\dagger(y_{p_d})\exp\left(-\int d^4x\, J^\mu(x)A^\mu(x)\right)\, |0\rangle\big|_{A^\mu=0}\ . \ (3.12)$$

"Gauging" is an operation which achieves the same result by the following simple rules [70]:

1. Notation: $F^\mu = -\dfrac{\delta}{\delta A^\mu(0)}\, F_A\bigg|_{A^\mu=0}$ where

   $F = \mathrm{F.T.}\ \langle 0|\, q(x_1)\ldots\bar{q}(y_1)\ldots\ldots|0\rangle$ and
   $F_A = \mathrm{F.T.}\ \langle 0|\, q(x_1)\ldots\bar{q}(y_1)\ldots\exp\left(-\int d^4x\, J^\mu(x)A^\mu(x)\right)\, |0\rangle.$

2. It is a linear operation, and for a constant c its action yields zero, $c^\mu = 0$.

3. It fulfills Leibniz' rule, $(F_1 F_2)^\mu = F_1^\mu F_2 + F_1 F_2^\mu$.

4. Gauging the inverse, F^{-1}, is accomplished by applying rule 2 and 3, *i.e.* $(F^{-1}F)^\mu = 0 \rightarrow (F^{-1})^\mu = -F^{-1}F^\mu F^{-1}$.

Besides the above mentioned contributions to G^μ from attaching photons to propagators and diquark-quark vertices (which are obtained by gauging $G^{\mathrm{q-dq}}$), there exist other contributions that cannot be obtained this way: Although a transition from scalar to axialvector diquark cannot occur, $\langle 0 | \, T d_a^\nu \, d_s^\dagger \, | 0 \rangle = 0$, this transition is possible if mediated by a photon, $\langle 0 | \, T d_a^\nu \, d_s^\dagger J^\mu \, | 0 \rangle_{\mathrm{irred}} \neq 0$. The special feature of this scalar-to-axialvector transition is that it satisfies gauge invariance on its own, *i.e.* its contribution vanishes upon contraction with Q^μ.

We know from gauge invariance that the five-point function G^μ must obey a Ward-Takahashi identity,

$$Q^\mu G^\mu(k_q, k_d; p_q, p_d) =$$
$$q_{q_f} G^{\mathrm{q-dq}}(k_q - Q, k_d; p_q, p_d) + q_{d_f} G^{\mathrm{q-dq}}(k_q, k_d - Q; p_q, p_d) -$$
$$q_{q_i} G^{\mathrm{q-dq}}(k_q, k_d; p_q + Q, p_d) - q_{d_i} G^{\mathrm{q-dq}}(k_q, k_d; p_q, p_d + Q) \,. \qquad (3.13)$$

The charges $q_{q_f[q_i]}$ refer to the quark charges in the final [initial] state, likewise $q_{d_f[d_i]}$ refer to the respective diquark charges. The notation is somewhat sloppy, since $G^{\mathrm{q-dq}}$ is a matrix that describes the propagation between the different charge eigenstates of quark and diquark. Therefore, eq. (3.13) is to be understood *for each matrix element* of $G^{\mathrm{q-dq}}$.

We will show that gauging $G^{\mathrm{q-dq}}$ leads to a G^μ that fulfills the Ward-Takahashi identity (3.13). First, we fix some notation for the basic quark and diquark vertices. Defining $-(S^{-1})^\mu = \Gamma_q^\mu$ to be the quark-photon vertex, we find for the gauged quark propagator,

$$S^\mu(k_q; p_q) := S(k_q) \, \Gamma_q^\mu \, S(p_q) \,. \qquad (3.14)$$

The Ward-Takahashi identity for it reads

$$Q^\mu S^\mu(k_q; p_q) = q_q \left(S(k_q - Q) - S(p_q + Q) \right) \,. \qquad (3.15)$$

In the same manner we gauge the diquark propagator, given by eq. (2.67), and write its Ward-Takahashi identity as

$$\tilde{D}^\mu(k_d; p_d) \;\; := \;\; \tilde{D}(k_d) \, \Gamma_{dq}^\mu \, \tilde{D}(p_d) \qquad\qquad (3.16)$$
$$= \;\; \begin{pmatrix} D(k_d) & 0 \\ 0 & D^{\alpha\alpha'}(k_d) \end{pmatrix} \begin{pmatrix} \Gamma_{sc}^\mu & 0 \\ 0 & \Gamma_{ax}^{\mu,\alpha'\beta'} \end{pmatrix} \begin{pmatrix} D(p_d) & 0 \\ 0 & D^{\beta'\beta}(p_d) \end{pmatrix}$$
$$Q^\mu \tilde{D}^\mu(k_d; p_d) \;\; = \;\; \begin{pmatrix} q_{sc} & 0 \\ 0 & q_{ax} \end{pmatrix} \left(\tilde{D}(k_d - Q) - \tilde{D}(p_d + Q) \right) \,, \qquad (3.17)$$

where we have introduced the photon vertex with the scalar diquark, Γ_{sc}^μ and the vertex with the axialvector diquark, $\Gamma_{ax}^{\mu,\alpha\beta}$. For the gauged free quark-diquark

propagator we obtain after applying Leibniz' rule,

$$(G_0^{\text{q}-\text{dq}})^\mu := G_0^{\text{q}-\text{dq}} \, \Gamma_0^\mu \, G_0^{\text{q}-\text{dq}} \, , \qquad (3.18)$$

$$\Gamma_0^\mu = \Gamma_q^\mu \, \tilde{D}^{-1} + S^{-1} \, \Gamma_{dq}^\mu \, . \qquad (3.19)$$

The rules 2 and 3 can now be applied to the *inhomogeneous* quark-diquark Bethe-Salpeter equation in order to find G^μ,[1]

$$G^{\text{q}-\text{dq}} = G_0^{\text{q}-\text{dq}} + G_0^{\text{q}-\text{dq}} \, K^{\text{BS}} \, G^{\text{q}-\text{dq}} \, . \qquad (3.20)$$

After simple algebraic manipulations using the above equation we find

$$G^\mu = (G_0^{\text{q}-\text{dq}})^\mu + \left(G_0^{\text{q}-\text{dq}} \, K^{\text{BS}} \, G^{\text{q}-\text{dq}} \right)^\mu \, , \qquad (3.21)$$

$$= G^{\text{q}-\text{dq}} \left(\Gamma_0^\mu + (K^{\text{BS}})^\mu \right) G^{\text{q}-\text{dq}} \, . \qquad (3.22)$$

Since the Ward-Takahashi identities for the free diquark and quark vertices hold, eqs. (3.15,3.17), a Ward-Takahashi identity for Γ_0^μ follows trivially. Now we consider: *if* the following identity for $(K^{\text{BS}})^\mu$ holds,

$$Q^\mu (K^{\text{BS}})^\mu (k_q, k_d; p_q, p_d) =$$
$$q_{q_f} K^{\text{BS}}(k_q - Q, k_d; p_q, p_d) + q_{d_f} K^{\text{BS}}(k_q, k_d - Q; p_q, p_d) -$$
$$q_{q_i} K^{\text{BS}}(k_q, k_d; p_q + Q, p_d) - q_{d_i} K^{\text{BS}}(k_q, k_d; p_q, p_d + Q) \, , \qquad (3.23)$$

then the identity

$$Q^\mu \left(\Gamma_0^\mu + (K^{\text{BS}})^\mu \right) =$$
$$q_{q_i} (G^{\text{q}-\text{dq}})^{-1}(k_q, k_d; p_q + Q, p_d) + q_{d_i} (G^{\text{q}-\text{dq}})^{-1}(k_q, k_d; p_q, p_d + Q) -$$
$$q_{q_f} (G^{\text{q}-\text{dq}})^{-1}(k_q - Q, k_d; p_q, p_d) - q_{d_f} (G^{\text{q}-\text{dq}})^{-1}(k_q, k_d - Q; p_q, p_d) \quad (3.24)$$

is valid, as can be inferred from eq. (3.22) and $(G^{\text{q}-\text{dq}})^{-1} = (G_0^{\text{q}-\text{dq}})^{-1} - K^{\text{BS}}$, eq. (2.70). The Ward-Takahashi identity for G^μ itself, eq. (3.13), follows immediately after left and right multiplication with $G^{\text{q}-\text{dq}}$. Indeed, eq. (3.23) which we will call the Ward-Takahashi identity for the quark exchange kernel is derived from a Ward-Takahashi identity[2] for $(G_0^{\text{q}-\text{dq}} K^{\text{BS}} G_0^{\text{q}-\text{dq}})^\mu$ and eqs. (3.15,3.17). Therefore we have established eq. (3.13).

Matrix elements of the current between bound states are obtained from the expression for G^μ, eq. (3.22). The full quark-diquark propagator, which sandwiches

---

[1]As for $G^{\text{q}-\text{dq}}$, the kernel K^{BS} has not exactly the form as given in eq. (2.72) but is rather written as a larger matrix describing the quark exchange between all charge eigenstate combinations of quark and diquark.

[2]Any perturbative graph with external legs and an external photon can be shown to fulfill a corresponding Ward-Takahashi identity.

the full vertex $\Gamma_0^\mu + (K^{\mathrm{BS}})^\mu$, can be approximated at the nucleon bound state pole by

$$G^{\mathrm{q-dq}} \sim \frac{\Psi \left(i\slashed{P} - M_n\right) \bar{\Psi}}{P^2 + M_n^2} + \text{regular terms} \tag{3.25}$$

as will be shown in the beginning of section 3.1.3. Inserted into eq. (3.22), we find for the current matrix element (the residue term of the leading pole)

$$\langle P_f| \, J^\mu \, |P_i\rangle = \bar{\Psi}_f \, \left(\Gamma_0^\mu + (K^{\mathrm{BS}})^\mu\right) \, \Psi_i \,. \tag{3.26}$$

This expression describes how to obtain bound state matrix elements from its Bethe-Salpeter wave function and is usually referred to as *Mandelstam's formalism* [63] although in the original paper only contributions in impulse approximation have been discussed.

   When contracting eq. (3.26) with Q^μ, we can use the Ward-Takahashi identity (3.24). Current conservation, $Q^\mu\langle P_f| \, J^\mu \, |P_i\rangle = 0$, follows immediately upon using the Bethe-Salpeter equations

$$(G^{\mathrm{q-dq}})^{-1} \, \Psi = \bar{\Psi} \, (G^{\mathrm{q-dq}})^{-1} = 0 \,. \tag{3.27}$$

We have arrived at an important point in this chapter. The nucleon current defined in eq. (3.26) above is conserved. To guarantee gauge invariance, we must include in the definition of the current operator the gauged Bethe-Salpeter kernel $(K^{\mathrm{BS}})^\mu$ besides the photon coupling to the free propagators Γ_0^μ. The latter contribution is commonly referred to as the *impulse approximation*. Incidentally, the necessity of including current contributions from the Bethe-Salpeter kernel for a gauge invariant matrix element was first discussed in ref. [74] in a deuteron bound state equation where the binding is provided by meson exchange.

   We turn now to the construction of explicit expressions for the current operator in impulse approximation, Γ_0^μ, and the gauged kernel $(K^{\mathrm{BS}})^\mu$.

3.1.1   Impulse approximation

Let us specify the electromagnetic vertices of the basic constituents, quark and diquark. For the quark-photon vertex, we employ the perturbative expression as the model propagator in eq. (2.64) is the tree-level one,

$$\Gamma_q^\mu = -iq_q\gamma^\mu \,. \tag{3.28}$$

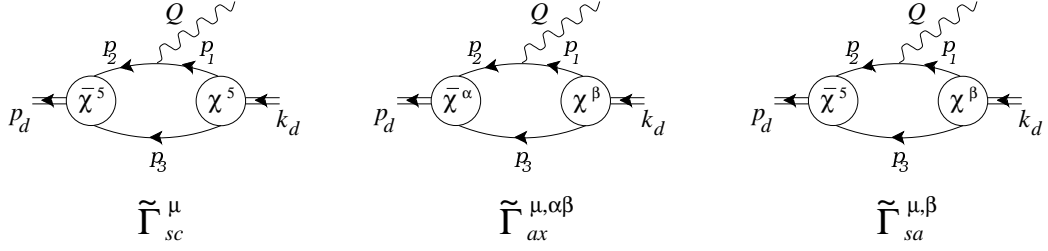Of course it satisfies the corresponding Ward identity (3.15).

Figure 3.1: Resolved vertices: photon-scalar diquark, photon-axialvector diquark and anomalous scalar-axialvector diquark transition.

The diquark propagators are the ones of a free spin-0 and spin-1 particle, therefore we also employ the corresponding free vertices

$$\Gamma^{\mu}_{dq} = \begin{pmatrix} \Gamma^{\mu}_{sc} & 0 \\ 0 & \Gamma^{\mu,\alpha\beta}_{ax} \end{pmatrix} , \tag{3.29}$$

$$\Gamma^{\mu}_{sc} = -q_{sc} \, (k_d + p_d)^{\mu} , \tag{3.30}$$

$$\Gamma^{\mu,\alpha\beta}_{ax} = q_{ax} \left(-(p_d + k_d)^{\mu} \, \delta^{\alpha\beta} + (p_d^{\alpha} - \xi \, k_d^{\alpha}) \, \delta^{\mu\beta} + (k_d^{\beta} - \xi \, p_d^{\beta}) \, \delta^{\mu\alpha} + \right.$$
$$\left. \kappa \, (Q^{\beta} \, \delta^{\mu\alpha} - Q^{\alpha} \, \delta^{\mu\beta}) \right) . \tag{3.31}$$

As the spin-1 vertex is not necessarily textbook material, we refer to ref. [75] for its derivation. The constant κ which appears in eq. (3.31) denotes a possible anomalous magnetic moment of the axialvector diquark. We obtain its value from a calculation for vanishing momentum transfer ($Q^2 = 0$) in which the quark substructure of the diquarks is resolved, *i.e.* in which a (soft) photon couples to the quarks within the diquarks, *cf.* the second graph in figure 3.1. The calculation of κ is provided in appendix B.1.1. Although the parameters presented in table 2.8 differ for the two sets, especially the diquark width parameter λ, we obtain in both cases $\kappa = 1.0$ (*cf.* table B.1 in appendix B.1.1). This might seem understandable from nonrelativistic intuition: the magnetic moments of two quarks with charges q_1 and q_2 add up to $(q_1 + q_2)/m_q$, the magnetic moment of the axialvector diquark is $(1 + \kappa)(q_1 + q_2)/m_{ax}$ and if the axialvector diquark is weakly bound, $m_{ax} \simeq 2m_q$, then $\kappa \simeq 1$.

As already mentioned, there is one contribution to the current which cannot be obtained by the gauging method: photon-induced anomalous[3] transitions from a scalar to axialvector diquark and *vice versa*. The corresponding vertex describing

---

[3]If the product of the parity eigenvalues π_i of the three particles at some vertex that describes their interaction is (-1) we call the vertex *anomalous*. For the scalar-axialvector transitions, we have $\pi_\gamma = \pi_{sc} = -\pi_{ax} = 1$, thus the corresponding vertex is anomalous.

the transition from axialvector (with index β) to scalar diquark must have the form

$$\hat{\Gamma}^{\mu\beta}_{sa} = -i\frac{\kappa_{sa}}{2M_n}\,\epsilon^{\mu\beta\rho\lambda}(p_d + k_d)^\rho Q^\lambda\;, \tag{3.32}$$

and that for the reverse transition from an scalar to axialvector (index α) is given by,

$$\hat{\Gamma}^{\mu\alpha}_{as} = i\frac{\kappa_{sa}}{2M_n}\,\epsilon^{\mu\alpha\rho\lambda}(p_d + k_d)^\rho Q^\lambda\;. \tag{3.33}$$

The tensor structure of these anomalous diagrams is derived in appendix B.1.1 by resolving the diquarks in a way as represented by the right diagram in figure 3.1. The explicit factor $1/M_n$ was introduced to isolate a dimensionless constant κ_{sa}. Its value is obtained roughly as $\kappa_{sa} \simeq 2.1$ (with the next digit depending on the parameter set, *cf.* table B.1). Since the only possible transition for nucleons involves the scalar (ud) diquark and the axialvector $[ud]$ diquark, there is only a constant charge (or flavor) factor in eqs. (3.32,3.33). It is $(q_d - q_u)/2 = -1/2$. We see immediately that nucleon current contributions using these vertices are transversal and thus do not affect current conservation.

The current operator associated with the anomalous transitions reads

$$\bar{\Psi}_f\,\Gamma^\mu_{\mathrm{sc-ax}}\,\Psi_i = w_{[ud]}\left(\langle J^\mu_{sa}\rangle^{\mathrm{sc-ax}} + \langle J^\mu_{as}\rangle^{\mathrm{ax-sc}}\right) \tag{3.34}$$

$$= w_{[ud]}\left(\begin{array}{cc}\bar{\Psi}^5 & \bar{\Psi}^\alpha\end{array}\right)\left(\begin{array}{cc}0 & S^{-1}\hat{\Gamma}^{\mu\beta}_{sa}\\ S^{-1}\hat{\Gamma}^{\mu\alpha}_{as} & 0\end{array}\right)\left(\begin{array}{c}\Psi^5\\ \Psi^\alpha\end{array}\right). \tag{3.35}$$

As for nucleons only the transition between scalar (ud) diquark and axialvector $[ud]$ diquark is possible, the flavor weight factor $w_{[ud]}$ for the strength of the $[ud]$ diquark correlations in the total axialvector correlations is included, *cf.* eqs. (A.18,A.20).

To conclude this subsection, we write down the explicit expressions for the proton and neutron current matrix elements in the extended impulse approximation,

$$\begin{aligned}{}_{\mathrm{p}}\langle P_f|\,J^\mu\,|P_i\rangle^{\mathrm{e-imp}}_{\mathrm{p}} &= \frac{2}{3}\langle J^\mu_q\rangle^{\mathrm{sc-sc}} + \frac{1}{3}\langle J^\mu_{sc}\rangle^{\mathrm{sc-sc}} + \langle J^\mu_{ax}\rangle^{\mathrm{ax-ax}} +\\ &\quad \frac{\sqrt{3}}{3}\left(\langle J^\mu_{sa}\rangle^{\mathrm{sc-ax}} + \langle J^\mu_{as}\rangle^{\mathrm{ax-sc}}\right)\;, \tag{3.36}\end{aligned}$$

$$\begin{aligned}{}_{\mathrm{n}}\langle P_f|\,J^\mu\,|P_i\rangle^{\mathrm{e-imp}}_{\mathrm{n}} &= -\frac{1}{3}\left(\langle J^\mu_q\rangle^{\mathrm{sc-sc}} - \langle J^\mu_q\rangle^{\mathrm{ax-ax}} - \langle J^\mu_{sc}\rangle^{\mathrm{sc-sc}} +\right.\\ &\quad \left.\langle J^\mu_{ax}\rangle^{\mathrm{ax-ax}}\right) - \frac{\sqrt{3}}{3}\left(\langle J^\mu_{sa}\rangle^{\mathrm{sc-ax}} + \langle J^\mu_{as}\rangle^{\mathrm{ax-sc}}\right).\tag{3.37}\end{aligned}$$

The superscript 'sc-sc' indicates that the current operator is to be sandwiched between scalar nucleon amplitudes for both the final and the initial state. Likewise
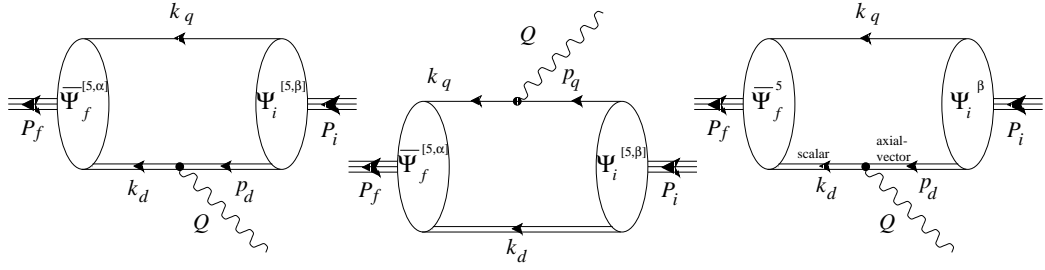
Figure 3.2: Impulse approximate contributions to the electromagnetic current. For the scalar-axialvector transition, a diagram analogous to the third one (with initial and final nucleon states interchanged) has to be computed.

'sc-ax' denotes current operators that are sandwiched between scalar amplitudes in the final and axialvector amplitudes in the initial state, *etc.* As an example we give

$$
\langle J_q^\mu \rangle^{\mathrm{ax-ax}} = \bar{\Psi}^\alpha \, (D^{-1})^{\alpha\beta} \, \hat{\Gamma}_q^\mu \, \Psi^\beta \qquad (\hat{\Gamma}_q^\mu = \Gamma_q^\mu / q_q) \tag{3.38}
$$

$$
= \int \frac{d^4 p}{(2\pi)^4} \bar{\Psi}^\alpha(P_f, p + (1-\eta)Q) \, (D^{-1})^{\alpha\beta}(k_d) \, \hat{\Gamma}_q^\mu \, \Psi^\beta(P_i, p) \, . \tag{3.39}
$$

The weight factors multiplying the single matrix elements arise from flavor algebra: we have chosen to define the matrix elements to be independent of the charge of the struck particle, *cf.* eq. (3.38). The nucleon is decomposed into its charge eigenstates of quark and diquark as in eqs. (A.18,A.20). Then the weight factors for the matrix elements are composed of the weight factors of the charge eigenstates and the charge of the struck quark or diquark.

We note that the axialvector amplitudes contribute to the proton current only in combination with diquark current couplings.

For visualization, the diagrams of the extended impulse approximation are shown in figure 3.2.

3.1.2   Seagulls

A matrix element of the quark exchange kernel (between charge eigenstates) is given by

$$
K_{ba}^{\mathrm{BS}} = -f_{ba} \, \chi^b(k_q, q) \, S^T(q) \, \bar{\chi}^a(q, p_q) \tag{3.40}
$$

cf. figure 3.3. The corresponding flavor factor which is unimportant in the following is given by f_{ba}. As in the actual solutions of the nucleon Bethe-Salpeter equation we have assumed that the diquark-quark vertices depend on just the relative

Figure 3.3: Left panel: The quark exchange kernel. Right panel: The seagull vertices. The charges belonging to the incoming and outgoing particles are enclosed in brackets, the other labels denote their momenta.

momentum between the two "participating" quarks, $\chi^a(k, p) \rightarrow \chi^a((k - p)/2)$. Gauging the kernel leads to three terms,

$$(K_{ba}^{\mathrm{BS}})^\mu = -f_{ba} \left[(M^b)^\mu \, S^T \, \bar{\chi}^a + \chi^b \, (S^\mu)^T \, \bar{\chi}^a + \chi^b \, S^T \, (\bar{M}^a)^\mu \right] . \qquad (3.41)$$

The gauged diquark-quark vertices χ^a and $\bar{\chi}^a$ are called $(M^a)^\mu$ and $(\bar{M}^a)^\mu$, respectively. These are the seagull vertices mentioned in the beginning of the chapter.

The Ward-Takahashi identity (3.23) which leads to a conserved nucleon current constrains the longitudinal part of the seagull vertices. Contracting (3.41) with Q^μ, inserting on the left hand side eq. (3.23) and using the Ward-Takahashi identity (3.15) for the gauged exchanged quark on the right hand side, we find

$$
\begin{aligned}
Q^\mu (M^a)^\mu (p_\alpha, p_\beta) \;\; &\overset{!}{=} \;\; q_\alpha \left[\chi^a(p_\alpha - Q, p_\beta) - \chi^a(p_\alpha, p_\beta) \right] + \\
&\qquad q_\beta \left[\chi^a(p_\alpha, p_\beta - Q) - \chi^a(p_\alpha, p_\beta) \right] \qquad (3.42) \\
&\qquad (\text{with} \quad p_d + Q = p_\alpha + p_\beta) \;, \\
Q^\mu (\bar{M}^a)^\mu (p_\alpha, p_\beta) \;\; &\overset{!}{=} \;\; -q_\alpha \left[\bar{\chi}^a(p_\alpha + Q, p_\beta) - \bar{\chi}^a(p_\alpha, p_\beta) \right] - \\
&\qquad q_\beta \left[\bar{\chi}^a(p_\alpha, p_\beta + Q) - \bar{\chi}^a(p_\alpha, p_\beta) \right] \qquad (3.43) \\
&\qquad (\text{with} \quad p_d - Q = p_\alpha + p_\beta) \;.
\end{aligned}
$$

The notation is explained in the right panel of figure 3.3. Of course, such constraints do not fix the seagull vertices completely. We choose a form which solves for this constraint and is regular in the limit $Q \rightarrow 0$. With $p = (p_\alpha - p_\beta)/2$ the

vertices read

$$
\begin{aligned}
(M^a)^\mu(p, Q; q_\alpha, q_\beta) &= q_\alpha \frac{(4p - Q)^\mu}{4p \cdot Q - Q^2} \left[\chi^a(p - Q/2) - \chi^a(p) \right] + \\
&\quad q_\beta \frac{(4p + Q)^\mu}{4p \cdot Q + Q^2} \left[\chi^a(p + Q/2) - \chi^a(p) \right] , \quad (3.44) \\
(\bar{M}^a)^\mu(p, Q; q_\alpha, q_\beta) &= -q_\alpha \frac{(4p - Q)^\mu}{4p \cdot Q - Q^2} \left[\chi^a(p + Q/2) - \chi^a(p) \right] + \\
&\quad -q_\beta \frac{(4p + Q)^\mu}{4p \cdot Q + Q^2} \left[\chi^a(p - Q/2) - \chi^a(p) \right] . \quad (3.45)
\end{aligned}
$$

In the limit $Q \to 0$ they simplify to

$$
(M^a)^\mu(p, 0; q_\alpha, q_\beta) = -\frac{1}{2} (q_\alpha - q_\beta) \, p^\mu \, \frac{d\,\chi^a}{d\,p^2} , \quad\quad\quad (3.46)
$$

$$
(\bar{M}^a)^\mu(p, 0; q_\alpha, q_\beta) = -\frac{1}{2} (q_\alpha - q_\beta) \, p^\mu \, \frac{d\,\bar{\chi}^a}{d\,p^2} . \quad\quad\quad (3.47)
$$

We add as a side remark that these seagull terms were derived a little bit differently in ref. [23]. There the Ward-Takahashi identity for the matrix element $\langle 0 | \, T q q \bar{q} \bar{q} J^\mu \, | 0 \rangle$ has been considered. Using the separable *ansatz* for the two-quark correlations, eq. (2.43), for expressions like $\langle 0 | \, T q q \bar{q} \bar{q} \, | 0 \rangle$, the constraints (3.42,3.43) have been derived under the assumption that the photon-diquark vertices contain no quark loop, *i.e.* they are given by the perturbative expressions (3.30,3.31). However, in the limit $Q \to 0$ the seagulls *must* have the form as in eqs. (3.46,3.47), as here the Ward-Takahashi identities reduce to the (differential) Ward identities which fix the vertices completely. In this kinematical situation a dressing quark loop in the photon-diquark vertices must yield the diquark charge (for an on-shell diquark).

Furthermore we note that seagull vertices of a similar kind were first considered in ref. [76]. The author discusses extended meson-baryon vertices and derives meson-baryon-photon vertices from a Lagrangian point of view by applying the minimal substitution rule.

For completeness we give the explicit expressions for the seagull and exchange quark contributions that are obtained when recombining the quark-diquark charge eigenstates to the correct nucleon flavor state. The symbolic matrix multiplications are to be understood as accompanied by an integration over the relative quark-diquark momenta in the initial and final states, respectively, and a summation over Dirac and Lorentz indices. First we write down the current term for

the proton that corresponds to the diagram in the lower right of figure 3.4,

$$\langle J^\mu_{sg} \rangle^{\text{proton}} = -\tfrac{1}{2} \left(\begin{array}{cc} \bar\Psi^5 & \bar\Psi^\alpha \end{array} \right) \left(\begin{array}{cc} K^\mu_{sg,ss} & K^\mu_{sg,sa} \\ K^\mu_{sg,as} & K^\mu_{sg,aa} \end{array} \right) \left(\begin{array}{c} \Psi^5 \\ \Psi^\beta \end{array} \right) , \tag{3.48}$$

$$K^\mu_{sg,ss} = (M^5)^\mu(p'_1, Q; q_u, q_d)\, S^T(q')\, \bar\chi^5(p_2) ,$$

$$K^\mu_{sg,sa} = -\tfrac{1}{3}\sqrt{3}\, (M^\beta)^\mu(p'_1, Q; 3q_u, 2q_u + q_d)\, S^T(q')\, \bar\chi^5(p_2) ,$$

$$K^\mu_{sg,as} = -\tfrac{1}{3}\sqrt{3}\, (M^5)^\mu(p'_1, Q; q_u + 2q_d, 2q_u + q_d)\, S^T(q')\, \bar\chi^\alpha(p_2) ,$$

$$K^\mu_{sg,aa} = -\tfrac{1}{3}\, (M^\beta)^\mu(p'_1, Q; q_u + 2q_d, 4q_u - q_d)\, S^T(q')\, \bar\chi^\alpha(p_2) ,$$

to be followed by the conjugated seagull contributions as depicted in the diagram to the lower left in figure 3.4,

$$\langle J^\mu_{\overline{sg}} \rangle^{\text{proton}} = -\tfrac{1}{2} \left(\begin{array}{cc} \bar\Psi^5 & \bar\Psi^\alpha \end{array} \right) \left(\begin{array}{cc} K^\mu_{\overline{sg},ss} & K^\mu_{\overline{sg},sa} \\ K^\mu_{\overline{sg},as} & K^\mu_{\overline{sg},aa} \end{array} \right) \left(\begin{array}{c} \Psi^5 \\ \Psi^\beta \end{array} \right) , \tag{3.49}$$

$$K^\mu_{\overline{sg},ss} = \chi^5(p_1)\, S^T(q)\, (\bar M^5)^\mu(p'_2, Q; q_d, q_u) ,$$

$$K^\mu_{\overline{sg},sa} = -\tfrac{1}{3}\sqrt{3}\, \chi^\beta(p_1)\, S^T(q)\, (\bar M^5)^\mu(p'_2, Q; q_d + 2q_u, q_u + 2q_d) ,$$

$$K^\mu_{\overline{sg},as} = -\tfrac{1}{3}\sqrt{3}\, \chi^5(p_1)\, S^T(q)\, (\bar M^\alpha)^\mu(p'_2, Q; 2q_u + q_d, 3q_u) ,$$

$$K^\mu_{\overline{sg},aa} = -\tfrac{1}{3}\, \chi^\beta(p_1)\, S^T(q)\, (\bar M^\alpha)^\mu(p'_2, Q; 4q_u - q_d, q_u + 2q_d) ,$$

and to be completed finally by the exchange quark contribution, *cf.* the upper diagram in figure 3.4,

$$\langle J^\mu_{ex} \rangle^{\text{proton}} = -\tfrac{1}{2} \left(\begin{array}{cc} \bar\Psi^5 & \bar\Psi^\alpha \end{array} \right) \left(\begin{array}{cc} K^\mu_{ex,ss} & K^\mu_{ex,sa} \\ K^\mu_{ex,as} & K^\mu_{ex,aa} \end{array} \right) \left(\begin{array}{c} \Psi^5 \\ \Psi^\beta \end{array} \right) , \tag{3.50}$$

$$K^\mu_{ex,ss} = q_d\, \chi^5(p_1)\, S^T(q)\, (\Gamma^\mu_q)^T\, S^T(q')\, \bar\chi^5(p_2) ,$$

$$K^\mu_{ex,sa} = -\tfrac{1}{3}\sqrt{3}\, (2q_u + q_d)\, \chi^\beta(p_1)\, S^T(q)\, (\Gamma^\mu_q)^T\, S^T(q')\, \bar\chi^5(p_2) ,$$

$$K^\mu_{ex,as} = -\tfrac{1}{3}\sqrt{3}\, (2q_u + q_d)\, \chi^5(p_1)\, S^T(q)\, (\Gamma^\mu_q)^T\, S^T(q')\, \bar\chi^\alpha(p_2) ,$$

$$K^\mu_{ex,aa} = -\tfrac{1}{3}\, (4q_u - q_d)\, \chi^\beta(p_1)\, S^T(q)\, (\Gamma^\mu_q)^T\, S^T(q')\, \bar\chi^\alpha(p_2) .$$

The respective contributions to the neutron current are obtained by interchanging the charges of the u and d quarks, $q_u \leftrightarrow q_d$. The relative momenta in the diquark-quark vertices and seagulls are according to figure 3.4: $p_1 = k_q - q$, $p'_1 = k_q - q'$, $p_2 = q' - p_q$ and $p'_2 = q - p_q$.
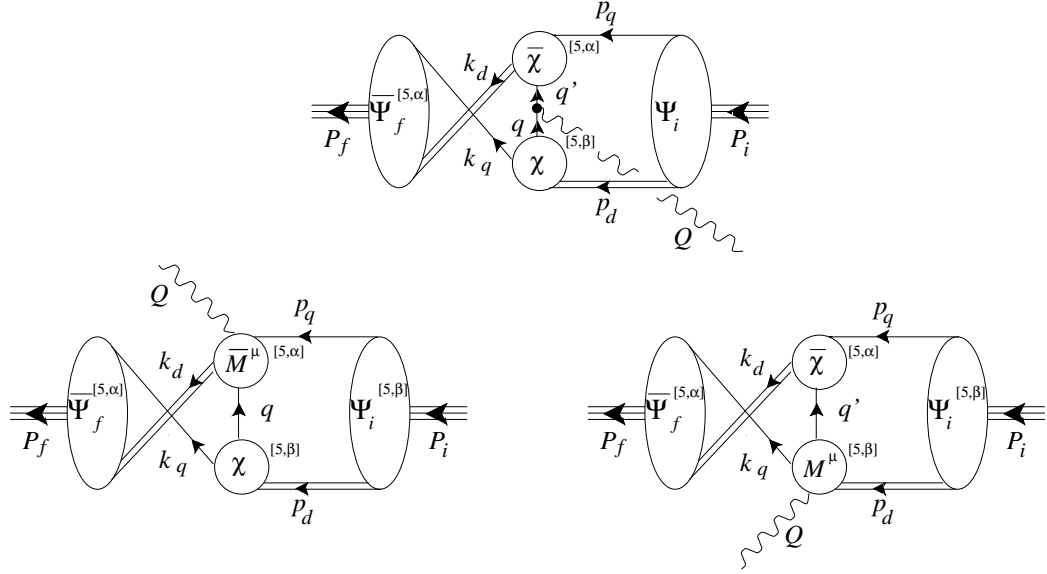
Figure 3.4: Exchange quark and seagull diagrams.

The nucleon current operator is now complete. We recapitulate that the current matrix element is written as,

$$\langle P_f | \, J^\mu \, | P_i \rangle := \bar{\Psi}_f \, \Gamma^\mu_{\text{nuc}} \, \Psi_i = \bar{\Psi}_f \, \left(\Gamma^\mu_0 + \Gamma^\mu_{\text{sc}-\text{ax}} + (K^{\text{BS}})^\mu \right) \, \Psi_i \, , \qquad (3.51)$$

including all the discussed elements. The impulse approximation operator Γ^μ_0 involves the couplings to quark and diquark, *cf.* eqs. (3.19,3.28–3.31). The extended impulse approximation comprises additionally the anomalous transitions between scalar and axialvector diquarks. Their operator $\Gamma^\mu_{\text{sc}-\text{ax}}$ is given in eq. (3.35). Finally we have discussed the coupling to the exchange quark kernel, $(K^{\text{BS}})^\mu$, in the last subsection.

3.1.3 Normalization of the Bethe-Salpeter wave function and the nucleon charges

A bound state Bethe-Salpeter equation is a homogeneous integral equation, therefore its solutions need subsequent normalization. The canonical normalization condition is derived by demanding that the bound state contributes a pole to the full two-body propagator with residue 1. As the nucleons are spin-1/2 particles, we demand that near the nucleon pole the full quark-diquark propagator behaves

like a free fermion propagator,

$$S(P) = \frac{i\slashed{P} - M_n}{P^2 + M_n^2} \;\; = \;\; (-2M_n) \sum_\sigma \frac{u_\sigma \, \bar{u}_\sigma}{P^2 + M_n^2} \;\; \Rightarrow \tag{3.52}$$

$$(G^{\mathrm{q-dq}})_{\mathrm{pole}} \;\; \overset{!}{=} \;\; (-2M_n) \frac{(\Psi u_\sigma) \, (\bar{u}_\sigma \bar{\Psi})}{P^2 + M_n^2} \; . \tag{3.53}$$

Now we write the inhomogeneous Bethe-Salpeter equation (2.70) for the full quark-diquark propagator in the form

$$G^{\mathrm{q-dq}} = G^{\mathrm{q-dq}} \left((G_0^{\mathrm{q-dq}})^{-1} - K^{BS} \right) G^{\mathrm{q-dq}} \tag{3.54}$$

and insert the pole form (3.53) on both sides to find the condition

$$\lim_{P^2 \to -M_n^2} = \bar{u}_\sigma \bar{\Psi} \, \frac{(G_0^{\mathrm{q-dq}})^{-1} - K^{BS}}{P^2 + M_n^2} \, \Psi u_\sigma \overset{!}{=} -\frac{1}{2M_n} \; . \tag{3.55}$$

Summing over spins, applying l'Hôspital's rule and writing the result covariantly yields the final normalization condition

$$-\frac{1}{2M_n} \, \mathrm{Tr} \, \bar{\Psi} \left[P^\mu \frac{\partial}{\partial P^\mu} \left((G_0^{\mathrm{q-dq}})^{-1} - K^{BS} \right) \right]_{P=P_n} \Psi \overset{!}{=} 1 \; , \tag{3.56}$$

where P_n denotes the on-shell nucleon momentum.

On the other hand, the electric form factor G_E is normalized to yield the physical nucleon charges in the soft limit, $Q \to 0$. Using eq. (3.8) that extracts G_E from the current matrix element and eq. (3.26) for the definition of the current operator[4] we find another condition,

$$-\frac{1}{2M_n} \, \mathrm{Tr} \, \bar{\Psi} \left(\Gamma_0^\mu + (K^{\mathrm{BS}})^\mu \right) \Psi \overset{!}{=} q_N \; . \tag{3.57}$$

In fact, the two conditions (3.56,3.57) are equivalent for the proton which has non-zero charge q_N. In the literature, a proof of this statement can be found [77] where the authors treat the case of one interaction channel and the momentum partitioning fixed by $\eta = 1/2$. Crucial for their proof is the differential form of the Ward-Takahashi identity for the gauged full 2-particle propagator which corresponds in our case to the gauged quark-diquark propagator, eq. (3.13). The proof is easily accomodated for our purposes and here it comes.

In our notation for the full quark-diquark propagator indicating all four particle momenta, $G^{\mathrm{q-dq}}(k_q, k_d; p_q, p_d)$, the momenta are not independent. We employ

---

[4]As the scalar-to-axialvector transitions are transversal, they do not contribute to the nucleon charges.

therefore the equivalent notation $G^{\mathrm{q-dq}}(k, p; P)$ with $P = k_q + k_d = p_q + p_d$ and p, k being the relative momenta. Our usual conventions hold:

$$k_q[p_q] = \eta P + k[p] , \quad k_d[p_d] = (1 - \eta)P - k[p] . \tag{3.58}$$

For the gauged propagator $G^\mu(k_q, k_d; p_q, p_d)$ the four momenta are independent, and here we define

$$P_f = p_q + p_d , \quad P_i = k_q + k_d . \tag{3.59}$$

The Ward-Takahashi identity (3.13) can now be formulated as

$$(P_f - P_i)^\mu G^\mu = \tag{3.60}$$
$$q_{q_f}G^{\mathrm{q-dq}}(k - (1 - \eta)(P_f - P_i), p; P_i) + q_{d_f}G^{\mathrm{q-dq}}(k + \eta(P_f - P_i), p; P_i) -$$
$$q_{q_i}G^{\mathrm{q-dq}}(k, p + (1 - \eta)(P_f - P_i); P_f) - q_{d_i}G^{\mathrm{q-dq}}(k, p - \eta(P_f - P_i); P_f) .$$

As we remarked earlier, this identity holds for each matrix element of $G^{\mathrm{q-dq}}$ that connects initial and final charge eigenstates of the quark-diquark system. We differentiate both sides with respect to P_f^μ and subsequently assume the soft limit, $P_i = P_f =: P$, to find

$$G^\mu = -(q_{q_i} + q_{d_i})\frac{\partial G^{\mathrm{q-dq}}}{\partial P^\mu}(k, p; P) + \tag{3.61}$$
$$(\eta q_{d_f} - (1 - \eta)q_{q_f})\frac{\partial G^{\mathrm{q-dq}}}{\partial k^\mu}(k, p; P) + (\eta q_{d_i} - (1 - \eta)q_{q_i})\frac{\partial G^{\mathrm{q-dq}}}{\partial p^\mu}(k, p; P) .$$

Since $q_{q_i} + q_{d_i} = 1$ (proton charge) for all the matrix elements of $G^{\mathrm{q-dq}}$, we employ for the first term on the right hand side

$$\frac{\partial}{\partial P^\mu}\left[G^{\mathrm{q-dq}}(G^{\mathrm{q-dq}})^{-1} \right] = 0 \quad \Rightarrow$$
$$\frac{\partial G^{\mathrm{q-dq}}}{\partial P^\mu} = -G^{\mathrm{q-dq}}\frac{\partial(G^{\mathrm{q-dq}})^{-1}}{\partial P^\mu}G^{\mathrm{q-dq}} . \tag{3.62}$$

On the other hand, we can use eq. (3.22) for G^μ on the left hand side of eq. (3.61). Therefore we obtain

$$G^{\mathrm{q-dq}}\left(\Gamma_0^\mu + (K^{\mathrm{BS}})^\mu\right)G^{\mathrm{q-dq}} = -G^{\mathrm{q-dq}}\frac{\partial(G^{\mathrm{q-dq}})^{-1}}{\partial P^\mu}G^{\mathrm{q-dq}} +$$
$$(\eta q_{d_f} - (1 - \eta)q_{q_f})\frac{\partial G^{\mathrm{q-dq}}}{\partial k^\mu} + (\eta q_{d_i} - (1 - \eta)q_{q_i})\frac{\partial G^{\mathrm{q-dq}}}{\partial p^\mu} . \tag{3.63}$$

Near the bound state the full quark-diquark propagator can be written in the pole form of eq. (3.53). We see that the first terms on the left and right hand side

of eq. (3.63) have a double pole at $P^2 = -M_n^2$, whereas the remaining terms can only contribute a single pole. Fortunately these drop out when comparing residues and we are left with

$$\bar{u}_\sigma \bar{\Psi} \, \frac{\partial (G^{\mathrm{q-dq}})^{-1}}{\partial P^\mu} \, \Psi u_{\sigma'} = \bar{u}_\sigma \bar{\Psi} \, \left(\Gamma_0^\mu + (K^{\mathrm{BS}})^\mu \right) \, \Psi u_{\sigma'} \; . \qquad (3.64)$$

Putting $\sigma = \sigma'$, performing the spin summation and contracting with P^μ, we indeed find the equality of the canonical normalization condition (3.56) and the charge normalization condition (3.57). Also the neutron has the correct charge: Although the overall normalization cannot be fixed in this case, eq. (3.61) guarantees that its electric form factor is zero in the soft limit since $q_{q_i} + q_{d_i} = 0$ for all quark-diquark channels.

It is possible to prove the equivalence of eqs. (3.56,3.57) without explicitly recurring to the Ward-Takahashi identity (3.13). The proof is slightly more technical and for the scalar diquark sector of the model it is described in ref. [23].

3.1.4   Summary

In conclusion we want to emphasize the power of the general Ward-Takahashi identity for the full quark-diquark propagator, eq. (3.13). Its implications allowed us to derive (i) conservation of the nucleon current, (ii) constraints on the longitudinal part of *all* contributing graphs, notably of the irreducible quark-diquark-photon vertices (seagulls) and finally (iii) the equivalence of the canonical and the charge normalization condition. It is interesting to note that actually current conservation holds for *each single diagram* depicted in figures 3.2 and 3.4. This has been proved in ref. [62] by using just the transformation properties of the respective matrix elements under time reversal and parity. But as we know, gauge invariance provides *more* information than conserved current matrix elements on-shell. This additional information is manifest in the (off-shell) Ward-Takahashi identities and it is certainly wrong to restrict oneself to assorted current contributions since at least the correct nucleon charges cannot be obtained in general. This is a shortcoming of a quark-diquark model investigated in refs. [78, 79]. The authors employ parametrized nucleon Faddeev amplitudes and calculate form factors in a generalized impulse approximation which, besides containing overcounted contributions [73], does not respect a Ward-Takahashi identity like eq. (3.13). The immediate consequence turned out to be that the correct nucleon charges have been obtained only for a special choice of parameters.

3.2   Numerical calculations

Before we present the results for the nucleon electric and magnetic form factors, we will discuss shortly the numerical method. As we have calculated the Bethe-Salpeter wave functions Ψ in the rest frame of the nucleon, we have to discuss their boosting to a moving frame. Thereby we will find that an accurate description of the boosted wave function is linked to the accuracy of its Chebyshev expansion in the rest frame. Since the *vertex* function Φ show better convergence in the Chebyshev expansion, it would be desirable to use Φ instead of the wave function Ψ. We find that this is feasible only for the diagrams of the extended impulse approximation but that due to their singularity structure the diagrams evaluated with the vertex function acquire additional residue contributions in a certain kinematical region. In this region the (Euclidean) vertex function Φ is not connected to the (Euclidean) wave function Ψ by simply cutting quark and diquark legs off Ψ.

3.2.1   Numerical method

The numerical computation of the form factors is done in the Breit frame where

$$
\begin{aligned}
Q^\mu &= (\boldsymbol{Q}, 0)\,, \\
P_i^\mu &= (-\boldsymbol{Q}/2, i\omega_Q)\,, \\
P_f^\mu &= (\boldsymbol{Q}/2, i\omega_Q)\,, \\
P^\mu = (P_i + P_f)/2 &= (\boldsymbol{0}, i\omega_Q)\,,
\end{aligned}
\tag{3.65}
$$

with $\omega_Q = \sqrt{M_n^2 + \boldsymbol{Q}^2/4}$.

The total current operator, eq. (3.51), employs the wave functions Ψ in the initial and final state. These are determined by the basic covariants and the corresponding scalar functions $\hat{S}_i(p^2, z = \hat{p}\cdot\hat{P}_n)$, $\hat{A}_i(p^2, z = \hat{p}\cdot\hat{P}_n)$, *cf.* eq. (2.129). We recall that we absorbed the angular (z) dependence in the Chebyshev expansion, eq. (2.136). In the rest frame, $P_n = (\boldsymbol{0}, iM_n)$, z is real and $|z| \leq 1$, therefore the expansion is *always* convergent. In the Breit frame we have the real relative momenta in the initial state, p, and the final state, k, which are integrated over. Therefore the angular variables $z_k = \hat{k}\cdot\hat{P}$ and $z_p = \hat{p}\cdot\hat{P}$ are real and not larger than 1. The angular variables that enter the initial and final state wave functions as an argument are, however,

$$
z_i = \hat{p}\cdot\hat{P}_i = \frac{\omega_Q}{M_n} z_p - i\frac{1}{2}\frac{|\boldsymbol{Q}|}{M_n}\hat{p}\cdot\hat{Q}\,,
\tag{3.66}
$$

$$
z_f = \hat{k}\cdot\hat{P}_f = \frac{\omega_Q}{M_n} z_k + i\frac{1}{2}\frac{|\boldsymbol{Q}|}{M_n}\hat{k}\cdot\hat{Q}\,.
\tag{3.67}
$$

Therefore, in order to use the rest frame solutions, analytical continuation to complex values for z_i and z_f is necessary. This can be justified for the bound-state Bethe-Salpeter wave functions Ψ. These can be expressed as vacuum expectation values of local (quark field) and almost local operators (diquark field) and we can resort to the domain of holomorphy of such expectation values to continue the relative momenta of the bound-state Bethe-Salpeter wave function $\Psi(p, P)$ into the 4-dimensional complex Euclidean space necessary for the computation of Breit-frame matrix elements from rest frame nucleon wave functions. The necessary analyticity properties are manifest in the expansion in terms of Chebyshev polynomials with complex arguments.

There is a practical obstacle in the outlined procedure. As the maximum of the squared absolute values $|z_{i[f]}|^2_{\max} = 1 + Q^2/(4M_n^2)$ rises with increasing Q^2, we encounter convergence problems for the current matrix elements as the Chebyshev moments of higher order n become more and more important (T_n is a polynomial of degree n). Consider the strengths of the wave function Chebyshev moments presented in appendix A.3 (Set I). The fourth Chebyshev moment of the dominating function $\hat{S}_1$ is about 7 % of the zeroth moment. With $T_4(z) = 8z^4 - 8z^2 + 1$ one can estimate the critical Q^2 for which contributions from $\hat{S}_1^4$ are comparable to the ones from $\hat{S}_1^0$,

$$|\hat{S}_1^4 \, T_4(z_f)|_{\max} \sim |\hat{S}_1^0 \, T_0(z_f)|_{\max} \quad \Rightarrow \quad Q^2 \sim 1.4 \text{ GeV}^2 \, . \tag{3.68}$$

As a consequence, the grid size in the angular integrations has to be increased beyond this value of Q^2 because the higher Chebyshev polynomials introduce rapid oscillations in the integrand. Since the Chebyshev moments of the vertex function converge much more rapidly ($|S_1^4|_{\max} = 0.01 \, |S_1^0|_{\max}$ for Set II), it would be desirable to use Φ instead of Ψ in the expressions for the current, eq. (3.51). Having $\Psi = G_0^{\text{q}-\text{dq}} \, \Phi$, the free quark and diquark propagators with the corresponding singularities are introduced in the integrand. For sufficiently small Q^2 these are outside the complex integration domain. For larger Q^2, these singularities enter the integration domain, therefore, a proper treatment of these singularities is required when they come into the domain of interest.

For the impulse approximation contributions to the form factors we have been able to take the corresponding residues into account explicitly in the integration. Here the integration is reduced to one four-dimensional integral over either p or k due to the inherent δ-function of the free quark-diquark propagator $G_0^{\text{q}-\text{dq}}$. Being technically somewhat involved, we have placed the matter into appendix B.2. For these contributions, one can compare the calculations with boosted Ψ and Φ and verify numerically that they yield the same, unique results (up to several Q^2). This is demonstrated in appendix B.2.

For the current contributions from the gauged Bethe-Salpeter kernel, *cf.* figure 3.4, two four-dimensional integrations over p and k are required. The complex

singularity structure of the integrand did not allow a similar treatment as described in appendix B.2 for the diagrams of the impulse approximation. Therefore we have resorted to employ the boosted wave functions Ψ. As a result, the numerical uncertainty (for these diagrams only) exceeded the level of a few percent beyond momentum transfers of 2.5 GeV^2. Due to this limitation (which could be avoided by increasing simply the used computer time) the form factor results presented in section 3.2.2 are restricted to the region of momentum transfers below 2.5 GeV^2.

In addition to the aforementioned complications, there is another bound on the value of Q^2 above which the exchange and seagull diagrams cannot be evaluated. It is due to the singularities in the diquark-quark vertices $\chi^{5[\mu]}(p_i)$ and in the exchange quark propagator. The rational n-pole forms of the diquark-quark vertices, $V_{n-\text{pole}}(p^2) = (\lambda_n^2/(\lambda_n^2 + p^2))^n$ for example yield the following upper bound,

$$Q^2 < 4 \left(\frac{4\lambda_n^2}{(1 - 3\eta)^2} - M_n^2 \right) . \tag{3.69}$$

A free constituent propagator for the exchange quark gives the additional constraint,

$$Q^2 < 4 \left(\frac{m_q^2}{(1 - 2\eta)^2} - M_n^2 \right) . \tag{3.70}$$

It turns out, however, that these bounds on Q^2 are insignificant for the model parameters employed in the calculations described herein.

3.2.2 Results

For the scalar diquark sector, we have presented results for the nucleon electric form factors, radii and magnetic moments already in section 2.5.2. There we found a good description of both the proton and neutron electric form factor, whereas the magnetic moments turned out to be less than half of the respective experimental value. We attributed this failure to the absence of axialvector diquarks (which carry spin and therefore contribute to the spin-flip currents) and to the high constituent quark mass employed for the solutions. Furthermore there is a substantial contribution to the electric form factors by the exchange quark and the seagull diagrams [23] with the latter being of the order of 30 %. We attribute this finding to the relatively small diquark width in momentum space and the quite sizeable nucleon binding energy (which is around 300 MeV for the parameter sets from table 2.5).

We turn now to the form factors for the two parameter sets of table 2.8 which include axialvector diquark correlations. First we want to judge the strength of the axialvector correlations within the nucleon by evaluating the contributions
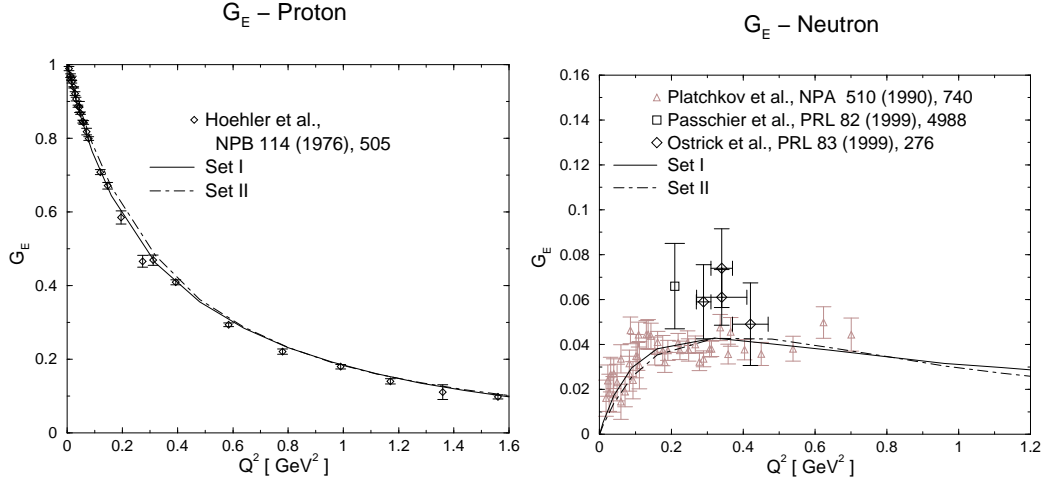
Figure 3.5: Electric form factors of both nucleons for the parameter sets of table 2.8. Experimental data for the proton is taken from [60]. The older neutron data analysis [61] contains more systematic uncertainties (due to specific nucleon-nucleon potentials) than the more recent data from [80, 81].

of Ψ^5 and Ψ^μ to the *norm* integral, eq. (3.56). The strength of the axialvector correlations is rather weak for Set II, since the scalar diquark contributes 92 % to the norm integral of eq. (3.56) while the axialvector correlations and scalar-axialvector transition terms together give rise only to the remaining 8 % for this set. Scalar diquark contributions are terms $\sim \bar{\Psi}^5\Psi^5$, axialvector contributions are $\sim \bar{\Psi}^\mu\Psi^\nu$ and the transition terms account for the two cross terms. For Set I, the fraction of the scalar correlations is reduced to 66 %, the axialvector correlations are therefore expected to influence nucleon properties more strongly for Set I than for Set II.

The results for the nucleon electric form factors are presented in figure 3.5. For the two sets we show here the sum of *all* diagrams, formed by the extended impulse approximation and the exchange kernel graphs. In table 3.1 we have collected the corresponding radii.[5] The phenomenological dipole behavior of the proton G_E is well reproduced by both parameter sets. In the neutron case, the slope at the soft point and the general behavior are well accounted for although the data points of ref. [61] have to be interpreted with care since here the electric form factor has been extracted from electron-deuteron scattering data using specific nucleon-nucleon potentials. Data from more recent experiments which

---

[5]A radius r_F corresponding to a form factor F is defined by $r_F^2 = -6\frac{dF}{dQ^2}|_{Q^2=0}/F(0)$ if $F(0)$ is non-zero. For the neutron electric charge radius, the quotient $F(0)$ is simply omitted.

		Set I	Set II	experiment
$(r_p)_{\rm el}$	[fm]	0.88	0.81	0.836 ± 0.013
$(r_n^2)_{\rm el}$	[fm^2]	-0.12	-0.10	-0.113 ± 0.007
$(r_p)_{\rm mag}$	[fm]	0.84	0.83	0.843 ± 0.013
$(r_n)_{\rm mag}$	[fm]	0.84	0.83	0.840 ± 0.042

Table 3.1: Nucleon electric and magnetic radii for the two parameter sets compared to the experimental values from [82] (for $(r_n^2)_{\rm el}$) and [60] (for the remaining radii).

largely avoid this model dependence are still rare. Our results lie here at the lower experimental bound.

In figure 3.6 we evaluate the contributions from the single diagrams for Set I. For the notation of the single current matrix elements we refer to eqs. (3.36,3.37) and (3.48–3.50). As can be seen, the overall behavior of the impulse approximation diagrams is close to the total form factor. Clearly the ones sandwiched between the scalar nucleon correlations (straight thin line) dominate over the matrix elements of the axialvector correlations (dashed thin line). Seagulls and exchange quark represent just a correction below 10 % but are nevertheless important to guarantee the correct behavior for $Q \to 0$. On the other side, the neutron electric form factor is much more sensitive to the behavior of the single diagrams as it arises as a result of delicate cancellations. Especially we want to point to the contribution from the impulse approximation graphs which are proportional to the nucleon axialvector correlations in the initial and final states, *i.e.* to the matrix elements $\langle J_q^\mu \rangle^{\rm ax-ax}$ and $\langle J_{dq}^\mu \rangle^{\rm ax-ax}$ (dashed thin line): At $Q^2 = 0$, they add positively to the neutron charge but for increasing Q^2 their contribution quickly drops. As a consequence, stronger axialvector correlations tend to suppress the peak in the form factor which the data suggest to be located at $Q^2 = 0.2 \ldots 0.5 \,{\rm GeV}^2$. Again, the seagulls and the exchange quark graph provide for the correct neutron charge.

The results for the proton magnetic form factor are shown in figure 3.7. Correspondingly, we have collected the single diagram contributions to the magnetic moment $\mu = G_M(0)$ in table 3.2. There, the influence of two parameters is visible. First, in contrast to non-relativistic constituent models, the dependence of the proton magnetic moment on the ratio M_n/m_q is stronger than linear. As a result, the quark impulse contribution to μ_p with the scalar diquark being spectator, which is the dominant one, yields about the same for both sets, even though the corresponding nucleon amplitudes of Set I contribute about 25 % less to the
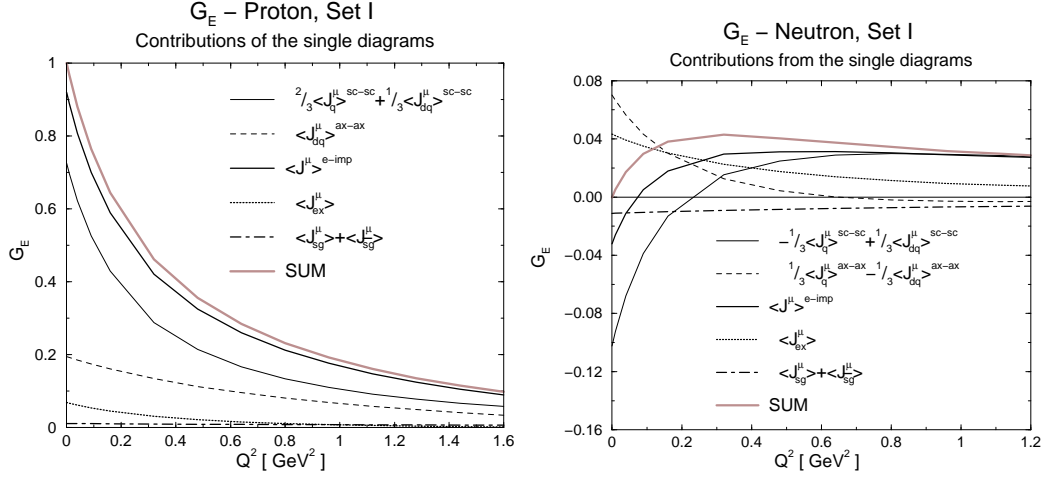
Figure 3.6: Contributions of the single diagrams to the nucleon electric form factors for Set I. They are obtained by applying eq. (3.8) to the current matrix elements.
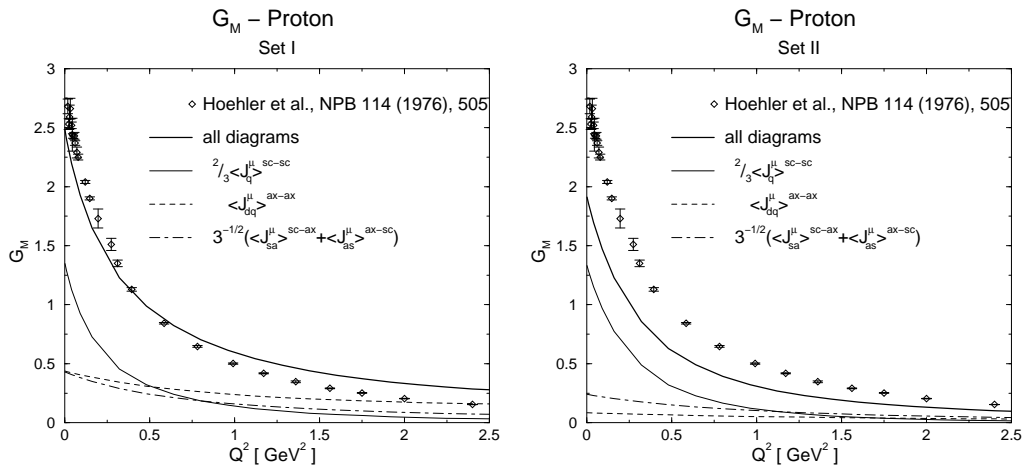

Figure 3.7: The proton magnetic form factor for Set I and II along with the dominating contributions from the impulse approximation. Experimental data are provided by ref. [60].

		Set I	Set II	experiment
	$\langle J_q^\mu \rangle^{\mathrm{sc-sc}}$	1.35	1.33	
	$\langle J_{dq}^\mu \rangle^{\mathrm{ax-ax}}$	0.44	0.08	
μ_p	$\langle J_{sa}^\mu \rangle^{\mathrm{sc-ax}} + \langle J_{as}^\mu \rangle^{\mathrm{ax-sc}}$	0.43	0.24	
	$\langle J_{ex}^\mu \rangle$	0.25	0.22	
	SUM	2.48	1.92	2.79
μ_n	SUM	-1.53	-1.35	-1.91
$\mu_p + \mu_n$	isoscalar	0.95	0.57	0.88
$\mu_p - \mu_n$	isovector	4.01	3.27	4.70

Table 3.2: Magnetic moments of proton and neutron. The contributions from the indicated current matrix elements are to be understood as coming with the appropriate flavor factors, *cf.* eq. (3.36).

norm than those of Set II. Secondly, the scalar-axialvector transitions contribute equally strong (Set I) or stronger (Set II) than the spin flip of the axialvector diquark itself. While for Set II (with weaker axialvector diquark correlations) the magnetic moments are about 30 % too small, the stronger diquark correlations of Set I yield an isovector contribution which is only 15% below and an isoscalar magnetic moment slightly above the phenomenological value.

Stronger axialvector diquark correlations are favorable for larger values of the magnetic moments as expected. If the isoscalar magnetic moment is taken as an indication that those of Set I are somewhat too strong, however, a certain mismatch with the isovector contribution remains, also with axialvector diquarks included. Looking at the left panel of figure 3.7, we note that the axialvector diquark diagram (dashed thin line) falls very slowly with increasing Q^2 and eventually causes a violation of the observed dipole shape. For Set II, this effect is absent due to the weakness of the axialvector correlations.

We can add another twist to the story by comparing our results to the recently measured ratio $\mu_p G_E/G_M$ for the proton [69], *cf.* figure 3.8. The ratio obtained from Set II with weak axialvector correlations lies above the experimental data, and that for Set I below. The experimental observation that this ratio decreases significantly with increasing Q^2 (about 40 % from $Q^2 = 0$ to 3.5 GeV^2), can be well reproduced with axialvector diquark correlations of a certain strength included. The reason for this is the following: The impulse-approximated photon-diquark couplings yield contributions that tend to fall off slower with increasing Q^2 than
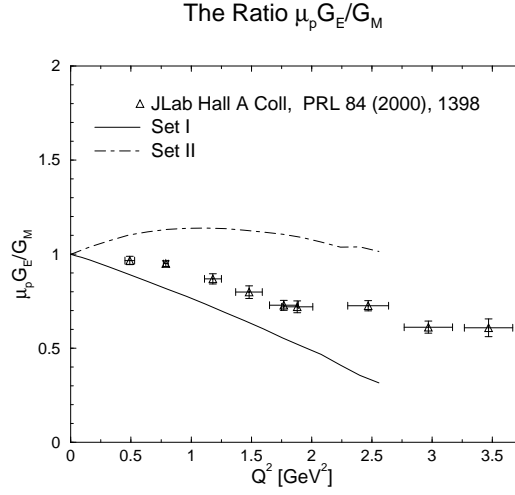
The Ratio $\mu_p G_E/G_M$

Figure 3.8: The ratio $(\mu_p\, G_E)/G_M$ compared to the data from ref. [69].

those of the quark. This is the case for both, the electric and the magnetic form factor. If no axialvector diquark correlations inside the nucleon are maintained, however, the only diquark contribution to the electromagnetic current arises from $\langle J^\mu_{sc}\rangle^{\mathrm{sc-sc}}$, see eqs. (3.36,3.37). Although this term does provide a substantial contribution to G_E, its respective contribution to G_M is of the order of 10^{-3}. This reflects the fact that an on-shell scalar diquark would have no magnetic moment at all, and the small contribution to G_M may be interpreted as an off-shell effect. Consequently, too large a ratio $\mu_p\, G_E/G_M$ results, if only scalar diquarks are maintained [23]. For Set II (with weak axialvector correlations), this effect is still visible, although the scalar-to-axialvector transitions already bend the ratio towards lower values at larger Q^2. These transitions almost exclusively contribute to G_M, and it thus follows that the stronger axialvector correlations of Set I enhance this effect. Just as for the isoscalar magnetic moment, the axialvector diquark correlations of Set I tend to be somewhat too strong here again.

3.2.3 Conclusions

The numerical results for the electric form factors support the already emphasized importance of using the Ward-Takahashi identities for constructing a suitable current operator. The correct value for $G_E(0) = q_N$, the nucleon charge, has been obtained not only for the two parameter sets that have been presented here but also for a general choice of parameters and of the momentum partitioning η. Furthermore, the proton and neutron electric form factors are described very well in the diquark-quark-model.

The strength of axialvector correlations Ψ^μ within the nucleon turns out to be constrained by two observations:

- The impulse approximation graphs involving Ψ^μ tend to suppress the neutron electric form factor. This becomes effective only for stronger correlations than presented here, though.

- Although larger axialvector correlations are favorable for the magnetic moments as expected, the ratio $\mu_p \, G_E / G_m$ provides tight bounds. As a result, Ψ^μ should contribute to the nucleon norm around 20 %.

As has been mentioned, a considerable improvement in the description of the nucleon magnetic moments has been achieved compared to the scalar diquark sector. The anomalous transitions between scalar and axialvector diquark are in this connection equally important as the contributions of the axialvector diquark itself. We hereby confirm the conjecture from ref. [41] where the nucleon magnetic moments have been ascertained in a simple additive diquark-quark picture including scalar and axialvector diquark.

Nevertheless, the isovector magnetic moments are still too small by about 15 %. We discuss two possibilities that might account for the mismatch.

- As we will see in the next chapter on the pionic and the axial form factor of the nucleon, *vector* diquarks need to be included in the parametrization of the two-quark correlations on theoretical grounds. Although their contributions to the nucleon *binding energy* are expected to be negligible, *cf.* the discussion in the beginning of section 2.2, the *photon coupling* of the vector diquarks could be strong enough to compensate the underestimated magnetic moments.

- The tree-level form of the employed quark and diquark propagators is certainly too naïve an assumption. As an example, a non-trivial quark propagator would lead to some effective *anomalous* magnetic moment of the (constituent) quark via the associated non-trivial quark-photon vertex. The effect of the latter would be visible, *e.g.*, in an enhanced magnetic moment contribution of the quark impulse approximation diagram. In chapter 5 we will therefore discuss some aspects of a dressed quark propagator and employ an especially simple parametrization (which avoids the free-particle threshold) in calculations of the octet-decuplet spectrum and of form factors.

Chapter 4

Strong and Axial Form Factors

In this chapter we will investigate the pion-nucleon form factor as an example of a strong form factor and the isovector axial form factor which is of interest in the description of nucleon weak interactions. In the first case, we are interested in the matrix elements of a pseudoscalar current operator J_5^a and in the second case it is the pseudovector[1] current operator $J_5^{a,\mu}$ whose matrix elements are the object under scrutiny. The superscript a labels the component of the isovector triplet which both current operators belong to.

If the squared momentum transfer is equal to the pion mass, $Q^2 = -m_\pi^2$, then the pseudoscalar matrix element is entirely determined by the *pion-nucleon coupling constant* $g_{\pi NN}$ which is accessible experimentally. There appears to be no experimentally feasible scattering process which is dominated by one-pion exchange such that the form factor could be determined away from the pion mass shell. Therefore corresponding theoretical results from microscopic nucleon models such as the diquark-quark model only serve as a guideline for effective nucleon potential models which incorporate one-pion exchange.

The matrix element of the pseudovector current at $Q^2 = 0$ is determined by the β decay and the corresponding *weak decay* or *axial coupling constant* g_A is known quite accurately[2]. For spacelike Q^2, the form factor may be determined by neutrino-deuteron scattering [85] but these experiments are difficult to perform. Thus the axial structure of the nucleon is known far less precisely than its electromagnetic structure.

As it is well-known, these seemingly unrelated constants g_A and $g_{\pi NN}$ are linked with each other by the famous *Goldberger-Treiman relation*, see below. It can be derived from the assumption of chiral symmetry of an underlying La-

---

[1] We reserve the label *pseudovector* for the external currents to distinguish them from *axialvector* diquarks. Both objects have of course the same Lorentz and parity transformation properties.

[2] Although in 1959 the constant was assumed to be known precise enough, $g_A|_{1959} = 1.17 \pm 0.02$, it is quite different from the presently known value, $g_A|_{2000} = 1.267 \pm 0.0035$ [83, 84].

grangian which conserves the pseudovector current. Additionally it is assumed that this chiral symmetry is spontaneously broken and pions appear as massless Goldstone bosons. Now the physical pion is massive, albeit its mass is small, so chiral symmetry is explicitly broken and the pseudovector current can be only partially conserved (*PCAC hypothesis*). However, it can be shown that the Goldberger-Treiman relation is still valid under the assumption that the axial form factor is slowly varying in the vicinity of $Q^2 = 0$. Furthermore, the Goldberger-Treiman relation holds experimentally on the five per cent accuracy level which, among other observations, lends support to the concept of spontaneously broken chiral symmetry and the partially conserved pseudovector current.

We tried to show by these introductory arguments that the pion-nucleon coupling constant and the weak decay constant are related with each other in a model independent way. Thereby we imply that if one were to start with a chirally symmetric *quark* theory one should always recover the Goldberger-Treiman relation for the *nucleon*, similar to the case of electromagnetic interactions where the nucleon charges should always come out correctly. Again similar to the electromagnetic case, there are powerful *chiral* Ward identities which constrain the pseudovector current vertices.

Unfortunately we will not be able to comply with the demand of a conserved pseudovector current and to actually derive the Goldberger-Treiman relation in the diquark-quark model in its present form. As will become clear in section 4.1, *vector* diquark correlations are inevitably needed to conserve the pseudovector current. These are neglected in our model, for their influence on the binding energy is assumed to be small and they introduce six additional scalar functions in the nucleon vertex function Φ, therefore being a substantial numerical complication. Our calculations presented in this chapter aim therefore at quantitative results for the expected discrepancy and at possible explanations for the measured weak coupling constant. In contrast to the anomalous magnetic moments, the non-relativistic quark model estimate $g_A = 5/3$ is 31 % larger than the measured value, $g_A = 1.27$, and therefore a relativistic treatment such as taken up here might offer an explanation for this difference.

We will begin with fixing our conventions for the matrix elements and re-derive quickly the Goldberger-Treiman relation. Section 4.1 explains the necessity of vector diquarks for pseudovector current conservation. In section 4.2 we are concerned with the construction of the pseudoscalar and pseudovector current operator for our model. Here we start with a suitable quark-pion vertex which in conjunction with a chiral Ward identity yields the quark-pseudovector vertex. The structures and strengths of the couplings of the diquarks to the pion and the pseudovector current are obtained from resolving the diquarks in a way similar to their electromagnetic couplings. The numerical results, again obtained by employing the two parameter sets from table 2.8, are presented in section 4.3. We will find

a slight overestimation of g_A and a violation of the Goldberger-Treiman relation of around 15 %. The axial form factor results for finite Q^2 are consistent with the presently available experimental results.

Let us start with a few definitions. The (spin-summed) matrix element of the pseudoscalar current J_5^a is parametrized as

$$\langle P_f | \, J_5^a \, | P_i \rangle = \Lambda^+(P_f) \, \tau^a \gamma^5 g_{\pi NN}(Q^2) \, \Lambda^+(P_i) \, , \qquad (4.1)$$

which defines the pion-nucleon form factor $g_{\pi NN}(Q^2)$. As before, $Q = P_f - P_i$ holds. For numerical evaluation, we will choose the neutral component, J_5^3, and sandwich between proton flavor states, indicated by the subscript $_\mathrm{p}$. Straightforward algebra allows to extract the form factor as the following Dirac trace,

$$g_{\pi NN}(Q^2) = -\frac{2M_n^2}{Q^2} \, \mathrm{Tr} \, \left[_\mathrm{p}\langle P_f | \, J_5^3 \, | P_i \rangle_\mathrm{p} \, \gamma^5 \right] \, . \qquad (4.2)$$

We take for granted in the following that $g_{\pi NN}(0)$ is close to the pion-nucleon coupling constant $g_{\pi NN} = g_{\pi NN}(-m_\pi^2)$ as consistent with the assumption of PCAC.

The matrix elements of the pseudovector current are parametrized by the form factor $g_A(Q^2)$ and the induced pseudoscalar form factor $g_P(Q^2)$,

$$\langle P_f | \, J_5^{a,\mu} \, | P_i \rangle = \Lambda^+(P_f) \frac{\tau^a}{2} \left[i\gamma^\mu \gamma^5 g_A(Q^2) + Q^\mu \gamma^5 g_P(Q^2) \right] \Lambda^+(P_i) \, . \qquad (4.3)$$

For $Q^2 \to 0$, the induced pseudoscalar form factor will be dominated by the pion pole,

$$\lim_{Q^2 \to 0} g_P(Q^2) = 2 \frac{f_\pi \, g_{\pi NN}(0)}{Q^2} \, . \qquad (4.4)$$

We denote the pion decay constant by $f_\pi = 92.7$ MeV. The Goldberger-Treiman relation follows from current conservation, $Q^\mu \langle J_5^{a,\mu} \rangle = 0$, and after replacing g_P by eq. (4.4) we find,

$$g_A(0) = f_\pi g_{\pi NN}(0) / M_n \, . \qquad (4.5)$$

The regular part of the matrix element, $g_A(Q^2)$, and the pion pole part, $g_P(Q^2)$, can be extracted from eq. (4.3) as follows:

$$g_A(Q^2) = -\frac{i}{2 \left(1 + \frac{Q^2}{4M_n^2} \right)} \, \mathrm{Tr} \, \left[_\mathrm{p}\langle P_f | \, J_5^{3,\mu} \, | P_i \rangle_\mathrm{p} \left(\gamma^5 \gamma^\mu - i\gamma^5 \frac{2M_n}{Q^2} Q^\mu \right) \right] \, ,$$
$$(4.6)$$

$$g_P(Q^2) = \frac{2M_n}{Q^2} \left(g_A(Q^2) - \frac{2M_n}{Q^2} \, \mathrm{Tr} \, \left[_\mathrm{p}\langle P_f | \, J_5^{3,\mu} \, | P_i \rangle_\mathrm{p} \, Q^\mu \gamma^5 \right] \right) \, . \qquad (4.7)$$

Having specified our conventions, we turn now to a short discussion about the consequences of excluding vector diquarks from our considerations.

4.1   Scalar and vector/axialvector diquarks as chiral multiplets

The necessity of including vector diquarks along with the axialvectors was observed only very recently in ref. [86] within the context of an NJL model. Remember that diquarks as separable 2-quark correlators are in the NJL model solutions of the t matrix integral equation, with the interaction kernel given in lowest order in the coupling constant. The separable interaction kernel describes here the 4-quark point interaction: two quarks in a channel with certain diquark quantum numbers interact locally with two antiquarks with respective antidiquark quantum numbers, see *e.g.* eq. (2.41) for the scalar channel. The statement of ref. [86] is summarized as follows: Chiral invariance of the NJL Lagrangian requires the inclusion of quark-quark interaction kernels with both vector and axialvector diquark quantum numbers and the same coupling constant. Solutions for the separable vector diquark t matrix do not have the same form as the axialvector t matrix, *e.g.*, a possible vector diquark mass pole will appear at larger invariant momentum values than an axialvector pole. Nevertheless vector diquarks have to be carried all the way through the nucleon Faddeev problem in order to comply with chiral invariance.

In our model, we have parametrized the diquark correlations without recurring to a specific model Lagrangian. To adapt the above argument to our case, we introduce interpolating diquark fields as done in section 3.1. Let $d_s^\dagger$ denote scalar diquark creation operators and $d_v^{\mu\dagger}, d_a^{b\mu\dagger}$ the ones for vector and axialvector diquarks. Scalar and vector diquarks are flavor singlets, the axialvector diquark belongs to a flavor triplet, with its components denoted by the index b. The appropriate color indices are suppressed as they are unimportant for the argument. The interaction of (pointlike) diquarks with quarks can now be written as an interaction Lagrangian,

$$
\begin{aligned}
\mathcal{L}_{\text{int}} \;=\;& g_s \left(q^T\, C\gamma^5\, \tau^2\, q \right) d_s^\dagger + g_v \left(q^T\, Ci\gamma^\mu\gamma^5\, \tau^2\, q \right) d_v^{\mu\dagger} + \\
& g_a \left(q^T\, Ci\gamma^\mu\, \tau^2\tau^b\, q \right) d_a^{b\mu\dagger} + \quad \text{herm. conj.} \,,
\end{aligned} \tag{4.8}
$$

where q denotes as usual the quark field. A combined infinitesimal chiral and isospin variation of the quark field reads

$$
\delta q = -i\omega_b\tau^b\gamma^5\, q \,, \tag{4.9}
$$

with ω_b denoting a set of three infinitesimal parameters. Straightforward evaluation to first order in the variation yields

$$
\delta \left(q^T\, C\gamma^5\, \tau^2\, q \right) \;=\; 0 \,, \tag{4.10}
$$

$$
\delta \left(q^T\, Ci\gamma^\mu\gamma^5\, \tau^2\, q \right) \;=\; -i\omega_b \left(q^T\, Ci\gamma^\mu\, \tau^2\tau^b\, q \right) \,, \tag{4.11}
$$

$$
\delta \left(q^T\, Ci\gamma^\mu\, \tau^2\tau^b\, q \right) \;=\; -i\omega_b \left(q^T\, Ci\gamma^\mu\gamma^5\, \tau^2\, q \right) \,. \tag{4.12}
$$

We demand that the interaction Lagrangian (4.8) be invariant under an infinitesimal chiral variation. Substituting eqs. (4.10–4.12) into eq. (4.8), we see that this leads to the requirements

$$\delta\, d_a^{b\mu\dagger} = i\omega_b d_v^{\mu\dagger}, \quad \delta\, d_v^{\mu\dagger} = i\omega_b d_a^{b\mu\dagger} \quad \text{and} \quad g_a = g_v\,. \tag{4.13}$$

Vector and axialvector diquarks mix under a chiral (isovector) transformation. The scalar diquark channel is unaffected by the transformation as its variation is zero. This is equivalent to the statement that a pseudovector (isovector) current does not couple to the scalar diquark. Summarizing these findings we have found that the scalar diquark on the one side and vector/axialvector diquarks on the other side belong to different chiral multiplets [86].

We learn something else. The above argument is only valid for a *local* quark-diquark interaction. If we introduced extended diquarks by a non-local interaction with some momentum dependent vertex we would find additional *chiral seagull vertices* as a result of the variation. This is very similar to the electromagnetic case. Although we derived the seagulls in section 3.1.2 by requiring gauge invariance via a Ward-Takahashi identity for the Bethe-Salpeter interaction kernel, they can also be obtained from an interaction Lagrangian with momentum-dependent vertices [76] in much the same way as indicated here.

In the following we will neglect both the chiral seagulls and the vector diquark correlations. As we remarked earlier, the expected high mass of the vector diquarks would suppress the strength of the corresponding vector correlations within the nucleon. Another argument is concerned with the numerical feasibility. In the Dirac algebra, the vector correlations could be decomposed similarly to the axialvector correlations, leading to six additional scalar functions. This would increase the numerical effort considerably and since the numerical calculations are already very involved at this stage, the inclusion of vector diquarks is beyond the scope of this thesis. On the other hand, we have no serious argument for the neglect of the seagulls. However, we can estimate from the numerical results presented in section 4.3 that their contribution to the weak coupling constant should be below ten per cent.

4.2   Pseudoscalar and pseudovector current operator

First we will specify the quark vertices with pseudoscalar and pseudovector current operators and then continue with a discussion of the effective diquark vertices that can be obtained by coupling the currents to an intermediate quark loop.

As we use a free fermion propagator for the quark, eq. (2.64), the scalar functions A, B in the parametrization $S^{-1} = -i\not{p}A - B$ reduce to $A = 1$ and $B = m_q$. This suggests that we use for the pion-quark vertex[3]

$$\Gamma_{5,q} = -\gamma^5 \frac{B(k^2) + B(p^2)}{2f_\pi} = -\gamma^5 \frac{B}{f_\pi} \, , \tag{4.14}$$

and discard the three additionally possible Dirac structures. The momenta of outgoing and incoming quark are k and p, respectively. The reason is that in the chiral limit eq. (4.14) represents the exact pion Bethe-Salpeter amplitude (on-shell, *i.e.* $Q^2 = 0$) for equal quark and antiquark momenta, since in this limit, with constant A, the Dyson-Schwinger equation for the scalar function B agrees with the Bethe-Salpeter equation for a pion of zero momentum. Of course, the subdominant amplitudes should in principle be included for physical pions (with momentum $P^2 = -m_\pi^2$), when solving the Dyson-Schwinger equation for A and B and the Bethe-Salpeter equation for the pion in mutually consistent truncations [48, 87, 64]. The generalization to pion off-shell momenta as used in eq. (4.14) is by no means unique but certainly the most simple one.

We use chiral symmetry constraints to construct the pseudovector-quark vertex $\Gamma_{5,q}^\mu$. In the chiral limit, the Ward-Takahashi identity for this vertex reads,

$$Q^\mu \Gamma_{5,q}^\mu = S^{-1}(k)\gamma^5 + \gamma^5 S^{-1}(p) \, , \quad (Q = k - p) \, . \tag{4.15}$$

To satisfy this constraint we use the form of the vertex proposed in ref. [88],

$$\Gamma_{5,q}^\mu = -i\gamma^\mu \gamma^5 + \frac{Q^\mu}{Q^2} 2f_\pi \Gamma_{5,q} \, . \tag{4.16}$$

The physical picture behind this form of the vertex is clear. In the spontaneously broken phase of chiral symmetry the quark acquires mass and at the same time the Goldstone boson pole must appear in the full quark-pseudovector vertex, and the Goldstone boson pole in turn is proportional to the generated quark mass. The second term which contains the massless pion pole does not contribute to g_A as can be seen from eq. (4.6).

The pion and the pseudovector current can couple to the diquarks by an intermediate quark loop. As for the anomalous contributions to the electromagnetic current, we derive the Lorentz structure of the diquark vertices and calculate their effective strengths from this quark substructure of the diquarks in appendix B.1.2. For momentum definitions at these vertices we refer to figure 3.1.

---

[3]We drop the flavor indices on the vertices in the following. Each pseudoscalar vertex comes with a factor of τ^a and each pseudovector vertex with a factor of $\tau^a/2$ as these are widely used conventions.

As already mentioned in the last section, no such couplings arise for the scalar diquark. This can be inferred from parity or covariance or, simpler, one considers the flavor trace of an isovector current between two isoscalar states (scalar diquark vertex) which yields zero. The axialvector diquark and the pion couple by an anomalous vertex. Its Lorentz structure is similar to that for the photon-induced scalar-to-axialvector transition in eq. (3.32),

$$\Gamma_{5,ax}^{\alpha\beta} = \frac{\kappa_{ax}^5}{2M_n}\frac{m_q}{f_\pi}\epsilon^{\alpha\beta\mu\nu}(p_d + k_d)^\mu Q^\nu \; . \tag{4.17}$$

Here, α and β are the Lorentz indices of outgoing and incoming diquark, respectively. The factor m_q/f_π comes from the quark-pion vertex (4.14) in the quark loop (see appendix B.1.2), and the nucleon mass was introduced to isolate a dimensionless constant κ_{ax}^5.

The pseudovector current and the axialvector diquark are also coupled by anomalous terms. As before, we denote with α and β the Lorentz indices of outgoing and incoming diquark, respectively, and with μ the pseudovector index. Out of three possible Lorentz structures for the regular part of the vertex,

$$p_d^\mu \; \epsilon^{\alpha\beta\rho\lambda}p_d^\rho Q^\lambda \; , \quad \epsilon^{\mu\alpha\beta\rho}Q^\rho \quad \text{and} \quad \epsilon^{\mu\alpha\beta\rho}(p_d + k_d)^\rho \; ,$$

only the last term contributes to g_A in the limit $Q \to 0$. We furthermore verified numerically that the first two terms yield negligible contributions to the form factor also for nonzero Q. Again, the pion pole contributes proportionally to Q^μ, and our *ansatz* for the vertex thus reads

$$\Gamma_{5,ax}^{\mu\alpha\beta} = \frac{\kappa_{\mu,ax}^5}{2}\epsilon^{\mu\alpha\beta\nu}(p_d + k_d)^\nu + \frac{Q^\mu}{Q^2}2f_\pi\Gamma_{5,ax}^{\alpha\beta} \; . \tag{4.18}$$

For both coupling strengths in the vertices $\Gamma_{5,ax}^{\alpha\beta}$ and $\Gamma_{5,ax}^{\mu\alpha\beta}$ we roughly obtain $\kappa_{ax}^5 \simeq \kappa_{\mu,ax}^5 \simeq 4.5$ slightly dependent on the parameter set, see table B.2 in appendix B.1.2.

Scalar-to-axialvector transitions are also possible by the pion and the pseudovector current. An effective vertex for the pion-mediated transition has one free Lorentz index to be contracted with the axialvector diquark. Therefore, two types of structures exist, one with the pion momentum Q, and the other with any combination of the diquark momenta p_d and k_d. If we considered this transition as being described by an interaction Lagrangian of scalar, axialvector and pseudoscalar fields, terms of the latter structure would be proportional to the divergence of the axialvector field which is a constraint that can be set to zero. We therefore adopt the following form for the transition vertex,

$$\Gamma_{5,sa}^\beta = -i\kappa_{sa}^5\frac{m_q}{f_\pi}Q^\beta \; . \tag{4.19}$$

Here the Lorentz index of the participating axialvector diquark is given by β. This vertex corresponds to a derivative coupling of the pion to scalar and axialvector diquark.

The pseudovector-induced transition vertex has two Lorentz indices, denoted by μ for the pseudovector current and β for the axialvector diquark. From the momentum transfer Q^μ and one of the diquark momenta altogether five independent tensors can be constructed,

$$\delta^{\mu\beta} , \quad Q^\mu Q^\beta , \quad Q^\mu p_d^\beta , \quad p_d^\mu Q^\beta \quad \text{and} \quad p_d^\mu p_d^\beta .$$

Note that a term constructed with the totally antisymmetric tensor would have the wrong parity. We assume, as before, that all terms proportional to Q^μ are contained in the pion part. They do not contribute to g_A anyway. From the diquark loop calculation in appendix B.1.2 we find that the terms proportional to $p_d^\mu Q^\beta$ and $p_d^\mu p_d^\beta$ can again be neglected with an error on the level of one per cent. Therefore, we use a vertex of the form,

$$\Gamma_{5,sa}^{\mu\beta} = i M_n \kappa_{\mu,sa}^5 \, \delta^{\mu\beta} + \frac{Q^\mu}{Q^2} 2 f_\pi \Gamma_{5,sa}^\beta. \tag{4.20}$$

For the strengths of these two transition vertices we obtain $\kappa_{sa}^5 \simeq 3.9$ and (on average) $\kappa_{\mu,sa}^5 \simeq 2.1$, *cf.* table B.2 in appendix B.1.2.

The vertices $\Gamma_{5,as}^\beta$, $\Gamma_{5,as}^{\mu\beta}$ for the reverse transitions are obtained by simply reversing the sign of Q.

Having constructed all vertices, we can now perform the flavor algebra and write down the pseudoscalar current matrix element in the extended impulse approximation. As done in section 3.1.1 we introduce quark current matrix elements by

$$\langle J_{5,q} \rangle^{\text{sc-sc}} = \bar{\Psi}^5 \, D^{-1} \, \Gamma_{5,q} \, \Psi^5 , \tag{4.21}$$

where this time *no* flavor matrix factor comes with $\Gamma_{5,q}$ as we compute the flavor factors separately. Likewise scalar/axialvector diquark and the transition matrix elements are defined. With these definitions we find for the matrix element of the extended impulse approximation

$$\begin{aligned} {}_\text{p}\langle P_f| \, J_5^3 \, |P_i\rangle_\text{p}^{\text{e-imp}} &= \langle J_{5,q} \rangle^{\text{sc-sc}} - \frac{1}{3} \langle J_{5,q} \rangle^{\text{ax-ax}} + \frac{2}{3} \langle J_{5,dq} \rangle^{\text{ax-ax}} + \\ &\quad \frac{\sqrt{3}}{3} \left(\langle J_{5,sa} \rangle^{\text{sc-ax}} + \langle J_{5,as} \rangle^{\text{ax-sc}} \right) . \end{aligned} \tag{4.22}$$

As we neglect seagull contributions, the only contribution from the Bethe-Salpeter

kernel is due to the coupling to the exchange quark and it reads explicitly

$$
\begin{aligned}
{}_{\mathrm{p}}\langle P_f|\, J_5^3\, |P_i\rangle_{\mathrm{p}}^{\mathrm{BS-ker}} &= \langle J_{5,ex}\rangle \\
&= -\tfrac{1}{2}\left(\begin{array}{cc} \bar{\Psi}^5 & \bar{\Psi}^\alpha \end{array}\right)
\left(\begin{array}{cc} K_{ex,ss}^5 & K_{ex,sa}^5 \\ K_{ex,as}^5 & K_{ex,aa}^5 \end{array}\right)
\left(\begin{array}{c} \Psi^5 \\ \Psi^\beta \end{array}\right) , \\
K_{ex,ss}^5 &= \chi^5(p_1)\, S^T(q)\, (\Gamma_{5,q})^T\, S^T(q')\, \bar{\chi}^5(p_2) , \\
K_{ex,sa}^5 &= \tfrac{1}{3}\sqrt{3}\, \chi^\beta(p_1)\, S^T(q)\, (\Gamma_{5,q})^T\, S^T(q')\, \bar{\chi}^5(p_2) , \\
K_{ex,as}^5 &= \tfrac{1}{3}\sqrt{3}\, \chi^5(p_1)\, S^T(q)\, (\Gamma_{5,q})^T\, S^T(q')\, \bar{\chi}^\alpha(p_2) , \\
K_{ex,aa}^5 &= \tfrac{5}{3}\, \chi^\beta(p_1)\, S^T(q)\, (\Gamma_{5,q})^T\, S^T(q')\, \bar{\chi}^\alpha(p_2) .
\end{aligned}
\tag{4.23}
$$

The diagrams of the extended impulse approximation are equivalent to those displayed in figure 3.2 and likewise the exchange quark diagram is similar to the first diagram in figure 3.4. The black dot which represents the quark-photon or diquark-photon vertex should be replaced with the appropriate quark-pseudoscalar or diquark-pseudoscalar vertex. The matrix elements for the pseudovector current differ from eqs. (4.22,4.23) only by an overall factor of 1/2 after replacing the pseudoscalar vertices by their pseudovector counterparts.

4.3 Numerical results

Having defined the pseudoscalar and pseudovector current operators in the last section and having fixed all unknown coupling constants by appropriate quark loop calculations, *cf.* appendix B.1.2, we can now compute the form factors for the two parameter sets of table 2.8. Regarding the numerical procedure, the method and its intricacies have been lined out in section 3.2.1 and all the remarks made in this section also apply here. We summarize: impulse approximation diagrams are computed in the Breit frame employing boosted vertex functions Φ and taking into account the residue contributions, *cf.* appendix B.2. The exchange quark diagram can only be computed using boosted wave functions Ψ and therefore the related numerical accuracy becomes very limited beyond momentum transfers $Q^2 > 2.5$ GeV^2.

Examining $g_{\pi NN}(0)$ which is assumed to be close to the physical pion-nucleon coupling and the weak coupling constant $g_A(0)$, we find large contributions to both arising from the scalar-axialvector transitions, *cf.* table 4.1. As mentioned in the previous section, the various diquark contributions violate the Goldberger-Treiman relation. Some compensations occur between the small contributions from the axialvector diquark coupling in impulse approximation and the compar-

	Set I		Set II	
	$g_{\pi NN}(0)$	$g_A(0)$	$g_{\pi NN}(0)$	$g_A(0)$
$\langle J_{5,q}^{[\mu]} \rangle^{\text{sc-sc}}$	7.96	0.76	9.25	0.86
$\langle J_{5,q}^{[\mu]} \rangle^{\text{ax-ax}}$	0.50	0.04	0.10	0.01
$\langle J_{5,dq}^{[\mu]} \rangle^{\text{ax-ax}}$	1.44	0.18	0.34	0.04
$\langle J_{5,sa}^{[\mu]} \rangle^{\text{sc-ax}} + \langle J_{5,as}^{[\mu]} \rangle^{\text{ax-sc}}$	5.66	0.39	3.79	0.22
$\langle J_{5,ex}^{[\mu]} \rangle$	1.69	0.12	2.70	0.22
SUM	17.25	1.49	16.18	1.35
experiment	$g_{\pi NN}$ 13.14 ± 0.07 [89] 13.38 ± 0.12 [90]		g_A 1.267 ± 0.0035 [84]	

Table 4.1: Various contributions to $g_{\pi NN}(0)$ and $g_A(0)$, labelled as in table 3.2.

atively large ones from scalar-axialvector transitions which provide the dominant effect to yield $g_A(0) > 1$.

Summing all these contributions, the Goldberger-Treiman discrepancy,

$$\Delta_{GT} \equiv \frac{g_{\pi NN}(0)}{g_A(0)} \frac{f_\pi}{M_n} - 1 \qquad (4.24)$$

amounts to 0.14 for Set I and 0.18 for Set II. The larger discrepancy for Set II (with weaker axialvector correlations) is due to the larger violation of the Goldberger-Treiman relation from the exchange quark contribution in this case. This contribution is dominated by the scalar amplitudes, and its Goldberger-Treiman violation should therefore be compensated by appropriate *chiral seagulls* as already mentioned in section 4.1. For Set II which is dominated by scalar correlations within the nucleon, their contribution to $g_A(0)$ can be estimated to be around 0.1 because the seagulls together with the contributions from $\langle J_{5,q}^{[\mu]} \rangle^{\text{sc-sc}}$ and $\langle J_{5,ex}^{[\mu]} \rangle$ should approximately obey the Goldberger-Treiman relation.

The strong and weak radii are presented in table 4.2 and the corresponding form factors in figure 4.1. Experimentally the axial form factor is known much less precisely than the electromagnetic form factors. In the right panel of figure 4.1 the experimental situation is summarized by a band of dipole parametrizations of g_A that are consistent with a wide-(energy)band neutrino experiment [85]. Besides the slightly too large values obtained for $Q^2 \to 0$ which are likely to be due to the PCAC violations of axialvector diquarks and of the missing seagulls as

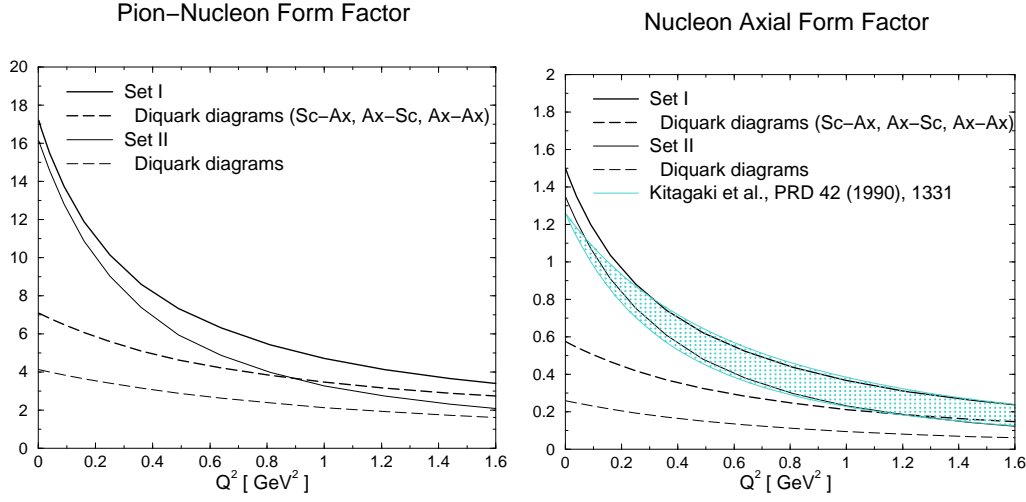Pion–Nucleon Form Factor   Nucleon Axial Form Factor

Figure 4.1: The pion-nucleon form factor $g_{\pi NN}(Q^2)$ and the axial form factor $g_A(Q^2)$. 'Diquark diagrams' labels the sum of the impulse-approximate axialvector contributions and scalar-axialvector transitions. The shaded region in the right panel represents the uncertainty in g_A as determined from quasi-elastic neutrino scattering when a dipole form is fitted to both, the vector and the axial form factor [85].

discussed in section 4.1, our results yield quite compelling agreement with the experimental bounds. As in the case of the electromagnetic form factors we observe a dominance of the diquark contributions for larger Q^2.

Turning to the pion-nucleon form factor we have fitted our results to an n-pole,

$$g_{\pi NN}(Q^2) = \frac{g_{\pi NN}(0)}{(1 + Q^2/\Lambda_n^2)^n} \ . \tag{4.25}$$

The form factor of Set I is close to a *monopole*, $n = 1$, with cut-off $\Lambda_1 = 0.6$ GeV, whereas the one of Set II is better approximated by a *dipole*, $n = 2$, with cut-off

		Set I	Set II	experiment
$r_{\pi NN}$	[fm]	0.83	0.81	
r_A	[fm]	0.82	0.81	0.70±0.09

Table 4.2: Strong radius $r_{\pi NN}$ and weak radius r_A, the experimental value of the latter is taken from [85].

$\Lambda_2 = 0.9$ GeV. The exponent n is determined by the strength of the diquark contributions whereas the cut-off has to comply with the slope at $Q^2 = 0$ (the radius). It is not a big surprise that the proton electromagnetic radii and the pionic/axial radii are very close to each other since the dominating impulse approximation diagrams have a very similar behavior for all observables.

As we have mentioned in the beginning of the chapter, pion-nucleon form factors are used in one-boson exchange potential *ansätze* to describe the NN force. Most of the potentials that fit the data employ a monopole with a large cut-off, $\Lambda_1 \geq 1.3$ GeV, see *e.g.* ref. [91]. However, other nucleon models, lattice and QCD sum rule calculations indicate a monopole behavior with a much smaller cut-off $\Lambda_1 \approx 0.5 - 0.95$ GeV, *cf.* ref. [92] and references therein. Our calculations support this point of view.

Summarizing the results of this section, we have found moderate violations of PCAC and the Goldberger-Treiman relation. These violations are estimated to be partitioned equally between the effects of neglecting chiral seagulls and vector diquarks. The inclusion of axialvector diquarks is essential to obtain values for the weak coupling constant $g_A > 1$. Of particular importance for this result are the transitions between scalar and axialvector diquarks, additionally they restrict the axialvector correlations within the nucleon to be small. For the pion-nucleon form factor, our model calculations support a monopole- or dipole-like fall-off with a cut-off well below 1 GeV.

Chapter 5

Effective Confinement

In this chapter we will investigate the possibility of incorporating confinement into the diquark-quark model by a suitable modification of quark and diquark propagators. As will become clear in the following, this will enable us to calculate the mass spectrum of octet and decuplet baryons. Electromagnetic form factors recomputed with the modified propagators reveal a drastic increase on the magnetic moments, being almost too much of an improvement. We have done the calculations for *pointlike* and for *extended* diquarks to demonstrate the necessity of the latter for a consistent description of masses and electromagnetic structure. Although the results for the spectrum and the magnetic moments are encouraging, there are serious difficulties associated with this approach of implementing confinement, both motivated from "theoretical" and "phenomenological" arguments.

Remember that the propagators along with the diquark vertices are the only ingredients of the model after the full 3-quark problem has been reduced, *cf.* the summary at the end of section 2.1. By choosing the most simple *ansätze* for them, *i.e.* free spin-1/2 and spin-0/spin-1 propagators for quark and diquark we have succeeded to describe quite successfully various spacelike nucleon form factors. However, shortcomings remain which might be cured by allowing for non-trivial propagators. These shortcomings are:

- To incorporate the Δ into the description, rather large quark and axialvector diquark masses have to be chosen, as their sum must be larger than the mass of the Δ. This problem extends to the strange quark mass and strange diquarks when aiming at including the whole octet-decuplet spectrum.

- The isovector part of the nucleon magnetic moments is too small, even after inclusion of the axialvector diquarks. The difference is substantial for parameter sets which fit the Δ mass. A reason for this, besides too large a constituent quark mass, might be the insufficiency of the bare quark-photon vertex to account for the quark contributions to the magnetic moments. Gauge

invariance demands, however, that a nonperturbative quark-photon vertex is intimately connected with a nonperturbative quark propagator.

- Hadronic reactions where *timelike* momenta of the order of 1 GeV are deposited onto nucleons, *e.g.* meson production processes, cannot be described within the model in its present form. The free-particle poles of quark and diquark cause unphysical thresholds in these processes.

As we see, the lack of confinement which is manifest in the poles of the quark and diquark propagators used so far is the main motivation to consider alterations in the model premises. At this stage we hope that the necessary modifications in the quark-photon vertex which are required by gauge invariance will improve the results on the magnetic moments as well.

5.1 Confinement in model propagators

Confinement is understood as the absence of colored states in the spectrum of observed particles. From a phenomenological point of view (as adopted here), calculations of S matrix elements using diagrams with internal quark loops must not have any imaginary parts which are associated with the singularities of the quark propagators. So, either they are absent or their contributions cancel in some manner [21]. In this way, one is led to consider the following possibilities, which are not necessarily the only ones:

a. Propagators are entire functions in the whole complex plane [93]. If they are to be analytic, they must possess an essential singularity in the infinite. An example is the function $f(x) = e^x$.

b. Propagators have complex conjugate poles [94]. In some sense the poles correspond to virtual excitations that cancel each other in physical amplitudes. Here an example is provided by the function $f(x) = x/(a^2 + x^2)$.

We will investigate the consequences of propagators being entire analytic functions. We insist here on analyticity in order not to loose the relativistic reparametrization invariance related to the choice of the momentum partitioning parameter η.[1] A word of caution is in order here. The Wick rotation which connects

---

[1]As explained in section 2.3.1, η invariance requires the following: If $\Psi(p, P; \eta_1)$ is a solution of the Bethe-Salpeter equation then $\Psi(p + (\eta_2 - \eta_1)P, P; \eta_2)$ with $\eta_2 \neq \eta_1$ is also one. In the rest frame of the bound state, $P = (\mathbf{0}, iM_n)$, this can be shown to be valid if the integration of the quark exchange kernel $K^{\mathrm{BS}}(p, k, P)$ over the component k^4 can be shifted as $k^4 \to k^4 + (\eta_2 - \eta_1)iM_n$. This is of course possible, if the propagators are analytic in the complex domain of k^4 given by $(\mathrm{Re}\, k^4, \mathrm{Im}\, k^4) \in ((-\infty, +\infty), [0, (\eta_2 - \eta_1)M_n])$.

Minkowski and Euclidean metric is no longer applicable as the propagators possess the essential singularity at infinity. Furthermore we are aware that this propagator contradicts general arguments about the behavior of propagators in gauge theories with confinement. Following ref. [95], it should vanish for $p^2 \to \infty$ in *all* directions of the complex p^2-plane faster than the free propagator (p is the particle momentum). Furthermore the propagators should have cuts along the *real p^2-axis*. Unphysical colored states associated with these cuts are then to be removed from the observable spectrum by other conditions such as a suitable definition of a physical subspace (*cf.* the long-known Gupta-Bleuler mechanism to remove scalar and longitudinal photons from the physical particle spectrum in QED [96]). It seems to be impossible to implement propagators which behave as indicated above and such a projection onto physical states in actual matrix element calculations at present, though. Therefore we believe it is instructive to investigate some phenomenological advantages and deficiencies of an "entire" propagator. In practical calculations, the quark propagator will be needed only on a limited domain in the complex plane and the essential singularity thus poses no practical difficulty, at least for the form factor calculations presented here.

The second possible form for the propagator mentioned above suffers from only one principal deficiency, as there are complex conjugate pole associated with it. The asymptotic conditions in the complex plane are in this case easy to incorporate. Actual calculations with this form are harder to perform and are currently under investigation.

Before we turn to the propagator parametrization chosen here, we discuss some aspects of the quark propagator that are known so far. We regard the quark propagator to be given in its most general form, $S^{-1} = -i\not{p}\,A - B$, with A, B being scalar functions. Information about the quark propagator may be obtained from calculations within the framework of Dyson-Schwinger equations, for a recent review see ref. [21]. In the near future, lattice results will provide us with more "empirical" information, for a recent study in quenched QCD see ref. [97]. Unfortunately, the quark propagator is usually computed in both schemes only for positive real p^2, where p is the Euclidean quark momentum, therefore the immediate benefit for phenomenological calculations is limited. However, these calculations have established an important generic feature. In rainbow truncation of the Dyson-Schwinger equations as well as in improved truncation schemes it could be shown that the quark acquires an effective constituent mass, *i.e.* $M(0) = B(0)/A(0)$ is non-zero for a vanishing current quark mass. This feature of dynamical chiral symmetry breaking has also been observed in the already mentioned lattice calculation [97]. For phenomenological calculations, the numerical results for A, B have been fitted to entire functions which has been successfully used in the description of (spacelike) meson [98] and nucleon properties [78, 79]. The most impressive success in this direction has been achieved in a combined rainbow/ladder

truncation scheme for quarks and mesons employing a specific gluon propagator which displays significant enhancement at momenta of the order of a few hundred MeV. Here the quark propagator has been computed from Dyson-Schwinger equations on *all* complex momentum points[2] where it has been needed to solve the Bethe-Salpeter equation for mesons and to compute their electric form factors [64, 65, 99]. Additionally the quark-photon vertex has been obtained from the solution of a corresponding inhomogeneous Bethe-Salpeter equation [100]. In these studies the solution for the quark propagator exhibited no poles for the (complex) momenta sampled by the meson calculations. These calculations support the working hypothesis of a quark propagator having no poles, at least in the interesting momentum regime.

In eq. (2.64) we have already indicated a possible parametrization of the quark propagator by multiplying the free one with a single dressing function $C(p^2, m)$. We choose a function for C which is entire and analytic and removes the free-particle pole in the denominator of the free propagator,

$$C(p^2, m) \equiv C^{\mathrm{exp}}(p^2, m) = 1 - \exp\left(-d\, \frac{p^2 + m^2}{m^2}\right) \ . \tag{5.1}$$

The essential singularity occurs here for $p^2 \to -\infty$. The parameter d regulates the modification as compared to the free propagator. If d is large, the spacelike properties remain nearly unchanged, whereas for timelike momenta the propagator blows up quickly. For small $d \lesssim 1$, even the spacelike behavior is substantially modified.

For simplicity, we apply the same modification to the propagators of scalar and axialvector diquarks, *cf.* eqs. (2.45,2.46). Additionally we choose $\xi = 1$ in eq. (2.46). This parameter is a gauge parameter when describing the interaction of a vector field with photons [75]. The photon vertex with the axialvector diquark has to be modified correspondingly.

We note that due to the absence of poles the "masses" m_q, m_{sc}, m_{ax} have no physical interpretation. They are merely width parameters of the propagator.

5.2   The octet-decuplet mass spectrum

Equipped with propagators which effectively mimic confinement we can calculate the mass spectrum of octet and decuplet baryons. This investigation has been reported in ref. [24]. In doing so, we have to extend all previous considerations to flavor $SU(3)$ and introduce explicit symmetry breaking as visible in the experimental spectrum. However, we will confine ourselves to the limit of unbroken

---

[2]This was rendered possible through the analytical *ansatz* for the gluon propagator.

isospin and, accordingly, the *strange* quark mass is the only source of symmetry breaking, $m_s \neq m_u = m_d$, where m_u, m_d denote the mass parameters of *up* and *down* quark.

In order to limit the number of parameters we assume the scalar and axialvector diquark mass parameters to be equal and introduce a diquark mass coefficient ζ by

$$m_{sc}^{ab} = m_{ax}^{ab} = \zeta(m_a + m_b) \quad (a, b \in \{u, d, s\}) . \tag{5.2}$$

Thus ab denotes the flavor content of the diquark. It will be interesting to see whether the mass differences between spin-1/2 and spin-3/2 baryons can be explained without an explicitly larger axialvector diquark mass parameter.

Diquark 3×3 flavor matrices $\left(t_{(ab)}\right)_{jk}$ are chosen antisymmetric for scalar diquarks,

$$t_{(ud)} = -\frac{i}{\sqrt{2}} \lambda^2 , \quad t_{(us)} = -\frac{i}{\sqrt{2}} \lambda^5 , \quad t_{(ds)} = -\frac{i}{\sqrt{2}} \lambda^7 . \tag{5.3}$$

Here we use for the λ's the standard Gell-Mann matrices [40]. Axialvector diquark matrices $\left(t_{[ab]}\right)_{jk}$ are symmetric in their indices j, k,

$$t_{[ud]} = \frac{1}{\sqrt{2}} \lambda^1 , \quad t_{[us]} = \frac{1}{\sqrt{2}} \lambda^4 , \quad t_{[ds]} = \frac{1}{\sqrt{2}} \lambda^6 ,$$
$$t_{[uu]} = \delta_{j1}\delta_{k1} , \quad t_{[dd]} = \delta_{j2}\delta_{k2} , \quad t_{[ss]} = \delta_{j3}\delta_{k3} . \tag{5.4}$$

To derive the Bethe-Salpeter equations for the octet (N, Λ, Σ, Ξ) and decuplet baryons (Δ, Σ^*, Ξ^*, Ω), one starts with their flavor wave functions prescribed by the Eightfold Way. The octet baryons have scalar diquark correlations, therefore this part of the flavor wave function is mixed antisymmetric. The axialvector diquark correlations for octet members are described in flavor space by a sum of two mixed antisymmetric states. For the decuplet members with only axialvector diquarks contributing these are either totally symmetric ($\Delta^{++}, \Delta^-, \Omega$) or mixed symmetric states. These wave functions may contain different mass eigenstates of quark-diquark pairs. For these mass eigenstates the system of coupled Bethe-Salpeter equations has to be solved, where the decomposition in the Dirac algebra according to section 2.4 can be used. As an example we consider the Σ^+ hyperon with its flavor wave function

$$|\Sigma^+\rangle_{\text{flavor}} = \begin{pmatrix} u(su) \\ \sqrt{\tfrac{1}{3}}u[us] - \sqrt{\tfrac{2}{3}}s[uu] \end{pmatrix} . \tag{5.5}$$

The scalar diquark part, $u(su)$ is clearly mixed antisymmetric and the axialvector diquark part is the normalized sum of $(us - su)u$ and $uus - suu$, both also mixed

		experi-ment	pointlike	extended diquark
			$V(p) = 1$	$V(p) = \left(\dfrac{\lambda^2}{\lambda^2 + p^2} \right)^4$ $\lambda = 0.5$ GeV
m_u	[GeV]		0.50	0.56
m_s	[GeV]		0.63	0.68
ξ			0.73	0.60
g_a/g_s			1.37	0.58
M_Λ		1.116	1.133	1.098
M_Σ		1.193	1.140	1.129
M_Ξ	[GeV]	1.315	1.319	1.279
M_{Σ^*}		1.384	1.380	1.396
M_{Ξ^*}		1.530	1.516	1.572
M_Ω		1.672	1.665	1.766

Table 5.1: Octet and decuplet masses.

antisymmetric. The Dirac-flavor wave function contains three independent terms $\Psi^5_{u(us)}$, $\Psi^\mu_{s[uu]}$ and $\Psi^\mu_{u[us]}$ with a total of 2+6+6=14 unknown scalar functions which shows the necessary increase of computer resources.

We have listed the Bethe-Salpeter equations for all octet and decuplet baryons in appendix A.4 and quote from the results given there just one remarkable fact. Due to the symmetry breaking, there occurs mixing of the flavor singlet wave function with the scalar diquark correlations within the Λ. This mixing is absent in quark potential models.

As the diquarks here can never be on-shell, we are not allowed to use the normalization conditions (2.59,2.60) to fix the quark-diquark coupling strengths g_s and g_a. Therefore we adjust them to the masses of nucleon and Δ, $M_n = 0.939$ GeV and $M_\Delta = 1.232$ GeV.

In table 5.1 we show results for the masses of the remaining baryons (i) for pointlike diquarks and (ii) for a quadrupole-like diquark vertex function. For both cases the octet-decuplet mass difference is a result of solely the relativistic dynamics; it is even overestimated for extended diquarks. The parameter set using the

extended diquarks allows a considerable reduction of the ratio g_a/g_s as compared to the ratio for pointlike diquarks. Still, axialvector correlations are somewhat too strong regarding the constraints which have been obtained in chapters 3 and 4.

As can be seen from table 5.1, the calculated baryon masses are higher for the spin-3/2 states than the sum of the quark and diquark mass parameters. Due to the absence of poles, it is possible to smoothly cross the tree-level thresholds given by the boundaries for the momentum partitioning parameter η in eqs. (2.154,2.155), *cf.* the discussion in refs. [58, 22].

These results have been obtained with the choice $d = 1$ in the propagator modification function C^{exp}, *cf.* eq. (5.1), corresponding to a quite substantial modification of the spacelike propagator properties. Since mainly these are important for solving the Bethe-Salpeter equation as well as for the calculation of form factors, we expect visible changes for the latter as well. We will now turn to this issue.

5.3   Electromagnetic form factors

In order to use the machinery developed in chapter 3 for calculating the form factors, we have to re-specify the basic quark and diquark vertices. To satisfy gauge invariance, the quark vertex must fulfill the Ward-Takahashi identity

$$(k - p)^\mu \, \Gamma_q^\mu = q_q \, \left(S^{-1}(k) - S^{-1}(p) \right) \; , \tag{5.6}$$

with the quark propagator being dressed by the function C^{exp} of eq. (5.1). The scalar functions A, B are given in terms of C^{exp} by

$$A(p^2) = \frac{1}{C^{\text{exp}}(p^2, m_q)} \; , \qquad B(p^2) = \frac{m_q}{C^{\text{exp}}(p^2, m_q)} \; . \tag{5.7}$$

It turns out that the longitudinal part of the quark vertex is unambiguously given by the Ball-Chiu *ansatz* [101], labelled by the superscript BC,

$$\Gamma_q^\mu \quad = \quad q_q \left(\Gamma_q^{\mu,\text{BC}} + \Gamma_{q,T}^\mu \right) \; , \tag{5.8}$$

$$\Gamma_q^{\mu,\text{BC}} \quad = \quad -i \, \frac{A(k^2) + A(p^2)}{2} \, \gamma^\mu - \tag{5.9}$$

$$i \, \frac{(k+p)^\mu}{k^2 - p^2} \left[(A(k^2) - A(p^2)) \frac{\slashed{k} + \slashed{p}}{2} - i \, (B(k^2) - B(p^2)) \right] \; .$$

Its exclusivity results if the following four conditions are valid:

1. It satisfies the Ward-Takahashi identity (5.6).

2. It does not possess any kinematical singularities.

3. It transforms under parity, charge conjugation and time reversal as the free vertex.

4. It reduces to the free vertex for $A = 1$ and $B = m_q$.

The transverse part of the vertex, $\Gamma_{q,T}^{\mu}$, remains undetermined. We will put it to zero in the following which is certainly an oversimplification regarding the information about it which has been obtained during the last years. It has been shown in ref. [102] that the requirement of multiplicative renormalizability greatly restricts the tensor structure of the transversal vertex. For large spacelike momenta Q, where no resonances are present, this leads to a phenomenologically unimportant vertex modification. For the small and moderate momentum transfers at which we investigate the form factors, a transversal term which contains the effect of the ρ meson pole might turn out to be of importance for the quark-photon vertex. The already mentioned study in ref. [100] has obtained the *full* quark-photon vertex as a solution of an inhomogeneous Bethe-Salpeter equation. The quark-antiquark scattering kernel in the vector channel must enter the equation for the quark-photon vertex as well, thereby the solution for the full vertex contains the vector meson pole as the pole also appears in the full quark-antiquark scattering amplitude. Besides having found this vector meson pole contribution (being transversal) to the quark-photon vertex, the study has numerically confirmed that the longitudinal part of the vertex is given by the Ball-Chiu recipe. Within this model context, the remnants of the vector meson pole have been shown to contribute about 30 % to the full pion charge radius r_π, with the remainder being attributable to the Ball-Chiu vertex.

In order to create a link to the old and, at this time, fairly successful picture of vector meson dominance, it would be interesting to investigate the influence of the vector meson pole also for the nucleon form factors. This requires, however, a tremendous effort to use an effective gluon interaction like the one from ref. [100] for the quark-antiquark and quark-quark scattering kernels to describe mesons *and* diquarks, to obtain the quark-photon vertex self-consistently, and to calculate or reliably parametrize the quark propagator in the complex plane where it is needed for calculations of nucleon properties. This is beyond the scope of this work.

Having introduced the Ball-Chiu vertex as an approximation to the full quark-photon vertex and having discussed possible shortcomings, let us turn to the diquark-photon vertices. We make use of the Ward-Takahashi identities for scalar and axialvector diquarks,

$$(k - p)^{\mu} \, \Gamma_{sc[ax]}^{\mu,[\alpha\beta]} = q_{sc[ax]} \, \left((D^{-1})^{[\alpha\beta]}(k) - (D^{-1})^{[\alpha\beta]}(p) \right) \, , \qquad (5.10)$$

to fix the longitudinal part of the respective photon vertices. Neglecting again transversal parts, we find for the vertices,

$$\Gamma^\mu_{sc} = -q_{sc} (k+p)^\mu \frac{\dfrac{k^2 + m^2_{sc}}{C^{\exp}(k^2, m_{sc})} - \dfrac{p^2 + m^2_{sc}}{C^{\exp}(p^2, m_{sc})}}{k^2 - p^2} , \qquad (5.11)$$

$$\Gamma^{\mu,\alpha\beta}_{ax} = -q_{ax} (k+p)^\mu \delta^{\alpha\beta} \frac{\dfrac{k^2 + m^2_{ax}}{C^{\exp}(k^2, m_{ax})} - \dfrac{p^2 + m^2_{ax}}{C^{\exp}(p^2, m_{ax})}}{k^2 - p^2} +$$

$$q_{ax} (1 + \kappa) \left(Q^\beta \delta^{\mu\alpha} - Q^\alpha \delta^{\mu\beta} \right) . \qquad (5.12)$$

The last term in eq. (5.12) is transversal and therefore no dressing can be inferred from the Ward-Takahashi identity. For this reason, we do not modify this term. Compared to the bare vertex, eq. (3.31), the transversal term appears with a modified prefactor, $(1 + \kappa)$ instead of κ where κ denotes the anomalous magnetic moment. This is a consequence of choosing the gauge parameter $\xi = 1$ in the dressed propagator [75].

Anomalous transitions between scalar and axialvector diquarks are of course possible as well. Their vertices remain unchanged, *cf.* eqs. (3.32,3.33).

We can determine the unknown anomalous magnetic moment κ appearing in eq. (5.12) and the strength of the scalar-to-axialvector transitions κ_{sa} from eqs. (3.32,3.33) by much the same procedure as described in section 3.1 and appendix B.1.1. That is, we calculate the resolved diquark vertices from figure 3.1, of course by using the dressed quark propagator and quark-photon vertex given above, and re-adjust the diquark normalization (coupling) constants $g_a \to g_a^{\text{resc}}$ and $g_s \to g_s^{\text{resc}}$ such that the differential Ward identity is fulfilled, *cf.* appendix B.1.1. Using these rescaled quantities g_a^{resc} and g_s^{resc}, we determine κ and κ_{sa}.

For pointlike diquarks as used by the first parameter set of table 5.1 the calculation of the resolved vertices leads to divergent integrals and therefore prohibits their use. We have performed the calculation for the second parameter set from

	g_s^{resc}/g_s	g_a^{resc}/g_a	κ	κ_{sa}
extended diquarks	0.73	1.33	0.69	1.76

Table 5.2: Rescaled diquark normalizations and constants of photon-diquark couplings for the parameter set with extended quarks, *cf.* table 5.1.
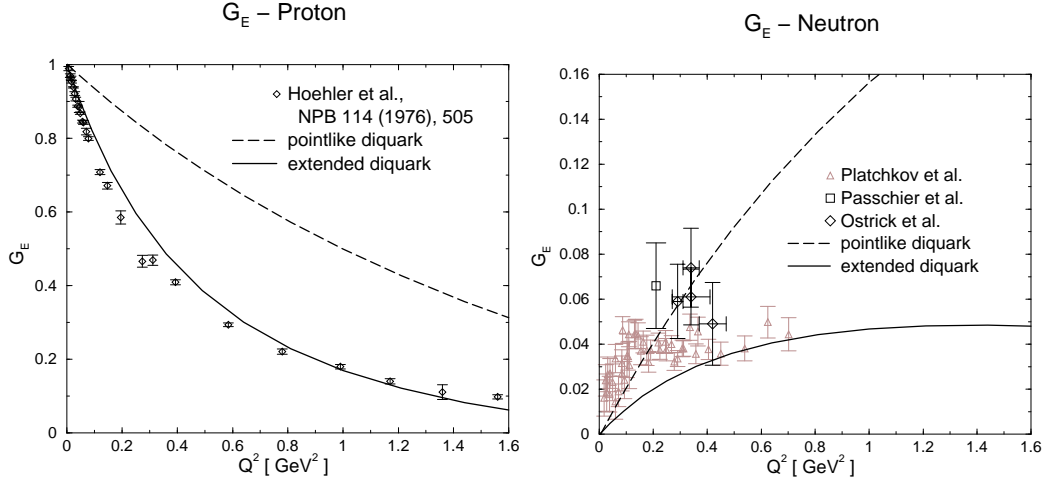
Figure 5.1: Electric form factors of both nucleons for the parameter sets of table 5.1.

table 5.1, *i.e.* the set which employs extended diquarks. From the results found in table 5.2 we see that the anomalous magnetic moment and the transition strength are reduced compared to the previous calculations with free propagators, *cf.* table B.1.

The form factors are now calculated as the sum of the extended impulse approximation diagrams, *cf.* figure 3.2, and of the quark exchange kernel diagrams depicted in figure 3.4. The relevant formulae for the impulse approximation are given by eqs. (3.36,3.37) and by eqs. (3.48–3.50) for the exchange kernel contributions.

Turning to the results for the electric form factors, shown in figure 5.1, we see the favorable influence of the diquark-quark vertices with finite width. They lead to a basically correct description of the proton electric form factor. The neutron electric form factor is also much better described by the parameter sets which employs extended diquarks. Here we see the already mentioned quenching effect of the axialvector correlations, though. They are quite strong as compared to the parameter sets from table 2.8, with the scalar diquark contributions to the norm integral reduced to 51 % (the numbers are 66 % for Set I and 92 % for Set II).

Regarding the overall shape of the calculated magnetic form factors, depicted in figure 5.2, we obtain the same conclusion as before. The parameter set with extended diquarks fairly well describes the empirical dipole shape whereas pointlike diquarks assume the nucleons to be far too rigid. It is interesting to observe that for the extended diquarks the calculated magnetic moments, $\mu_p = 3.32$ and $\mu_n = -2.14$, now exceed the experimental values by 19 and 12 per cent, respectively. We find that the magnetic moment contribution of *every single* diagram
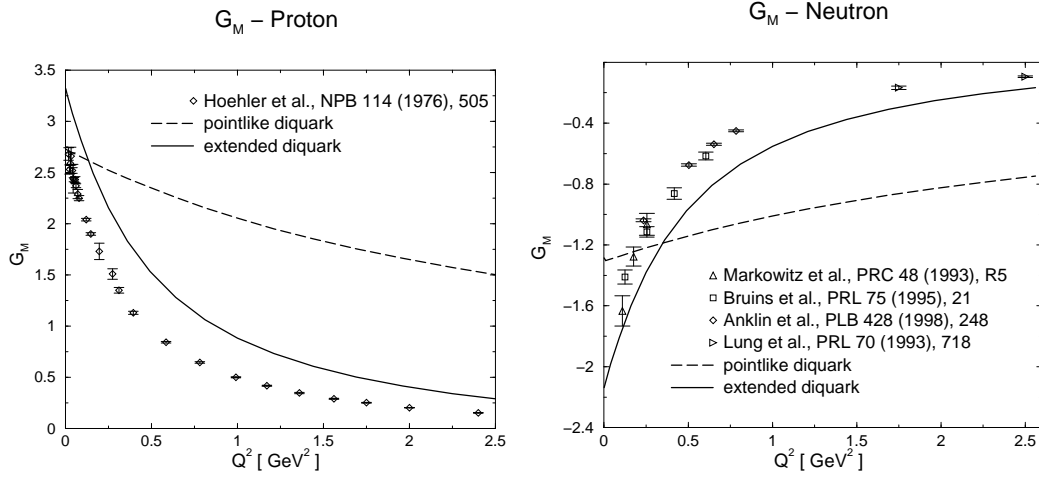
Figure 5.2: Magnetic form factors of both nucleons for the parameter sets of table 5.1. Experimental data for the neutron is taken from refs. [103, 104, 105, 106].

weighed with its contribution to the total nucleon charge is enhanced when comparing with the corresponding ratios for the Sets I and II which employ bare propagator and vertices. Clearly the dressing of propagators and vertices has a quite substantial effect on the magnetic moments and a more refined choice for them may provide for an exact description of both electric and magnetic form factors.

5.4 Discussion

We have employed a simple parametrization of quark and diquark propagators which renders them to be devoid of poles in the complex momentum plane except for an essential singularity at infinity. Thereby we could demonstrate that an overall satisfying description of both the electromagnetic form factors and the mass spectrum of octet and decuplet baryons has been achieved. However, these results have to be taken with a grain of salt as has been already alluded to. General arguments about the functional form of the quark propagator in QCD simply prohibit such a behavior for timelike momenta as has been assumed here. Since mass spectrum and form factor calculations test the propagator only to a moderate extent in the timelike region ($\mathrm{Re}(p^2) \gtrsim -0.3\ \mathrm{GeV}^2$) one might argue that the chosen form for the propagator parametrizes the momentum regime needed well enough for practical calculations of physical processes and only the continuation to large timelike momenta needs to be adapted.

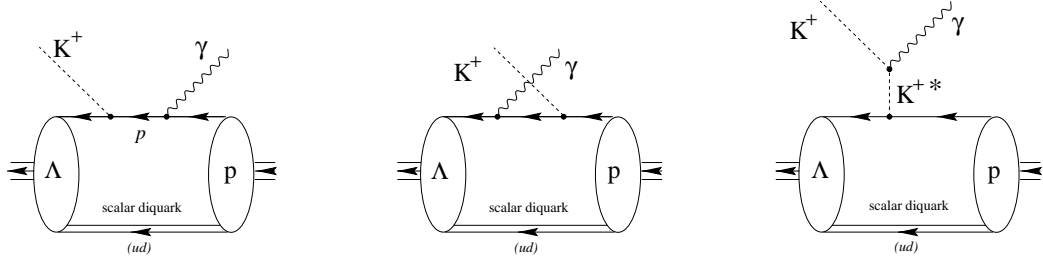On the other hand, there are processes which permit to test the quark propaga-

Figure 5.3: The dominating processes in the diquark-quark model for kaon photoproduction, assuming small axialvector correlations.

tor properties for larger timelike momenta. Consider the photoproduction of kaons off the proton ($\gamma p \to K^+ \Lambda$), measured by the SAPHIR collaboration [107]. The dominant contributions to this process in the diquark-quark model are depicted in figure 5.3. The threshold photon energy for this process to occur (with the proton being at rest) is $E_\gamma = 0.913$ GeV and a broad, dipped maximum for the total cross section is found for $E_\gamma = 1.1 \ldots 1.5$ GeV. Now consider the left diagram in figure 5.3. For the momentum p of the quark propagating between the points of the photon absorption and kaon emission we find the bound $\mathrm{Re}(p^2) \geq -(\eta M_n + E_\gamma)^2$ [108], with M_n being the nucleon mass and η the momentum partitioning parameter between quark and diquark. For photon energies larger than 1 GeV a propagator dressed as given by eq. (5.1) will show considerable enhancement and this has indeed been found [109, 108]. The calculation of the total cross section using the parameter set with pointlike diquarks from table 5.1 reveals an upshot of the cross section beyond $E_\gamma = 1.2$ GeV, clearly in contrast to the data. Only with a (non-analytical) modification function,

$$C(p^2, m) = 1 - \exp\left(-\frac{1}{4} \frac{|p^2 + m_q^2|}{m_q^2}\right) , \qquad (5.13)$$

which damps the propagator for timelike momenta, the experimental cross section could be reproduced. Unfortunately solutions of the Bethe-Salpeter equation and results for observables employing such a propagator do not exhibit invariance under shifts of the momentum partitioning parameter η anymore due to the non-analyticity of C. Thereby relativistic translation invariance seems to be lost.

Another phenomenological argument against the pole-free form for the quark propagator comes from the analysis of Deep Inelastic Scattering in the diquark-quark picture. In the Bjorken limit the leading contribution to the hadronic tensor is obtained by calculating the imaginary part of the "handbag diagram" shown in figure 5.4. This diagram constitutes the leading part of the Compton tensor in forward scattering. By Cutkosky's rule the imaginary part is obtained by cutting
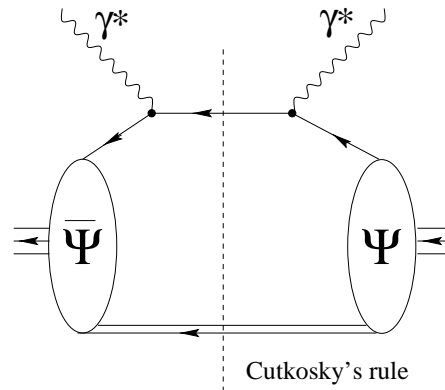
Figure 5.4: Handbag diagram for Virtual Compton Scattering in the diquark-quark model. The imaginary part of the forward amplitude is obtained by Cutkosky's rule, *i.e.* by setting the intermediate quark and diquark propagators on-shell, indicated by the dashed line.

the diagram as indicated in the figure and setting the propagators on-shell at the cuts. This procedure is of course not possible when employing pole-free propagators and in this case the imaginary part of the Compton scattering amplitude could only be obtained by calculating more complicated diagrams with intermediate mesons and baryons. In the limit of the squared photon momentum Q^2 going to infinity, each of these diagrams will be suppressed and the hadronic tensor vanishes, in obvious contradiction to the measured finite structure functions.

Therefore we are in the peculiar situation that results obtained by using free quark and diquark propagators compares favorably with experiments when calculating quark distributions. For the quark-diquark model with pointlike scalar diquarks this has been done in ref. [57]. A simple quark-diquark spectator model which parametrizes the nucleon vertex function in terms of the "s wave" covariants $\mathcal{S}_1$ and $\mathcal{A}_3$, *cf.* table 2.1, has been used in ref. [110] to calculate various distribution and fragmentation functions. These calculations indicate that the approximation of the plethora of intermediate (colorless) states possible in Compton scattering by a simple (colored) quark and a (colored) diquark works amazingly well. However, in the beginning of the chapter we have emphasized that exactly these thresholds are sought to avoid in other calculations such as those related to kaon photoproduction. It therefore remains an interesting task to resolve this puzzle in a consistent manner.

Chapter 6

The Salpeter Approximation

In this chapter we will critically compare results for vertex functions and nucleon observables obtained (i) by using the full solution as described in chapters 2–4 and (ii) in the *Salpeter approximation* [66] to the (ladder) Bethe-Salpeter equation. The Salpeter approximation, to be explained below, is a popular 3-dimensional reduction of the original 4-dimensional problem. We mention that the here obtained results are summarized in ref. [25].

We can identify two motivations to study semi-relativistic reductions to the Bethe-Salpeter equation. First, the gain in technical simplicity is substantial when the equation is transformed into a 3-dimensional problem which can be solved with the tried and tested methods from quantum mechanics. Secondly, excited states which have negative norm are absent in the spectrum of a Salpeter approximated equation. We will shortly dwell upon this point. Let us consider the spectrum of the Bethe-Salpeter equation in ladder approximation within two well-studied models, the Wick-Cutkosky model [111] and the positronium system [112, 113]. They have a class of "normal" solutions, *i.e.* solutions with a non-relativistic quantum mechanical analogue, which exist already for infinitesimally small coupling constants. On the other side, there are solutions which begin to exist only for a finite coupling constant, and these are called "abnormal" states. In the Wick-Cutkosky model, they are excitations in the relative time between the two constituents and clearly in a non-relativistic description with no separation in the time coordinate between the two constituents corresponding states do not exist. Furthermore, these abnormal states have partly negative norm [35]. Therefore, the interpretation of excited states within a given model employing the Bethe-Salpeter equation for modelling bound states is seriously hampered. Here, the Salpeter approximation allows a transformation of the problem into a Hamiltonian form with the Hamiltonian being hermitian and thus no negative norm states

can arise[1]. This transformation is possible as the interaction kernel in the Bethe-Salpeter equation is assumed to be independent of the relative time coordinate or, equivalently, independent of the fourth component of the relative momenta (*equal time approximation*). Studies employing this technique in solving for ground state and excited meson masses can be found in refs. [115, 116].

Appreciating the advantages of the Salpeter approximation in the computation of excited states one could proceed and calculate dynamical observables for the bound states. However, we will show in the following that nucleon form factors, the pion-nucleon and weak coupling constants calculated in the diquark-quark model differ substantially for the full solution and the Salpeter approximation. Therefore, results from the latter might lead to a misinterpretation of the model's parameters. As there exist studies for the diquark-quark model using the Salpeter approximation [62, 117], we will employ model parameters as chosen there to furnish the comparison.

6.1 Solutions for vertex functions

We will use the diquark-quark model as defined in chapter 2. Following refs. [62, 117], we employ free quark and diquark propagators, with the gauge parameter ξ for the axialvector diquark chosen to be 1, *cf.* eq. (2.46),

$$S(p) \;=\; \frac{i\!\not\!p - m_q}{p^2 + m_q^2} \,, \tag{6.1}$$

$$D(p) \;=\; -\frac{1}{p^2 + m_{sc}^2} \,, \qquad D^{\mu\nu}(p) = -\frac{\delta^{\mu\nu}}{p^2 + m_{ax}^2} \,. \tag{6.2}$$

The Dirac part of the diquark-quark vertices is given as in eqs. (2.51,2.52) by

$$\chi^5 = g_s \left(\gamma^5 C\right) V(q^2) \,, \qquad \chi^\mu = g_a \left(\gamma^\mu C\right) V(q^2) \,, \tag{6.3}$$

with the scalar function V chosen to be

$$V(q^2) = \exp(-4\lambda^2 q^2) \,. \tag{6.4}$$

The relative momentum between the quarks is denoted by q. We recapitulate the Bethe-Salpeter equation in short notation,

$$\Psi(p, P) \;=\; S(p_q) \, \tilde{D}(p_d) \, \Phi(p, P) \tag{6.5}$$

$$\Phi(p, P) \;=\; \int \frac{d^4k}{(2\pi)^4} K^{\mathrm{BS}}(p, k, P) \, \Psi(k, P) \,. \tag{6.6}$$

---

[1]Abnormal states may still exist, *cf.* ref. [114] for an investigation on the persistence of abnormal states in 3-dimensional reductions of a two-fermion Bethe-Salpeter equation.

All terms appearing here are defined in section 2.3.1. Let $q_T = q - \hat{P}(q \cdot \hat{P})$ denote the transversal part of any momentum q with respect to the bound state momentum P. The Salpeter approximation consists in reducing the momentum dependence of the quark exchange kernel in the following manner,

$$K^{\mathrm{BS}}(p, k, P) \to K^{\mathrm{BS}}(p_T, k_T) \ . \tag{6.7}$$

In the rest frame of the bound state, $K^{\mathrm{BS}}(p_T, k_T) \equiv K^{\mathrm{BS}}(\boldsymbol{p}, \boldsymbol{k})$, and hence the (other) names *equal time* or *instantaneous* approximation. It follows immediately from eq. (6.6) that $\Phi(p, P) \equiv \Phi(\boldsymbol{p})$. Although covariance is lost by assuming instantaneous interactions, the solutions for Φ are invariant against shifts in the parameter η which defines the distribution of momentum between quark and diquark.

Again following ref. [62], the reduced Bethe-Salpeter equation can be processed by introducing

$$\tilde{\Psi}(\boldsymbol{p}) = \gamma^4 \int \frac{dp^4}{2\pi} \Psi(p, P) \ , \tag{6.8}$$

integrating eq. (6.5) over p^4 likewise, and thus arriving at an equation with the formal structure,

$$H\tilde{\Psi} = M\tilde{\Psi} \ . \tag{6.9}$$

The "Hamiltonian" H is an integral operator which contains "kinetic" parts stemming from the propagators and a "potential", being the instantaneous quark exchange.

Instead of solving this Schrödinger-type equation, we will employ the numerical method developed in section 2.5.1. Having expanded the wave function Ψ and the vertex function Φ according to eqs. (2.91,2.129), we solve the Bethe-Salpeter equation for the sets of scalar functions $\{S_i, A_i\}$ and $\{\hat{S}_i, \hat{A}_i\}$. As described in section 2.5.1, each of the scalar functions depends on p^2 and $z = \hat{p} \cdot \hat{P}$. The dependence on z will be absorbed by the Chebyshev expansion of eqs. (2.135,2.136). Note that in the Salpeter approximation the scalar functions S_i, A_i pertaining to the vertex function depend only on the single variable $\boldsymbol{p}^2 = p^2(1 - z^2)$, thus their Chebyshev expansions contains just even moments.

As stated above we adopt the parameters of refs. [62, 117]. The first study investigates one parameter set in the scalar diquark sector only and the second one includes the axialvector diquark channel using another parameter set. In these studies, the author did not fix the diquark-quark coupling constants by a normalization condition like in eqs. (2.59,2.60), but rather adjusted g_s so as to obtain the physical nucleon mass for given values of quark and diquark mass, and of

Set		m_q [GeV]	m_{sc} [GeV]	m_{ax} [GeV]	λ [fm]	g_a/g_s	g_s	
Ia	Salpeter	0.35	0.65	-	0.18	-	20.0	(20.0)
	full						16.5	
IIa	Salpeter	0.35	0.65	0.65	0.24	1	12.3	(11.5)
	full						9.6	

Table 6.1: The two parameter sets of the model as taken from refs. [62, 117].

g_a/g_s when including the axialvector diquarks. This procedure is convenient as the Bethe-Salpeter equation is an eigenvalue problem for the eigenvalue g_s. In table 6.1 we have listed the two sets of parameters with their corresponding eigenvalues g_s obtained by us in the full calculation and the Salpeter approximation. The values in parentheses are the ones from refs. [62, 117]. Please note that due to a different flavor normalization these values had to be multiplied by $\sqrt{2}$ to be directly comparable to ours.

Although we could reproduce the eigenvalue for the model case with scalar diquarks only, this is not the case for Set IIa. We observe that the calculations of [117] involved only 4 instead of 6 axialvector components of Φ^μ, namely the projected ones onto zero orbital angular momentum and the corresponding lower components. Still one would expect a higher eigenvalue in the reduced system. The more striking observation is the amplification of the eigenvalue by about 20 ... 25 % in the Salpeter approximation although the binding energy is small, being only 6% of the sum of the constituent masses. This is in contrast to results obtained in the massive Wick-Cutkosky model [118] where the Salpeter approximation leads to a *reduction* of the eigenvalue. This may be attributed to the exchange of a boson instead of a fermion as here in the diquark-quark model.

The substantial difference between the two approaches is also reflected in the vertex function solutions themselves. Figure 6.1 shows the Chebyshev moments of the dominant scalar function S_1 for both methods using the parameters of Set Ia. Only the even momenta are given, since the odd ones are zero in the Salpeter approximation (but are present, of course, in the full calculation). Two things are manifest: the Salpeter amplitudes have a much broader spatial extent than the full amplitudes. Secondly, the expansion in Chebyshev polynomials that relies on an approximate $O(4)$ symmetry converges much more rapidly for the full solution but is hardly convincing in the Salpeter approximation. Again, since the scalar functions depend in the Salpeter approximation on just one variable, $p^2(1 - z^2)$,
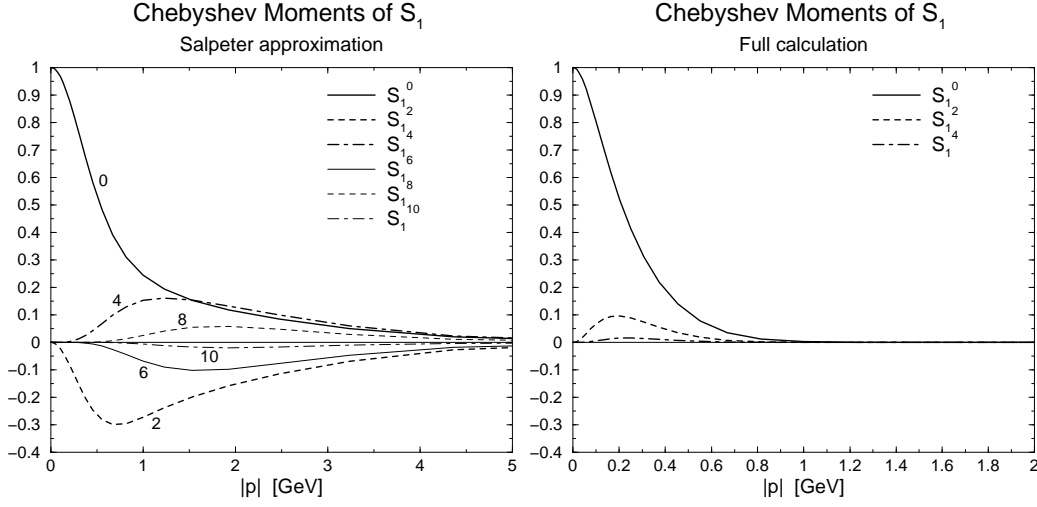
Figure 6.1: The Chebyshev expansion of the dominant scalar function $S_1(p, z)$ in the Salpeter approximation and the full calculation.

our expansion is a cumbersome way of visualizing the solution but makes clear that the Salpeter approximation does not exhibit an approximate $O(4)$-symmetry.

We remind ourselves that Salpeter in his original work [66] devised the instantaneous approximation of the Bethe-Salpeter kernel as the first term in a perturbation series for the full solution. We clearly see that one should not stop after the first term as the character of the exact and the approximated solution differ so profoundly.

6.2   Results for observables

Let us turn first to the calculation of the electromagnetic form factors G_E and G_M. They can be extracted from the current matrix element as prescribed by eqs. (3.8,3.9). In impulse approximation the current operator for proton and neutron reads

$$_{\mathrm{p}}\langle P_f|\, J^\mu\, |P_i\rangle_{\mathrm{p}}^{\mathrm{imp}} \;=\; \frac{2}{3}\langle J_q^\mu\rangle^{\mathrm{sc-sc}} + \frac{1}{3}\langle J_{sc}^\mu\rangle^{\mathrm{sc-sc}} + \langle J_{ax}^\mu\rangle^{\mathrm{ax-ax}}\,, \qquad (6.10)$$

$$_{\mathrm{n}}\langle P_f|\, J^\mu\, |P_i\rangle_{\mathrm{n}}^{\mathrm{imp}} \;=\; -\frac{1}{3}\left(\langle J_q^\mu\rangle^{\mathrm{sc-sc}} - \langle J_q^\mu\rangle^{\mathrm{ax-ax}} - \langle J_{sc}^\mu\rangle^{\mathrm{sc-sc}} + \langle J_{ax}^\mu\rangle^{\mathrm{ax-ax}}\right)\,.$$
$$\qquad (6.11)$$

Here we adopted the notation from section 3.1. Diagrammatically the single matrix elements correspond to the left two graphs of figure 3.2. The quark and di-
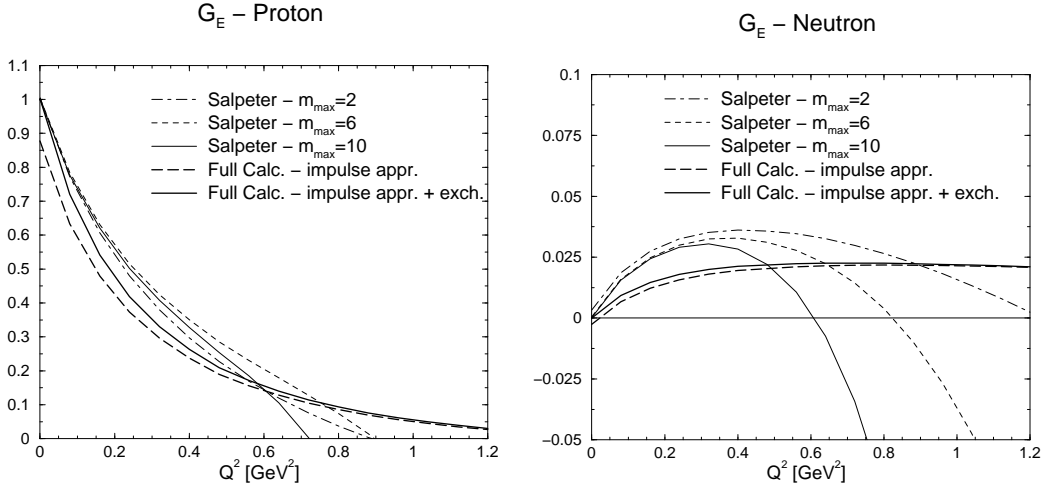
Figure 6.2: Nucleon electric form factors in the Salpeter approximation and in the full calculation. The curves for the Salpeter approximation have been obtained by including the Chebyshev moments of the vertex function up to order m_{max}.

quark vertices which are needed in these diagrams are given by eqs. (3.28–3.31). These diagrams are the only ones which have been calculated in refs. [62, 117], with the following justification given: as already mentioned in the summary of section 3.1, the diagrams of the impulse approximation separately conserve the current. Furthermore, peculiar identities at zero momentum transfer hold in the Salpeter approximation,

$$\langle J_q^4(Q^2 = 0)\rangle^{\mathrm{sc-sc}} \;=\; \langle J_{sc}^4(Q^2 = 0)\rangle^{\mathrm{sc-sc}} \tag{6.12}$$

$$\langle J_q^4(Q^2 = 0)\rangle^{\mathrm{ax-ax}} \;=\; \langle J_{ax}^4(Q^2 = 0)\rangle^{\mathrm{ax-ax}} \;, \tag{6.13}$$

which are proved by straightforward calculation. These identities, in conjunction with eqs. (6.10,6.11) and the normalization condition (3.56) for the nucleon wave function, guarantee that proton and neutron have their correct charge, *i.e.* the electric form factors satisfy $G_E^{\mathrm{proton}}(Q^2 = 0) = 1$ and $G_E^{\mathrm{neutron}}(Q^2 = 0) = 0$.

We have seen that in the full calculation we need the current contributions from the quark exchange kernel to establish the correct nucleon charges. This followed as a consequence of the general Ward-Takahashi identity, eq. (3.13), for the quark-diquark propagator. We will therefore compare the impulse approximation for the Salpeter calculation to the calculations with full vertex functions with and without the exchange diagrams of figure 3.4.

In figure 6.2 the electric form factors of proton and neutron are displayed, using the parameters of Set IIa. The first observation is that in the Salpeter approximation we could not obtain convergence with the expansion in Chebyshev

		$\langle J_q^\mu \rangle^{\mathrm{sc-sc}}$	— μ_p — $\langle J_{ax}^\mu \rangle^{\mathrm{ax-ax}}$	$\langle J_{ex}^\mu \rangle$	SUM
Ia	Salpeter	1.57	-	-	1.58 (1.58)
	full	2.04	-	0.31	2.38
IIa	Salpeter	0.92 (1.08)	1.37 (1.7)	-	2.29 (2.78)
	full	1.09	0.98	0.37	2.45

Table 6.2: The most important contributions to the proton magnetic moment from the single diagrams. The notation is as in table 3.2. In parentheses the values of refs. [62, 117] are given.

polynomials beyond $Q^2 \approx 0.4$ GeV^2. As described in section 3.2.1, we computed the form factors in the Breit frame where Q is real but $z_i = \hat{p} \cdot \hat{P}_i$ and $z_f = \hat{k} \cdot \hat{P}_f$, the angular variables which enter as their arguments the Chebyshev polynomials for the boosted vertex functions, have imaginary parts. Their absolute values may exceed one, except for the case of zero momentum transfer, *cf.* eqs. (3.66,3.67). So this expansion that works in the rest frame, and it does barely so for the Salpeter approximation, will not generally work in a moving frame. On the other hand, the decrease of the higher Chebyshev moments is good enough for the full four-dimensional solution that the numerical values for the form factors converge up to several GeV^2. However, as can be seen from fig. 6.2 the Salpeter approximation badly fails above 0.5 GeV^2 thereby revealing its semi-relativistic nature.

The second finding concerns the electromagnetic radii. The Salpeter approximation tends to underestimate the proton charge radius and to overestimate the absolute value of the neutron charge radius, see the first two result lines of table 6.3. The axialvector correlations tend to suppress the neutron electric form factor much more in the full calculation than in the Salpeter approximation. Remember that this suppression is due to the axialvector correlations which have been chosen to be rather strong for Set IIa, as $g_s = g_a$.

Turning to the magnetic moments, the contributions of the various diagrams are tabulated in table 6.2 for the proton. Following ref. [117] we ascribed to the axialvector diquark a rather large anomalous magnetic moment of $\kappa = 1.6$ which was needed in that study to fit the proton magnetic moment. As already observed earlier, we could reproduce the magnetic moment for Set Ia, however, for Set IIa, the values differ and especially the coupling to the axialvector diquark is much

Set		Ia			IIa		
		Salpeter	full		Salpeter	full	
		IA	IA	all	IA	IA	all
$(r_p)_{\mathrm{el}}$	[fm]	0.89	1.00	0.99	0.88	1.01	1.01
$(r_n^2)_{\mathrm{el}}$	[fm^2]	-0.28	-0.21	-0.23	-0.06	-0.04	-0.04
μ_p		1.58	2.05	2.58	2.29	2.07	2.45
$(r_p)_{\mathrm{mag}}$	[fm]	1.04	1.09	1.06	0.85	0.99	0.99
μ_n		-0.77	-1.02	-1.65	-0.98	-1.02	-1.26
$(r_n)_{\mathrm{mag}}$	[fm]	1.05	1.09	1.00	0.94	1.06	1.05
$g_{\pi NN}$		8.96	11.71	15.34	6.03	6.95	9.36
$r_{\pi NN}$	[fm]	1.04	1.07	1.04	1.15	1.21	1.15
g_A		0.93	1.16	1.46	0.53	0.65	0.82
r_A	[fm]	0.93	0.99	1.02	1.08	1.14	1.10

Table 6.3: Some static nucleon observables. The acronym 'IA' indicates that the results in these columns have been obtained in the impulse approximation whereas 'all' means that also the diagrams of the quark exchange kernel have been taken into account.

weaker in our Salpeter calculation. Rather more interesting is the comparison between the full calculations using either Set Ia or Set IIa: The axialvector diquark improves the magnetic moment only marginally, due to the neglect of the anomalous transitions between scalar and axialvector diquarks. The Salpeter approximation tends to overestimate the contribution of $\langle J_{ax}^\mu \rangle^{\mathrm{ax-ax}}$ quite drastically.

We have also calculated the pion-nucleon constant, the weak coupling constant and the corresponding radii for the two sets in a first approximation, taking into account only the diagrams where the pseudoscalar and pseudovector current couple to the spectator or the exchanged quark. Please refer to table 6.3 for the numerical results. Of course, the numbers for g_A and $g_{\pi NN}$ obtained for the parameters of Set IIa signal the missing contributions from the resolved axialvector diquark and from the scalar-to-axialvector transitions. But we want to emphasize another point: Already in impulse approximation the results vary strongly (on the level of 20 %) between the full and the Salpeter calculation with the Salpeter approximation *underestimating* the couplings. But as we have seen for the magnetic moments for Set IIa, the Salpeter approximation *overestimates* them, so we arrive at the conclusion that observables vary quite strongly and unpredictably when employing the equal time approximation. In this case, it is hardly of use to relate

parameters to the physical content which the model hopefully describes.

Let us summarize the results obtained in this chapter. The Bethe-Salpeter equation for the nucleon has been solved in a fully covariant way and in the instantaneous Salpeter approximation. As for the model with scalar diquarks only we have verified the results of ref. [62] whereas discrepancies remain if the axialvector diquark is included. These differences are partly due to the fact that in ref. [117] not all (ground state) axialvector components have been taken into account. Additionally, we take our result as an indication that the calculations presented in ref. [117] might suffer from some minor error.

However, the main purpose has been the comparison of observables calculated in the Salpeter approximation to the ones obtained in the fully four-dimensional scheme. The first very surprising observation is the overestimation of the Bethe-Salpeter eigenvalue in the Salpeter approximation. Phrased otherwise, for a given coupling constant the binding energy would be much too small in the Salpeter approximation. We have also demonstrated that the character of the vertex function solutions in the full treatment and for the Salpeter approximation is grossly different, since the full solutions exhibit an approximate $O(4)$ symmetry which is absent in the Salpeter approximation. This has drastic consequences for the resulting nucleon electromagnetic form factors if the photon virtuality exceeds 0.4 GeV^2. Although the non-convergence of the form factors in the Salpeter approximation in this momentum regime can be solely ascribed to the Chebyshev expansion which is inappropriate for the instantaneous approximation, we find nevertheless differences for static observables. On the one hand, different nucleon radii differ only mildly in these two approaches, with the exception of the neutron charge radius. On the other hand, one sees very clearly that the results (obtained in the Salpeter approximation) for the magnetic moments, the pion-nucleon coupling and the weak coupling constant deviate sizeably from the full calculation.

Chapter 7

Summary and Conclusions

In this thesis we have presented a framework for a fully covariant diquark-quark model of baryons and obtained solutions for bound states and certain nucleon observables having employed simple *ansätze* for the quark and diquark propagators, and the diquark-quark vertices. We derived the basic Bethe-Salpeter equations governing the dynamics of the quarks and the diquark quasi-particles by a suitable reduction of the relativistic three-quark problem. This reduction consists in neglecting three-quark irreducible interactions and assuming separable two-quark correlations, the diquarks. Scalar and axialvector diquarks have been included into the description as the presumably most important diquark correlations.

We solved the Bethe-Salpeter equation which sums up the continuous quark exchange between quark and diquark in a fully covariant manner, thereby obtaining relativistic baryon wave functions which contain far more structure than non-relativistic wave functions. These wave functions have been subsequently employed to calculate electromagnetic form factors. Here, we constructed the current operator for the electromagnetic field using Ward-Takahashi identities and thereby maintaining gauge invariance. Covariance and gauge invariance are manifest in the numerical results. For the nucleon electric form factors we found good agreement with the experimental data. The magnetic moments fall short by approximately 15 ... 30 %, depending on whether the Δ resonance is included in the description or not. A possible source of this failure is found in the free constituent quark and diquark propagators which have been employed in these calculations. The lack of confinement forced us to choose rather large quark and diquark masses to obtain a bound Δ, and the perturbative quark-photon vertex is probably insufficient to account for the observed magnetic moments. The recently measured ratio of electric to magnetic form factor of the proton restricts the strength of the axialvector correlations within the nucleon to be small, on the level of 20 %, if our results are to match the data.

In an attempt to circumvent the problem posed by the inclusion of the Δ reso-

nance and the underestimated magnetic moments, we have investigated a possible parametrization of confinement by modifying quark and diquark propagators to render them pole-free in the complex momentum plane. These modifications allowed us to calculate the mass spectrum of octet and decuplet baryons in fair agreement with experiment and the nucleon magnetic moments received additional contributions which even rendered them to be larger by 15 % than the experimental values. Nevertheless, there are serious doubts about the justification of such a modification. The modified propagators have an essential singularity at timelike infinity which is not in accordance with general theorems about the behavior of propagators in quantum field theory. Additionally, this singularity causes a spurious enhancement of the calculated cross section in kaon photoproduction, and would render the calculation of the leading twist contributions to Deep Inelastic Scattering impossible. Therefore, refined methods to incorporate confinement are needed and work on this problem is currently done.

The isovector axial form factor for the nucleon and the pion-nucleon form factor have also been calculated. Chiral symmetry could be used to construct the pseudovector and the pseudoscalar quark current operators. As it turns out, chiral symmetry requires also the inclusion of vector diquarks besides the axialvector diquarks, since they form a chiral multiplet. The neglect of the former leads to a moderate violation of the Goldberger-Treiman relation, and the pion-nucleon and the weak coupling constant are found to be somewhat too large compared to their experimental values. Since the transitions between scalar and axialvector diquarks proved to be the main source of the calculated Goldberger-Treiman discrepancy and the large pion-nucleon coupling constant, we again conclude that axialvector correlations within the nucleon should be small.

We also compared results for nucleon vertex function solutions and observables between the fully covariant treatment of the diquark-quark Bethe-Salpeter equation and the semi-relativistic Salpeter approximation. The vertex functions for the latter differed strongly from the full solution, on a qualitative as well as on a quantitative level. Furthermore, we found rather erratic deviations between the results for static observables obtained with both methods and therefore conclude that the semi-relativistic treatment is inadmissible within the diquark-quark model.

Regarding the simplicity of the quark-diquark picture, the model reproduces fairly well the basic nucleon observables investigated here. It should be considered a success that maintaining covariance is feasible in calculating the form factors and this is a good starting point to investigate more involved hadronic processes. For kaon photoproduction, $\gamma p \to K^+ \Lambda$, and associated strangeness production, $pp \to pK^+ \Lambda$, preliminary results are already available, *cf.* refs. [109, 119].

To check the viability of the chosen approach within QCD, some more in-

formation about the quark propagator and the two-quark correlations are needed. Whereas there is justified hope that lattice or Dyson-Schwinger calculations will provide us with more refined results for the quark propagator in the near future, it is not clear at all whether a non-perturbative characterization of the two-quark correlations can be found. To proceed further in this direction, one probably has to resort in a next step to an approximate model for the quark-gluon dynamics.

Appendix A

Varia

A.1 Conventions

Throughout the text we work in Euclidean space with the metric $g^{\mu\nu} = \delta^{\mu\nu}$. Accordingly, a hermitian basis of Dirac matrices $\{\boldsymbol{\gamma}, \gamma^4\}$ is used which is related to the matrices $\{\gamma_D^0, \boldsymbol{\gamma}_D\}$ of the Dirac representation by

$$\gamma^4 = \gamma_D^0 \ , \quad \boldsymbol{\gamma} = -i\boldsymbol{\gamma}_D \ . \tag{A.1}$$

Furthermore we define $\gamma^5 = -\gamma^1\gamma^2\gamma^3\gamma^4$. The charge conjugation matrix is defined by $C = -\gamma^2\gamma^4$. The free quark propagator $S(k)$ is determined by the relation, valid in the theory for a free, massive fermion,

$$\langle 0|Tq(x)\bar{q}(y)|0\rangle \ = \ \int \frac{d^4k}{(2\pi)^4} \exp(ik{\cdot}(x-y))S(k) \ , \tag{A.2}$$

$$S(k) \ = \ \frac{i\not{k} - m_q}{k^2 + m_q^2} \ . \tag{A.3}$$

We arrive at this equation, if we formulate the continuation between Minkowski and Euclidean space using the well-known rules

$$x_M^0 \to -ix^4 \ , \quad \boldsymbol{x}_M \to \boldsymbol{x} \ , \tag{A.4}$$

$$k_M^0 \to ik^4 \ , \quad \boldsymbol{k}_M \to -\boldsymbol{k} \tag{A.5}$$

for a formal transcription of position variables x_M and momentum variables k_M in Minkowski space to their Euclidean pendants x and k. Additionally we prescribe for the Euclidean momentum variables $k \to -k$. Furnished with an additional transcription rule for the metric tensor in Minkowski space,

$$g^{\mu\nu} \to -\delta^{\mu\nu} \ , \tag{A.6}$$

we find for the scalar and the Proca propagator,

$$D(p) = -\frac{1}{p^2 + m_{sc}^2} , \quad D^{\mu\nu}(p) = -\frac{\delta^{\mu\nu} + \frac{p^\mu p^\nu}{m_{ax}^2}}{p^2 + m_{ax}^2} . \tag{A.7}$$

Four-dimensional momentum integrals, appearing in the Bethe-Salpeter equation or in the expression for current matrix elements, are evaluated by using hyperspherical coordinates. We parametrize the Cartesian components of an Euclidean vector q^μ in the following way,

$$q^\mu = |q| \begin{pmatrix} \sin\phi \sin\theta \sin\Theta \\ \cos\phi \sin\theta \sin\Theta \\ \cos\theta \sin\Theta \\ \cos\Theta \end{pmatrix} . \tag{A.8}$$

With the abbreviations $z = \cos\Theta$ and $y = \cos\theta$ the four-dimensional volume integral measure is

$$\int \frac{d^4q}{(2\pi)^4} = \frac{1}{(2\pi)^4} \int_0^\infty |q|^3 d|q| \int_{-1}^1 \sqrt{1-z^2}\, dz \int_{-1}^1 dy \int_0^{2\pi} d\phi . \tag{A.9}$$

Hyperspherical harmonics are defined by

$$\mathcal{Y}_{nlm}(\Theta, \theta, \phi) = \sqrt{\frac{2^{2l+1}}{\pi} \frac{(n+1)(n-l)!(l!)^2}{(n+l+1)!}} \sin^l\Theta\, C_{n-l}^{1+l}(\cos\Theta) Y_{lm}(\theta, \phi), \tag{A.10}$$

where the polynomials $C_{n-l}^{1+l}(\cos\Theta)$ are the *Gegenbauer polynomials* [52] and the $Y_{lm}(\theta, \phi)$ are the familiar spherical harmonics. For vanishing three-dimensional angular momentum, $l = 0$, the Gegenbauer polynomials reduce to the Chebyshev polynomials of the second kind, $C_n^1 = U_n$, and the corresponding hyperspherical harmonics are simply

$$\mathcal{Y}_{n00} = \sqrt{\frac{1}{2\pi^2}} U_n(\cos\Theta) . \tag{A.11}$$

Thus, the expansion of relativistic ground state wave functions ($l = 0$) in terms of Chebyshev polynomials, as done in section 2.5 for the baryons, corresponds to an expansion into hyperspherical harmonics.

A.2 Color and flavor factors in the Bethe-Salpeter equations

A.2.1 Nucleon

For the derivation of the color factor, let us introduce the color singlet state of the nucleon as being proportional to a 3-dimensional unit matrix $(\mathbf{3} \otimes \bar{\mathbf{3}} = \mathbf{1} \oplus \mathbf{8})$

$$|0\rangle_{\text{color}} = \sqrt{\tfrac{1}{3}} (\lambda^0)_{AB} := \sqrt{\tfrac{1}{3}} \delta_{AB}, \qquad \langle 0|0 \rangle = 1 . \tag{A.12}$$

Since both diquarks are in an antitriplet representation, the color part of the Bethe-Salpeter kernel reads (see figure A.1)

$$K_{\text{color}}^{\text{BS}} = \tfrac{1}{2} \, \epsilon_{LKA} \, \epsilon_{JNA} = -\tfrac{1}{2}(\delta_{LN}\delta_{KJ} - \delta_{LJ}\delta_{KN}) . \tag{A.13}$$

Sandwiching between the nucleon color singlet state yields

$$\langle 0|K_{\text{color}}^{\text{BS}}|0 \rangle = -\tfrac{1}{6}\delta_{JK}(\delta_{LN}\delta_{KJ} - \delta_{LJ}\delta_{KN})\delta_{LN} = -1 . \tag{A.14}$$

The nucleon flavor state distinguishes of course between scalar and axialvector diquarks. We rewrite the diquarks as eigenstates of their total isospin and the projection onto the respective z axis. They are easily expressed by the combinations of u and d quark. $(ud) = -\sqrt{\tfrac{1}{2}}(ud - du)$ has isospin zero (scalar diquark). $[uu]$, $[ud] = \sqrt{\tfrac{1}{2}}(ud + du)$ and $[dd]$ have isospin one with the respective third (z) component being $+1, 0, -1$. Expressed with spherical isospin matrices τ_m, $\tau_{\pm 1} = \mp\sqrt{\tfrac{1}{2}}(\tau^1 \pm i\tau^2)$ and $\tau_0 = \tau^3$, they read

$$(ud) \equiv -\frac{1}{\sqrt{2}} \, i\tau^2 \tag{A.15}$$

$$\begin{pmatrix} [uu] \\ [ud] \\ [dd] \end{pmatrix} \equiv \frac{1}{\sqrt{2}} \begin{pmatrix} i\tau_1\tau^2 \\ i\tau_0\tau^2 \\ i\tau_{-1}\tau^2 \end{pmatrix} \tag{A.16}$$

Remember the expression for the nucleon Faddeev amplitude,

$$\Gamma_{\alpha\beta\gamma} = \chi_{\beta\gamma}^5 \, D \, \left(\Phi^5 u\right)_\alpha + \chi_{\beta\gamma}^\mu \, D^{\mu\nu} \, \left(\Phi^\nu u\right)_\alpha . \tag{A.17}$$

The two summands on the right hand side represent scalar and axialvector correlations, respectively, and the Greek indices contain also the flavor indices. We will write the nucleon flavor state as a 2-vector, with scalar and axialvector correlations as components, and keep in mind that they add up to the Faddeev amplitude

as indicated above. Then the proton flavor wave function can be constructed with the appropriate Clebsch-Gordan coefficients as

$$
|p\rangle_{\text{flavor}} = \begin{pmatrix} |p\rangle_{\text{sc}}^{abc} \\ |p\rangle_{\text{ax}}^{abc} \end{pmatrix} = \begin{pmatrix} u(ud) \\ \sqrt{\frac{1}{3}}u[ud] - \sqrt{\frac{2}{3}}d[uu] \end{pmatrix}
$$

$$
= \begin{pmatrix} \sqrt{\frac{1}{2}}\begin{pmatrix}1\\0\end{pmatrix}_a(i\tau^2)_{bc} \\ \sqrt{\frac{1}{6}}\begin{pmatrix}1\\0\end{pmatrix}_a(\tau^1)_{bc} - \sqrt{\frac{1}{3}}\begin{pmatrix}0\\1\end{pmatrix}_a(i\tau_{-1}\tau^2)_{bc} \end{pmatrix} . \tag{A.18}
$$

The scalar and axialvector flavor components are separately normalized to yield unity,

$$
{}^{acb}_{\text{sc[ax]}}\langle p|p\rangle^{abc}_{\text{sc[ax]}} \overset{!}{=} 1 , \tag{A.19}
$$

where the conjugate flavor states are obtained by Hermitian conjugation. The absolute strength of the scalar and axialvector correlations is determined by the solution to the Bethe-Salpeter equation. A redefinition of the diquark flavor matrices appearing in eq. (A.18) also affects the diquark normalization conditions, eqs. (2.59,2.60), and the Bethe-Salpeter kernel such that the contributions of the scalar and axialvector correlations to observables remain unchanged. The neutron flavor state accordingly writes

$$
|n\rangle_{\text{flavor}} = \begin{pmatrix} d(ud) \\ -\sqrt{\frac{1}{3}}d[ud] + \sqrt{\frac{2}{3}}u[dd] \end{pmatrix} \tag{A.20}
$$

The matrix representation of the Bethe-Salpeter kernel with respect to the diquark isospin eigenstates defined above is given by (see figure A.1)

$$
K_{\text{flavor}}^{\text{BS}} = \begin{matrix} {}^{I=0} \\ {}^{I=1} \end{matrix} \frac{1}{2} \begin{pmatrix} \overset{I=0}{(\tau^2\,\tau^2)_{kn}} & \overset{I=1}{-((\tau_{m'}\tau^2)\,\tau^2)_{kn}} \\ -(\tau^2\,(\tau^2\tau_m^\dagger))_{kn} & ((\tau_{m'}\tau^2)\,(\tau^2\tau_m^\dagger))_{kn} \end{pmatrix} . \tag{A.21}
$$

Sandwiching between either the proton or the neutron flavor state yields the identical flavor matrix

$$
\langle p|K_{\text{flavor}}^{\text{BS}}|p\rangle = \langle n|K_{\text{flavor}}^{\text{BS}}|n\rangle = \begin{matrix} {}^{I=0} \\ {}^{I=1} \end{matrix} \frac{1}{2} \begin{pmatrix} \overset{I=0}{+1} & \overset{I=1}{-\sqrt{3}} \\ -\sqrt{3} & -1 \end{pmatrix} . \tag{A.22}
$$

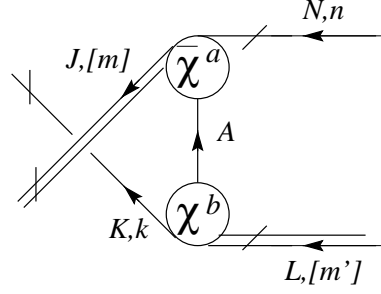Eqs. (A.14,A.22) provide for the explicit factors in the Bethe-Salpeter kernel of eq. (2.70).

Figure A.1: Color and flavor indices appearing in the Bethe-Salpeter kernel. Capital letters run from $1 \ldots 3$ and label the color state of quarks ($\mathbf{3}$) and of diquarks ($\bar{\mathbf{3}}$). Small letters $n, k = 1, 2$ label quark isospin and $m, m' = \pm 1, 0$ label the third component of the axialvector diquark isospin.

A.2.2 Δ

Taking over the notations from the previous subsection, we write the flavor states of the four nearly mass-degenerate Δ resonances as

$$
\begin{pmatrix} |\Delta^{++}\rangle \\ |\Delta^{+}\rangle \\ |\Delta^{0}\rangle \\ |\Delta^{-}\rangle \end{pmatrix} = \begin{pmatrix} u[uu] \\ \sqrt{\frac{2}{3}}u[ud] + \sqrt{\frac{1}{3}}d[uu] \\ \sqrt{\frac{2}{3}}d[ud] + \sqrt{\frac{1}{3}}u[dd] \\ d[dd] \end{pmatrix} .
\tag{A.23}
$$

The flavor matrix of the Bethe-Salpeter kernel involves only the axialvector diquark ($I = 1$) channel,

$$
(K_{\Delta}^{\mathrm{BS}})_{\mathrm{flavor}} = \left((\tau_{m'}\tau^2)\,(\tau^2\tau_m^{\dagger}) \right)_{kn} .
\tag{A.24}
$$

This yields for all Δ states $i \in \{++, +, 0, -\}$ identical flavor factors,

$$
\langle \Delta^{(i)} | (K_{\Delta}^{\mathrm{BS}})_{\mathrm{flavor}} | \Delta^{(i)} \rangle = 1 .
\tag{A.25}
$$

A.3   Wave functions

On the next pages the scalar functions describing the partial waves of nucleon and Δ are displayed. In figure A.2 we show the nucleon functions $\hat{S}_i$, $\hat{A}_i$ for the parameter Set I of table 2.8. The momentum partitioning parameter $\eta = 0.36$ has been chosen. This value is roughly half way between the bounds set by the constituent poles, *cf.* eq. (2.154),

$$
\eta \in [0.334, 0.383] .
\tag{A.26}
$$

The even Chebyshev momenta dominate the expansion of the scalar functions and therefore we show the three leading even momenta for each function. The two dominating s waves $\hat{S}_1$ and $\hat{A}_3$ converge quickly in their expansion. The p waves $\hat{S}_2$, $\hat{A}_2$ and $\hat{A}_6$ which follow next with respect to the overall magnitude display a more moderate convergence. One can estimate that these p waves will have an influence on observables on the level of below 10 %. All other functions are subdominant, especially the d wave $\hat{A}_5$ turns out to be extremely small.

The Δ partial waves depicted in figure A.3 have been calculated using the parameter Set II which fits the experimental Δ mass. The binding energy is only 24 MeV and consequently the range of allowed η values is restricted by eqs. (2.154,2.155) to

$$\eta \in [0.328, 0.345] \, . \tag{A.27}$$

We have chosen $\eta = 1/3$. The small binding energy is reflected in the scalar functions as follows. The only s wave $\hat{D}_1$ clearly dominates and the p waves $\hat{D}_2$, $\hat{D}_4$ and $\hat{D}_6$ represent corrections of the order of one per cent. All other partial waves are suppressed. Although the convergence of the Chebyshev expansion is still moderate for $\hat{D}_1$, the remaining functions possess a number of higher moments which are larger than one tenth of the zeroth moment. In figure A.3 we have picked the moments 0, 4 and 8 to illustrate this behaviour.

A.4   Bethe-Salpeter equations for octet and decuplet

Here we list the Bethe-Salpeter equations for octet and decuplet baryons needed in section 5.2. First we introduce the notation:

$\Psi^5_{c(ab)}, \Psi^\mu_{c[ab]}$	Spin-1/2 wave function for flavor components with spectator quark c and scalar (ab) or axialvector diquark $[ab]$, decomposed as in eq. (2.129)
$\Psi^{\mu\nu}_{c[ab]}$	Spin-3/2 wave function for flavor components with spectator quark c and axialvector diquark $[ab]$, decomposed as in eq. (2.131)
S_a	Quark propagator as in eq. (2.64) with $m_q = m_a$
$D_{(ab)}, D^{\mu\nu}_{[ab]}$	Diquark propagators as in eqs. (2.45,2.46) with $m_{sc} = m_{(ab)}$ and $m_{ax} = m_{[ab]}$
$K^{\sf ab}_a$	Quark exchange kernel with momentum definitions as below eq. (2.72): $K^{\sf ab}_a = -\frac{1}{2} \int \frac{d^4k}{(2\pi)^4} \chi^{\sf a} \, S^T_a \, \bar{\chi}^{\sf b}$ (${\sf a}, {\sf b} = 1, \ldots, 5$)

As we consider the isospin symmetric case, the flavor labels a, b, c will be chosen among up and $strange$ (u, s). We recapitulate the nucleon equation (2.69),

$$
\begin{pmatrix} S_u^{-1} D_{(uu)}^{-1} & 0 \\ 0 & S_u^{-1} (D_{[uu]}^{\mu\nu})^{-1} \end{pmatrix} \begin{pmatrix} \Psi_{u(uu)}^5 \\ \Psi_{u[uu]}^\nu \end{pmatrix} = \begin{pmatrix} K_u^{55} & -\sqrt{3}\, K_u^{\rho 5} \\ -\sqrt{3}\, K_u^{5\mu} & -K_u^{\rho\mu} \end{pmatrix} \begin{pmatrix} \Psi_{u(uu)}^5 \\ \Psi_{u[uu]}^\rho \end{pmatrix} .
$$

$$(\text{A}.28)$$

The Σ hyperon is described by

$$
\begin{pmatrix} S_u^{-1} D_{(us)}^{-1} & 0 & 0 \\ 0 & S_u^{-1} (D_{[us]}^{\mu\nu})^{-1} & 0 \\ 0 & 0 & S_s^{-1} (D_{[uu]}^{\mu\nu})^{-1} \end{pmatrix} \begin{pmatrix} \Psi_{u(us)}^5 \\ \Psi_{u[us]}^\nu \\ \Psi_{s[uu]}^\nu \end{pmatrix} =
$$

$$
\begin{pmatrix} K_s^{55} & -K_s^{\rho 5} & \sqrt{2}\, K_u^{\rho 5} \\ -K_s^{5\mu} & K_s^{\rho\mu} & \sqrt{2}\, K_u^{\rho\mu} \\ \sqrt{2}\, K_u^{5\mu} & \sqrt{2}\, K_u^{\rho\mu} & 0 \end{pmatrix} \begin{pmatrix} \Psi_{u(us)}^5 \\ \Psi_{u[us]}^\rho \\ \Psi_{s[uu]}^\rho \end{pmatrix} . \quad (\text{A}.29)
$$

The equation for the Ξ hyperon is obtained by interchanging $u \leftrightarrow s$. $SU(3)$ symmetry breaking couples the eightfold way state of the Λ to the flavor singlet, $s(ud) + u(ds) + d(su)$. We introduce the flavor states $f_1 = [d(us) - u(ds)]/\sqrt{2}$, $f_2 = s(ud)$ and $l = (d[us] - u[ds])/\sqrt{2}$ and the equation for the physical Λ hyperon reads

$$
\begin{pmatrix} S_u^{-1} D_{(us)}^{-1} & 0 & 0 \\ 0 & S_s^{-1} D_{(uu)}^{-1} & 0 \\ 0 & 0 & S_u^{-1} (D_{[us]}^{\mu\nu})^{-1} \end{pmatrix} \begin{pmatrix} \Psi_{f_1}^5 \\ \Psi_{f_2}^5 \\ \Psi_l^\nu \end{pmatrix} =
$$

$$
\begin{pmatrix} -K_s^{55} & \sqrt{2}\, K_u^{55} & K_s^{\rho 5} \\ \sqrt{2}\, K_u^{55} & 0 & \sqrt{2}\, K_u^{\rho 5} \\ K_s^{5\mu} & \sqrt{2}\, K_u^{5\mu} & -K_s^{\rho\mu} \end{pmatrix} \begin{pmatrix} \Psi_{f_1}^5 \\ \Psi_{f_2}^5 \\ \Psi_l^\rho \end{pmatrix} . \quad (\text{A}.30)
$$

The equation for the Δ reads, *cf.* eq. (2.80),

$$
S_u^{-1} (D_{[uu]}^{\mu\nu})^{-1} \Psi_{u[uu]}^{\nu\sigma} = 2\, K_u^{\rho\mu} \Psi_{u[uu]}^{\rho\sigma} . \quad (\text{A}.31)
$$

By interchanging $u \leftrightarrow s$ one finds the equation for the Ω. Finally the Σ^* obeys the equation

$$\begin{pmatrix} S_u^{-1} (D_{[us]}^{\mu\nu})^{-1} & 0 \\ 0 & S_s^{-1} (D_{[uu]}^{\mu\nu})^{-1} \end{pmatrix} \begin{pmatrix} \Psi_{u[us]}^{\nu\sigma} \\ \Psi_{s[uu]}^{\nu\sigma} \end{pmatrix} = \begin{pmatrix} K_s^{\rho\mu} & \sqrt{2}\, K_u^{\rho\mu} \\ \sqrt{2}\, K_u^{\rho\mu} & 0 \end{pmatrix} \begin{pmatrix} \Psi_{u[us]}^{\rho\sigma} \\ \Psi_{s[uu]}^{\rho\sigma} \end{pmatrix} .$$

$$(A.32)$$

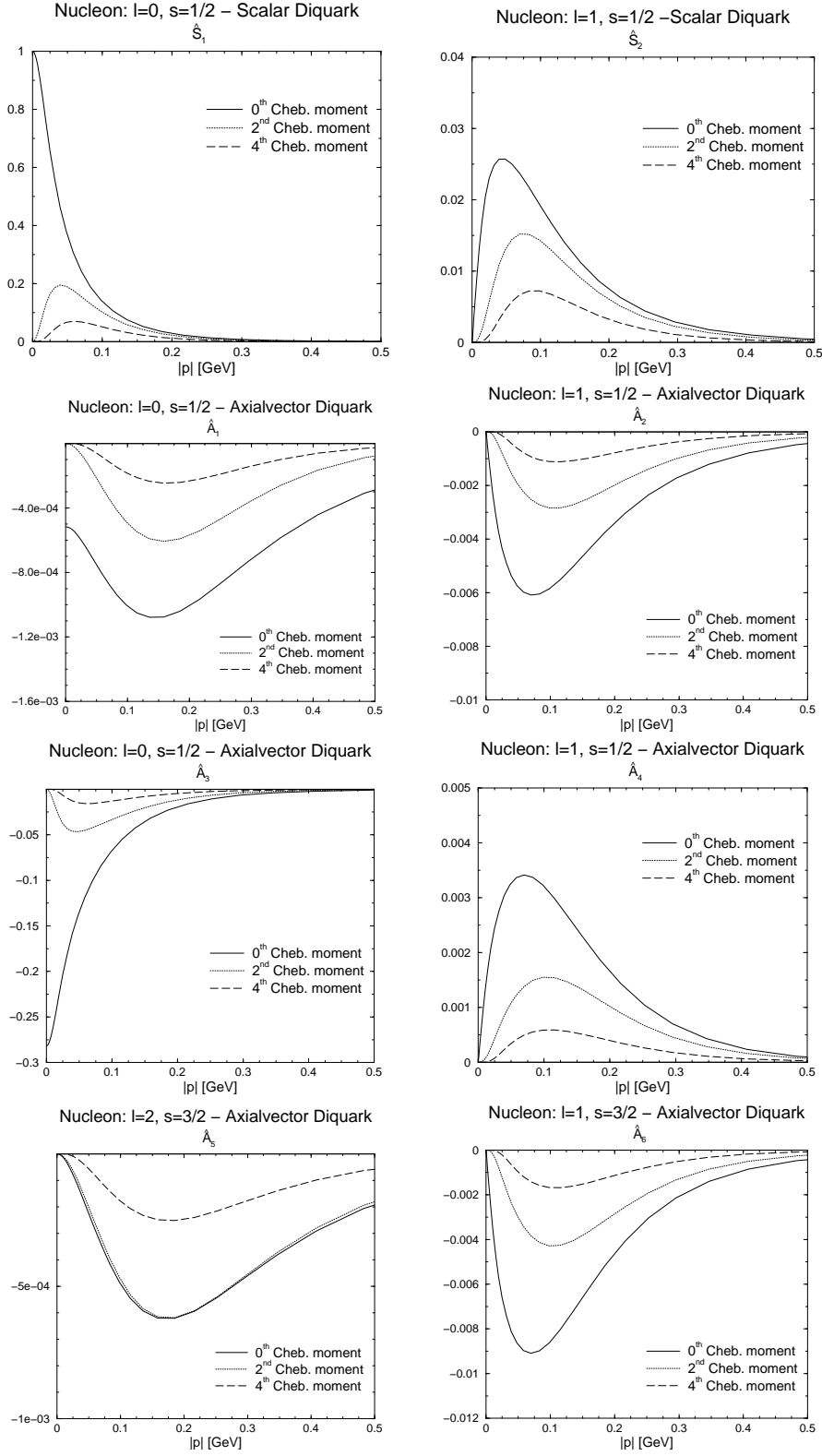In eq. (A.32) the interchange $u \leftrightarrow s$ leads to the Ξ^* equation.

Figure A.2: Chebyshev moments of the scalar functions $\hat{S}_i$ and $\hat{A}_i$ describing the nucleon wave function for parameter Set I.
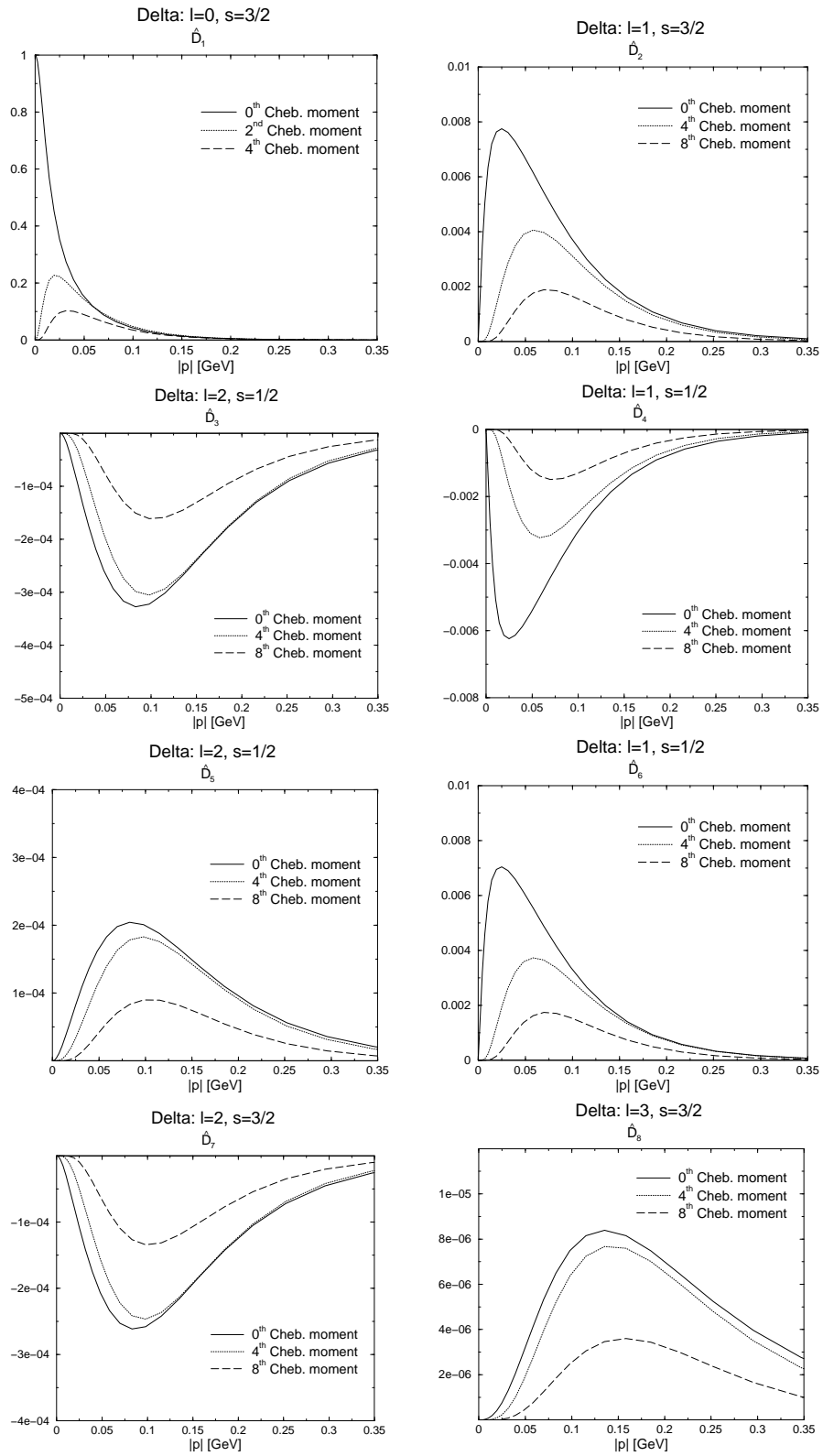
Figure A.3: Chebyshev moments of the scalar functions $\hat{D}_i$ describing the Δ wave function for parameter Set II.

Appendix B

Form Factor Calculations

B.1   Resolving diquarks

B.1.1   Electromagnetic Vertices

Here we adopt an impulse approximation to couple the photon directly to the quarks inside the diquarks obtaining the scalar, axialvector and the photon-induced scalar-axialvector diquark transition couplings as represented by the 3 diagrams in figure 3.1. For on-shell diquarks these yield diquark form factors and at the soft point ($Q = 0$) the electric form factors of scalar and axialvector diquark are equivalent to the normalization conditions (2.59,2.60). Hereby it is assumed that the diquark-quark vertices $\chi^{5[\mu]}$ could be obtained from a quark-quark scattering kernel which is independent of the total diquark momentum, *cf.* also section 3.1.3 where we discussed the equivalence of canonical and charge normalization in the nucleon case.

Due to the quark-exchange antisymmetry of the diquark amplitudes it suffices to calculate one diagram for each of the three contributions, *i.e.*, those of figure 3.1 in which the photon couples to the "upper" quark line. The color trace yields unity as in the normalization integrals, eqs. (2.59) and (2.60). To perform the traces over the diquark flavor matrices with the charge matrix acting on the quark line it is advantageous to choose the diquark charge eigenstates, *cf.* appendix A.2.1. With the definition

$$Q_c = \tfrac{1}{6}\mathbf{1} + \tfrac{1}{2}\tau^3 \tag{B.1}$$

we then obtain the following flavor factors

$$(\tilde{\Gamma}^\mu_{sc})_{\text{flavor}} = \tfrac{1}{2}\text{Tr}\,\tau^2 Q_c \tau^2 = \tfrac{1}{6}\,,\tag{B.2}$$

$$(\tilde{\Gamma}^{\mu,\alpha\beta}_{ax})_{\text{flavor}} = \tfrac{1}{2}\text{Tr}\,(\tau^2 \tau^\dagger_m) Q_c(\tau_m \tau^2) = \begin{pmatrix} \tfrac{2}{3} \\ \tfrac{1}{3} \\ -\tfrac{1}{3} \end{pmatrix}\,,\tag{B.3}$$

$$(\tilde{\Gamma}^{\mu,\beta}_{sa})_{\text{flavor}} = -\tfrac{1}{2}\text{Tr}\,\tau^2 Q_c(\tau_m \tau^2) = -\delta_{m0}\,\tfrac{1}{2}\,.\tag{B.4}$$

For the flavor factors of the scalar and axialvector diquarks we obtain half their total charges. The factor 1/2 is due to the antisymmetry of the vertices and also appears in the normalization conditions (2.59,2.60).

We are left with the quark loop that involves just a trace over the Dirac indices. Including the minus sign for fermion loops, we find for the Lorentz structure of the resolved vertices

$$\tilde{\Gamma}^\mu_{sc} = -\text{Tr}\int \frac{d^4q}{(2\pi)^4}\,\bar{\chi}^5\left(\frac{p_2-p_3}{2}\right)\,S(p_2)\,\Gamma^\mu_q\,S(p_1)\,\chi^5\left(\frac{p_1-p_3}{2}\right)\,S^T(p_3)\,,\tag{B.5}$$

$$\tilde{\Gamma}^{\mu,\alpha\beta}_{ax} = -\text{Tr}\int \frac{d^4q}{(2\pi)^4}\,\bar{\chi}^\alpha\left(\frac{p_2-p_3}{2}\right)\,S(p_2)\,\Gamma^\mu_q\,S(p_1)\,\chi^\beta\left(\frac{p_1-p_3}{2}\right)\,S^T(p_3)\,,\tag{B.6}$$

$$\tilde{\Gamma}^{\mu,\beta}_{sa} = -\text{Tr}\int \frac{d^4q}{(2\pi)^4}\,\bar{\chi}^5\left(\frac{p_2-p_3}{2}\right)\,S(p_2)\,\Gamma^\mu_q\,S(p_1)\,\chi^\beta\left(\frac{p_1-p_3}{2}\right)\,S^T(p_3)\tag{B.7}$$

$$= 4im_q\,\epsilon^{\mu\beta\rho\lambda}(p_d+k_d)^\rho Q^\lambda \int \frac{d^4q}{(2\pi)^4}\,\frac{g_s g_a\,V(q-Q/4)V(q+Q/4)}{(p_1^2+m_q^2)(p_2^2+m_q^2)(p_3^2+m_q^2)}\,.$$

The quark momenta herein are,

$$p_1 = \frac{p_d+k_d}{4} - \frac{Q}{2} + q\,,\quad p_2 = \frac{p_d+k_d}{4} + \frac{Q}{2} + q\,,$$

$$p_3 = \frac{p_d+k_d}{4} - q\,.\tag{B.8}$$

Even though current conservation can be maintained with these vertices on-shell, off-shell $\tilde{\Gamma}^\mu_{sc}$ and $\tilde{\Gamma}^{\mu,\alpha\beta}_{ax}$ do not satisfy the Ward-Takahashi identities for the free propagators in eqs. (2.45,2.46). Thus they cannot be directly employed to couple the photon to the diquarks inside the nucleon without violating gauge invariance. For $Q = 0$, however, they can be used to estimate the anomalous magnetic moment κ of the axialvector diquark and the strength of the scalar-axialvector transition, denoted by κ_{sa} in (3.32), as follows.

First we calculate the contributions of the scalar and axialvector diquark to the proton charge, *i.e.* the contribution of the first diagram in figure 3.2 to $G_E(0)$, upon replacing the vertices Γ^μ_{sc} and $\Gamma^{\mu,\alpha\beta}_{ax}$ given in eqs. (3.30,3.31) by the resolved

	g_s^{resc}/g_s	g_a^{resc}/g_a	κ	κ_{sa}
Set I	0.943	1.421	1.01	2.09
Set II	0.907	3.342	1.04	2.14

Table B.1: Rescaled diquark normalizations and constants of photon-diquark couplings.

ones, $\tilde{\Gamma}_{sc}^{\mu}$ and $\tilde{\Gamma}_{ax}^{\mu,\alpha\beta}$ in eqs. (B.5) and (B.6). Since the *bare* vertices satisfy the Ward-Takahashi identities, and since current conservation is maintained in the calculation of the electromagnetic form factors, the correct charges of both nucleons are guaranteed to result from the contributions to $G_E(0)$ obtained with these bare vertices, Γ_{sc}^{μ} and $\Gamma_{ax}^{\mu,\alpha\beta}$ of eqs. (3.30,3.31). In order to reproduce these correct contributions, we then adjust the values for the diquark couplings, g_s and g_a, to be used in connection with the resolved vertices of eqs. (B.5) and (B.6). This yields couplings g_s^{resc} and g_a^{resc}, slightly rescaled (by a factor of the order of one, *cf.* table B.1). We see that gauge invariance in form of the differential Ward identity provides an off-shell constraint on the diquark normalization where we have averaged over diquark off-shell states by performing the four-dimensional integration for the current matrix element. Once the "off-shell couplings" g_s^{resc} and g_a^{resc} are fixed we can continue and calculate the contributions to the magnetic moment of the proton that arise from the resolved axialvector and transition couplings, $\tilde{\Gamma}_{ax}^{\mu,\alpha\beta}$ and $\tilde{\Gamma}_{sa}^{\mu,\beta}$, respectively. These contributions determine the values of the constants κ and κ_{sa} for the couplings in eqs. (3.31) and (3.32,3.33). The results are given in table B.1. As can be seen, the values obtained for κ and κ_{sa} by this procedure are insensitive to the parameter sets for the nucleon amplitudes. In the calculations of observables we use $\kappa = 1.0$ and $\kappa_{sa} = 2.1$.

B.1.2 Pseudoscalar and pseudovector vertices

The pion and the pseudovector current do not couple to the scalar diquark. Therefore, in both cases only those two contributions have to be computed which are obtained from the middle and lower diagrams in figure 3.1 with replacing the photon-quark vertex by the pion-quark vertex of eq. (4.14), and by the pseudovector-quark vertex of eq. (4.16), respectively.

First we evaluate the flavor trace implicitly given in the diagrams of figure 3.1. As we employ only the third component (in isospace) of the pseudoscalar and the pseudovector currents to obtain $g_{\pi NN}$ and g_A, *cf.* eqs. (4.2,4.6), we just need the

following flavor factors,

$$(\tilde{\Gamma}^{\alpha\beta}_{5,ax})_{\text{flavor}} \;\; = \;\; \tfrac{1}{2}\text{Tr} \;(\tau^2\tau^\dagger_m)\tau^3(\tau_m\tau^2) = \begin{pmatrix} 1 \\ 0 \\ -1 \end{pmatrix} , \tag{B.9}$$

$$(\tilde{\Gamma}^{\beta}_{5,sa})_{\text{flavor}} \;\; = \;\; -\tfrac{1}{2}\text{Tr}\;\tau^2\tau^3(\tau_m\tau^2) = -\delta_{m0} . \tag{B.10}$$

The flavor factors for the pseudovector vertices are half of the above factors.

In the quark loop calculations we use the rescaled couplings from appendix B.1.1 which proved to yield consistent results with respect to the Ward identity for the nucleon. For the Dirac part of the vertex describing the pion coupling to the axialvector diquark we obtain,

$$\tilde{\Gamma}^{\alpha\beta}_{5,ax} \;\; = - \;\; 2\frac{m^2_q}{f_\pi}\epsilon^{\alpha\beta\mu\nu}(p_d + k_d)^\mu Q^\nu \;\times \tag{B.11}$$
$$\int \frac{d^4q}{(2\pi)^4} \frac{(g^{\text{resc}}_a)^2\; V(q - Q/4)V(q + Q/4)}{(p^2_1 + m^2_q)(p^2_2 + m^2_q)(p^2_3 + m^2_q)} ,$$

and fixes its strength (at $Q^2 = 0$) to $\kappa^5_{ax} \approx 4.5$, see table B.2.

For the effective pseudovector-axialvector diquark vertex in eq. (4.18) it is sufficient to consider the regular part, since its pion pole contribution is fully determined by eq. (B.11) already. The regular part reads,

$$\tilde{\Gamma}^{\mu\alpha\beta}_{5,ax} \;\; = \;\; \int \frac{d^4q}{(2\pi)^4} \frac{(g^{\text{resc}}_a)^2\; V(q - Q/4)V(q + Q/4)}{(p^2_1 + m^2_q)(p^2_2 + m^2_q)(p^2_3 + m^2_q)} \;\times \tag{B.12}$$
$$\left[-4m^2_q\epsilon^{\mu\alpha\beta\nu}\;(p_1 + p_2 + p_3)^\nu - \text{Tr}\,\gamma_5\gamma^\alpha\not{p}_2\gamma^\mu\not{p}_1\gamma^\beta\not{p}_3\right] .$$

Although after the q-integration the terms in brackets yield the four independent Lorentz structures discussed in the paragraph above eq. (4.18), only the first term contributes to $g_A(0)$ (with $p_1 + p_2 + p_3 = (3/4)(p_d + k_d) + q$).

The scalar-axialvector transition induced by the pion is described by the vertex

$$\tilde{\Gamma}^{\beta}_{5,sa} \;\; = \;\; 4i\frac{m_q}{f_\pi} \int \frac{d^4q}{(2\pi)^4} g^{\text{resc}}_s g^{\text{resc}}_a\; V(q - Q/4)V(q + Q/4) \;\times \tag{B.13}$$
$$\frac{(p_2\!\cdot\!p_3)p^\beta_1 - (p_3\!\cdot\!p_1)p^\beta_2 + (p_1\!\cdot\!p_2)p^\beta_3}{(p^2_1 + m^2_q)(p^2_2 + m^2_q)(p^2_3 + m^2_q)} ,$$

and the reverse (axialvector-scalar) transition is obtained by substituting $Q \to -Q$ (or $p_1 \leftrightarrow p_2$) in (B.14). The corresponding vertex for the pseudovector current

	κ_{ax}^5	$\kappa_{\mu,ax}^5$	κ_{sa}^5	$\kappa_{\mu,sa}^5$
Set I	4.53	4.41	3.97	1.97
Set II	4.55	4.47	3.84	2.13

Table B.2: Strengths for pion- and pseudovector-diquark couplings.

reads

$$\tilde{\Gamma}_{5,sa}^{\mu\beta} = -4im_q \int \frac{d^4q}{(2\pi)^4} \frac{g_s^{\text{resc}} g_a^{\text{resc}} V(q - Q/4) V(q + Q/4)}{(p_1^2 + m_q^2)(p_2^2 + m_q^2)(p_3^2 + m_q^2)} \times$$
$$\left[\delta^{\mu\beta}(m_q^2 - p_1 \cdot p_2 - p_2 \cdot p_3 - p_3 \cdot p_1) + \right. \tag{B.14}$$
$$\left. \{p_1 p_2\}_+^{\mu\beta} + \{p_1 p_3\}_+^{\mu\beta} - \{p_2 p_3\}_-^{\mu\beta} \right].$$

The short-hand notation for a(n) (anti)symmetric product used herein is defined as $\{p_1 p_2\}_\pm^{\mu\nu} = p_1^\mu p_2^\nu \pm p_1^\nu p_2^\mu$. The reverse transition is obtained from $Q \to -Q$ together with an overall sign change in (B.14). As already mentioned in the main text, the term proportional to $\delta^{\mu\beta}$ provides 99 % of the value for g_A as obtained with the full vertex. It therefore clearly represents the dominant tensor structure.

As explained for the electromagnetic couplings of diquarks, we use these resolved vertices in connection with the rescaled couplings g_s^{resc} and g_a^{resc} to compute $g_{\pi NN}$ and g_A in the limit $Q \to 0$. In this way the otherwise unknown constants that occur in the (pointlike) vertices of eqs. (4.17–4.20) are determined.

As seen from the results in table B.2, the values obtained for these effective coupling constants are only slightly dependent on the parameter set (the only exception being $\kappa_{\mu,sa}^5$ where the two values differ by 8 %). For the numerical calculations presented in section 4.3 we employ $\kappa_{ax}^5 = 4.5$, $\kappa_{\mu,ax}^5 = 4.4$, $\kappa_{sa}^5 = 3.9$ and $\kappa_{\mu,sa}^5 = 2.1$.

B.2 Calculation of the impulse approximation diagrams

In this appendix we discuss the difficulties in the formal transition from the Minkowski to the Euclidean metric. These are encountered in the connection between Bethe-Salpeter wave function Ψ and vertex functions Φ in a general (boosted) frame of reference of the nucleon bound state.
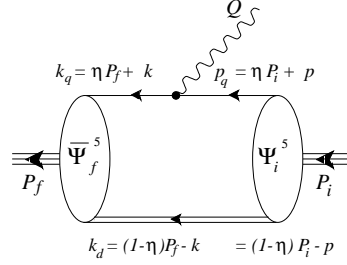
Figure B.1: The quark coupling diagram of the impulse approximation.

As the generic example for this discussion, we have chosen the second diagram in figure 3.2 which describes the impulse-approximated contribution arising from the coupling of the photon to the quark within the nucleon. Furthermore it is sufficient to restrict ourselves to scalar diquark correlations, retaining only Ψ^5 and Φ^5. The principle of the calculation will nevertheless become clear. We have singled out this diagram and, having added the appropriate momentum definitions, it is shown in figure B.1. We evaluate the diagram in the Breit frame, *cf.* the momentum definitions in eqs. (3.65).

Let us consider Mandelstam's formalism, eq. (3.26), in Minkowski space where it has been derived originally [63]. Here, the matrix elements between bound states are related to the corresponding Bethe-Salpeter wave functions in Minkowski space which for the moment are our nucleon Bethe-Salpeter wave functions Ψ_M.[1] Upon the transition to the Euclidean metric, the corresponding contribution to the observable, here to the nucleon form factors, is determined by the "Euclidean" Bethe-Salpeter wave function Ψ_E. In the rest frame of the nucleon bound state this transfer from $M \to E$ of the Bethe-Salpeter wave functions commutes with the replacement of the wave by the vertex functions; that is, unique results are obtained from the Euclidean contributions based on either employing the Minkowski space wave functions or the vertex functions which are related by the truncation of the propagators of the constituent legs, here $\Phi_M = \left. \left(G_0^{\mathrm{q-dq}}\right)^{-1}\right|_M \Psi_M$, or, *vice versa*, $\Psi_M = \left. G_0^{\mathrm{q-dq}}\right|_M \Phi_M$.

At finite momentum transfer Q^2 one needs to employ Bethe-Salpeter wave functions in a more general frame of reference, here we use the Breit frame in which neither the incoming nor the outgoing nucleon are at rest. As described in section 3.2.1, the "Euclidean wave function" Ψ_E in this frame is obtained from the solution to the Bethe-Salpeter equation in the rest frame by analytic continua-

---

[1]In the following the subscript $_M$ stands for definitions in Minkowski space and $_E$ for the corresponding ones in Euclidean space.

$$\int \bar{\Psi}_M \ D^{-1}\Gamma_q^\mu\Big|_M \ \Psi_M \quad \xrightarrow{\text{Wick rotation}} \quad \int \bar{\Psi}_E \ D^{-1}\Gamma_q^\mu\Big|_E \ \Psi_E$$

$$\Phi_M = (G_0^{\text{q}-\text{dq}})^{-1}\Big|_M \Psi_M \Bigg\downarrow \qquad\qquad\qquad \Bigg\downarrow \Phi_E \neq (G_0^{\text{q}-\text{dq}})^{-1}\Big|_E \Psi_E$$

$$\int \bar{\Phi}_M \ S\Gamma_q^\mu G_0^{\text{q}-\text{dq}}\Big|_M \ \Phi_M \quad \xrightarrow{\text{Wick rotation}} \quad \int \bar{\Phi}_E \ S\Gamma_q^\mu G_0^{\text{q}-\text{dq}}\Big|_E \ \Phi_E$$
$$+ \quad \text{residue terms}$$

Figure B.2: Interrelation of matrix elements in Minkowski and Euclidean space. The integral sign is shorthand for the four-dimensional integration over the relative momentum p, see equation (B.15).

tion, in particular, by inserting complex values for the argument of the Chebyshev polynomials, see eqs. (3.66,3.67). This corresponds to the transition from left to right indicated by the arrow of the upper line in figure B.2.

In the analogous transition on the other hand, when the truncated Bethe-Salpeter amplitudes are employed, the possible presence of singularities in the legs has to be taken into account explicitly. In the present example, these are the single particle poles of the propagators of the constituent quark and diquark that might be encircled by the closed path in the p^0-integration. The corresponding residues have to be included in the transition to the Euclidean metric in this case, which is indicated in the lower line of figure B.2.

The conclusion is therefore that the naïve relation between Bethe-Salpeter vertex and wave functions cannot be maintained in the Chebyshev expansion of the Euclidean spherical momentum coordinates when singularities are encountered in the truncation of the legs. Resorting to the Minkowski space definitions of vertex *vs.* wave functions, however, unique results are obtained from either employing the domain of holomorphy of the Bethe-Salpeter wave functions in the continuation to the Euclidean metric (with complex momenta) or, alternatively and technically more involved, from keeping track of the singularities that can occur in the Wick rotation when the truncated amplitudes and explicit constituent propagators are employed.

The rest of this section is concerned with the description of how to account for these singularities which, for our present calculations are affected by constituent poles for quark and diquark, give rise to residue terms as indicated in the lower right corner of figure B.2.

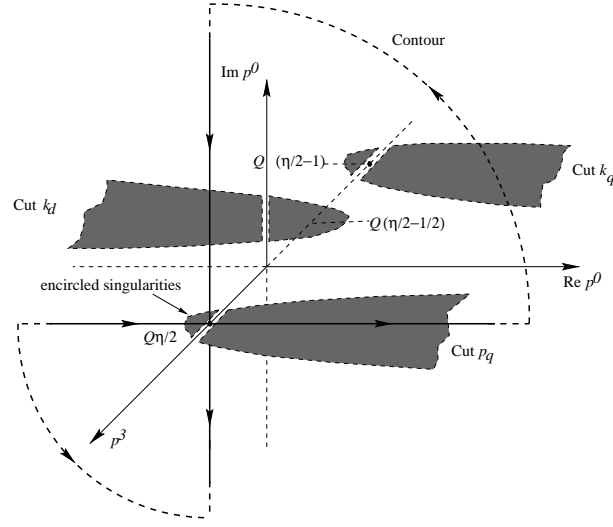To this end consider the quark contribution to the matrix elements of the elec-

Figure B.3: Location of the relevant singularities in the impulse-approximate quark contribution to the form factors. The relative momentum p is the integration variable in the loop diagram corresponding to equation (B.15).

tromagnetic current which is given by (*cf.* also eq. (3.39))

$$\langle J_q^\mu \rangle^{\text{sc}-\text{sc}} \; = \; \int_M \frac{d^4 p}{(2\pi)^4} \bar{\Phi}^5(p + (1-\eta)Q, P_f) \; D(k_d) S(k_q) \, \Gamma_q^\mu \, S(p_q) \; \Phi^5(p, P_i) \; .$$

$$\text{(B.15)}$$

We are interested in the location of the propagator poles herein (in Minkowski space). For these poles, solving the corresponding quadratic equation for the zeroth component of the relative momentum p^0 yields

$$p_q^2 - m_q^2 - i\epsilon \; = \; 0 \qquad \Leftrightarrow \qquad\qquad\qquad\qquad \text{(B.16)}$$
$$p_{\text{pole},1}^0 \; = \; -\eta \, \omega_Q \pm W(m_q, (\boldsymbol{p} - \eta/2 \, \boldsymbol{Q})^2)$$
$$k_q^2 - m_q^2 - i\epsilon \; = \; 0 \qquad \Leftrightarrow \qquad\qquad\qquad\qquad \text{(B.17)}$$
$$p_{\text{pole},2}^0 \; = \; -\eta \, \omega_Q \pm W(m_q, (\boldsymbol{p} - (\eta/2 - 1)\boldsymbol{Q})^2)$$
$$k_d^2 - m_{sc}^2 - i\epsilon \; = \; 0 \qquad \Leftrightarrow \qquad\qquad\qquad\qquad \text{(B.18)}$$
$$p_{\text{pole},3}^0 \; = \; (1-\eta) \, \omega_Q \pm W(m_{sc}, (\boldsymbol{p} - (\eta/2 - 1/2) \, \boldsymbol{Q})^2)$$

with $W(m, \boldsymbol{p}^2) = \sqrt{\boldsymbol{p}^2 + m^2 - i\epsilon}$. We used the momentum definitions given in figure B.1 and in eqs. (3.65).

For $Q = 0$, *i.e.* in the rest frame of the nucleon in which the Bethe-Salpeter equation was solved, the naïve Wick rotation is justified for $1 - \frac{m_{sc}}{M_n} < \eta < \frac{m_q}{M_n}$,

since there is always a finite gap between the cuts contained in the hypersurface $\operatorname{Re} p^0 = 0$ of the $\operatorname{Re} p^0 - \operatorname{Im} p^0 - \boldsymbol{p}$ space. As Q increases, these cuts are shifted along both, the p^3 and the p^0-axis, as sketched in Figure B.3. This eventually amounts to the effect that one of the two cuts arising from each propagator crosses the $\operatorname{Im} p^0$-axis. As indicated in the figure, the Wick rotation $p^0 \to i p^4$ is no longer possible for arbitrary values of p^3 without encircling singularities. The corresponding residues thus lead to

$$
\begin{aligned}
\langle J_q^\mu \rangle^{\text{sc-sc}} \quad \to \quad & \int_E \frac{d^4 p}{(2\pi)^4} \bar{\Phi}^5(p + (1-\eta)Q, P_f) \, D(k_d) S(p_q) \, \Gamma_q^\mu \, S(k_q) \, \Phi^5(p, P_i) \\
& + i \int \frac{d^3 \boldsymbol{p}}{(2\pi)^3} \, \theta_{\boldsymbol{p}} \, \bar{\Phi}^5(p_{\text{pole},1}^4, \boldsymbol{p} + (1-\eta)\boldsymbol{Q}, P_f) \, D(k_d) S(k_q) \, \times \\
& \qquad\qquad \Gamma_q^\mu \operatorname{Res}(S(p_q)) \, \Phi^5(p_{\text{pole},1}^4, \boldsymbol{p}, P_i) \\
& + \quad \text{analogous terms for } S(k_q) \text{ and } D(k_d) \qquad\qquad \text{(B.19)}
\end{aligned}
$$

upon transforming equation (B.15) to the Euclidean metric. Here, the residue integral is evaluated at the position of the pole in the incoming quark propagator $S(p_q)$ on the Euclidean p^4-axis

$$
p_{\text{pole},1}^4 = -i\eta \sqrt{M_n^2 + Q^2/4} + iW(m_q, (\boldsymbol{p} - \eta/2\, \boldsymbol{Q})^2), \qquad\qquad \text{(B.20)}
$$

where $\operatorname{Res}(S(k_q))$ denotes the corresponding residue, and the abbreviation

$$
\theta_{\boldsymbol{p}} \equiv \theta \left(\eta \, \omega_Q - W(m_q, (\boldsymbol{p} - \eta/2\, \boldsymbol{Q})^2) \right)
$$

was adopted to determine the integration domain for which the encircled singularities of figure B.3 contribute.

Analogous integrals over the spatial components of the relative momentum $\boldsymbol{p}$ arise from the residues corresponding to the poles in the outgoing quark propagator $S(k_q)$ and the diquark propagator $D(k_d)$ as given in eqs. (B.17,B.18).

One verifies that these cuts (as represented by the shaded areas in Fig. B.3) never overlap. Pinching of the deformed contour does not occur, since there are no anomalous thresholds for spacelike momentum transfer Q^2 in these diagrams.

We have numerically checked the procedure described here using the parameter set from the scalar diquark sector employing diquark-quark vertices of dipole shape, *cf.* table 2.5. We have calculated the contributions to the proton electric form factor from the (quark and diquark) impulse approximation diagrams for two different values of η, η_1 and η_2. Hereby $\eta_1 = 1/3$ is close to the left limit of the η range in which the (Euclidean) Bethe-Salpeter equation can be solved, *cf.* eq. (2.154). The second value, $\eta_2 = 0.4$, lies safely in the middle of this range. For each η value, we calculated the form factor in Euclidean space using (*i*) boosted

Proton Electric Form Factor
$m_q/M_n=0.62$, $m_{sc}/M_n=0.7$, $V(p^2)$: dipole

vertex function: $\eta=1/3$
wave function : $\eta=1/3$
vertex function: $\eta=0.4$
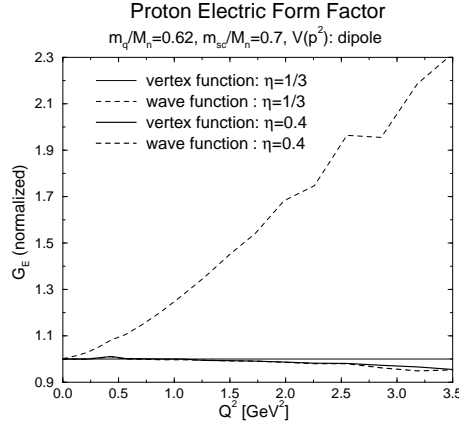wave function : $\eta=0.4$

G_E (normalized)

Q^2 [GeV^2]

Figure B.4: The impulse-approximated contribution, corresponding to the two left diagrams of figure 3.2, to the electric form factor of the proton. We have employed the dipole-V parameter set from the scalar diquark sector, *cf.* table 2.5. Results of the Bethe-Salpeter wave function calculations for the η values $1/3$ and 0.4 are compared to the respective vertex function plus residue calculations. The results are normalized to the latter that uses $\eta = 1/3$.

wave functions Ψ^5 and (ii) boosted vertex functions Φ^5 along with the residue prescription form eq. (B.19). The results are found in figure B.4. For η_1 the Chebyshev expansion of the Bethe-Salpeter wave function to 9 orders still turns out insufficient to provide for stable numerical results. This is due to being too close to the limit of the allowed range in η. The considerably weaker suppression of higher orders in the Chebyshev expansion of the wave function as compared to the expansion of the vertex function enhances the residual η-dependence of the observables obtained from the former expansion at a given order, in particular, when it has to reproduce close-by pole contributions in the constituent propagators. The impulse approximation contributions to G_E deviate substantially from those employing the vertex function and residue calculations in this case. On the other hand, for η_2 that has been employed to give the other results of figure B.4, unique results are obtained from both procedures. Both the Bethe-Salpeter wave function and vertex function calculation are in perfect agreement for values of the momentum partitioning that are closer to the middle of the range allowed to η. Furthermore the difference between the vertex function calculations for η_1 and η_2 show a good agreement and only deviate for larger momentum transfer ($Q^2 > 3$ GeV^2) by a few per cent. Thus, the independence of the form factor on the momentum distribution between quark and diquark holds in actual numerical calculations.

Bibliography

[1] T. P. Cheng and L. F. Li, *Gauge Theory of Elementary Particle Physics*, Clarendon, Oxford, UK, 1984.

[2] M. E. Peskin and D. V. Schroeder, *An Introduction to quantum field theory*, Addison-Wesley, Reading, USA, 1995.

[3] Y. Ne'eman M. Gell-Mann, *The Eightfold Way*, Benjamin, New York, USA, 1964.

[4] D. Faiman and A. W. Hendry, Phys. Rev. **173** (1968) 1720–1729.

[5] A. De Rujula, H. Georgi, and S. L. Glashow, Phys. Rev. **D12** (1975) 147–162.

[6] N. Isgur and G. Karl, Phys. Rev. **D18** (1978) 4187.

[7] B. Bakamjian and L. H. Thomas, Phys. Rev. **92** (1953) 1300–1310.

[8] H. Leutwyler and J. Stern, Ann. Phys. **112** (1978) 94.

[9] L. Ya. Glozman, Z. Papp, W. Plessas, K. Varga, and R. F. Wagenbrunn, Phys. Rev. **C57** (1998) 3406.

[10] G. Holzwarth and B. Schwesinger, Rept. Prog. Phys. **49** (1986) 825.

[11] T. H. R. Skyrme, Proc. Roy. Soc. Lond. **A262** (1961) 237.

[12] H. Weigel, Int. J. Mod. Phys. **A11** (1996) 2419–2544.

[13] E. Witten, Nucl. Phys. **B223** (1983) 422–432.

[14] E. Witten, Nucl. Phys. **B160** (1979) 57.

[15] R. Alkofer and H. Reinhardt, *Chiral Quark Dynamics*, Springer, Berlin, Germany, 1995, (Lecture notes in physics).

[16] R. Alkofer, H. Reinhardt, and H. Weigel, Phys. Rept. **265** (1996) 139–252.

[17] C. V. Christov et al., Prog. Part. Nucl. Phys. **37** (1996) 91.

[18] P. Hasenfratz and J. Kuti, Phys. Rept. **40** (1978) 75–179.

[19] R. K. Bhaduri, *Models of the Nucleon: From Quarks to Soliton.*, Addison-Wesley, Redwood City, USA, 1988, (Lecture notes and supplements in physics, 22).

[20] A. Hosaka and H. Toki, Phys. Rept. **277** (1996) 65–188.

[21] R. Alkofer and L. v. Smekal, *electronic preprint*, hep-ph/0007355, 2000, submitted to Phys. Rep.

[22] M. Oettel, G. Hellstern, R. Alkofer, and H. Reinhardt, Phys. Rev. **C58** (1998) 2459.

[23] M. Oettel, M. Pichowsky, and L. von Smekal, Eur. Phys. J. **A8** (2000) 251–281.

[24] M. Oettel, S. Ahlig, R. Alkofer, and C. Fischer, Form factors of baryons in a confining and covariant diquark-quark model, In *Hadron Physics - effective theories of low energy QCD: proceedings, AIP Press.*, 2000.

[25] M. Oettel and R. Alkofer, Phys. Lett. **B484** (2000) 243–250.

[26] M. Oettel, R. Alkofer, and L. von Smekal, Eur. Phys. J. **A8** (2000) 553–566.

[27] G. Hellstern, *Baryonen in einem kovarianten Diquark-Quark-Modell mit Confinement*, PhD thesis, Tübingen University, 1998, (in German).

[28] L. v. Smekal, *Perspectives for Hadronic Physics from Dyson-Schwinger Equations for the Dynamics of Quark and Glue*, Habilitation Thesis, Erlangen University, 1998.

[29] A. W. Thomas (ed.), *Fundamentals of Three Body Scattering Theory*, Springer, Berlin, Germany, 1977, (Topics In Current Physics, Vol.2).

[30] W. Glöckle, *The Quantum Mechanical Few-Body Problem*, Springer, Berlin, Germany, 1983.

[31] L. D. Faddeev, *Mathematical Aspects of the Three Body Problem in Quantum Scattering Theory*, Davey, New York, USA, 1965.

[32] C. Carimalo, J. Math. Phys. **34** (1993) 4930.

[33] N. Ishii, W. Bentz, and K. Yazaki, Nucl. Phys. **A587** (1995) 617.

[34] C. Itzykson and J. B. Zuber, *Quantum Field Theory*, McGraw-Hill, New York, USA, 1980, (International Series In Pure and Applied Physics), p.484.

[35] N. Nakanishi, Prog. Theor. Phys. Suppl. **43** (1969) 1–81.

[36] U. Vogl and W. Weise, Prog. Part. Nucl. Phys. **27** (1991) 195–272.

[37] H. Reinhardt, Phys. Lett. **B244** (1990) 316–326.

[38] M. Hess, F. Karsch, E. Laermann, and I. Wetzorke, Phys. Rev. **D58** (1998) 111502.

[39] J. Praschifka, R. T. Cahill, and C. D. Roberts, Int. J. Mod. Phys. **A4** (1989) 4929.

[40] D. J. Griffiths, *Introduction to elementary particles*, Wiley, New York, USA, 1987, p.282.

[41] C. Weiss, A. Buck, R. Alkofer, and H. Reinhardt, Phys. Lett. **B312** (1993) 6–12.

[42] C. Hanhart and S. Krewald, Phys. Lett. **B344** (1995) 55–60.

[43] A. Buck and H. Reinhardt, Phys. Lett. **B356** (1995) 168–174.

[44] H. Asami, N. Ishii, W. Bentz, and K. Yazaki, Phys. Rev. **C51** (1995) 3388.

[45] N. Ishii, Nucl. Phys. **A670** (2000) 68.

[46] C. J. Burden, R. T. Cahill, and J. Praschifka, Austral. J. Phys. **42** (1989) 147.

[47] G. Hellstern, R. Alkofer, and H. Reinhardt, Nucl. Phys. **A625** (1997) 697.

[48] A. Bender, C. D. Roberts, and L. von Smekal, Phys. Lett. **B380** (1996) 7–12.

[49] J. Praschifka, R. T. Cahill, and C. D. Roberts, Mod. Phys. Lett. **A3** (1988) 1595.

[50] D. Luriè, *Particles and Fields*, Interscience, New York, USA, 1968.

[51] S. Nozawa and D. B. Leinweber, Phys. Rev. **D42** (1990) 3567–3571.

[52] M. Abramowitz and I. A. Stegun, *Handbook of Mathematical Functions*, Dover, New York, USA, 1965.

[53] W. H. Press, B. P. Flannery, S. A. Teukolsky, and W. T. Vetterling, *Numerical Recipes (FORTRAN Version)*, Cambridge University Press, Cambridge, UK, 1989.

[54] N. Nakanishi, Prog. Theor. Phys. Suppl. **95** (1988) 1.

[55] R. E. Cutkosky, Phys. Rev. **96** (1954) 1135.

[56] T. Nieuwenhuis and J. A. Tjon, Few Body Syst. **21** (1996) 167.

[57] K. Kusaka, G. Piller, A. W. Thomas, and A. G. Williams, Phys. Rev. **D55** (1997) 5299–5308.

[58] G. Hellstern, R. Alkofer, M. Oettel, and H. Reinhardt, Nucl. Phys. **A627** (1997) 679.

[59] B. Povh, Nucl. Phys. **A532** (1991) 133c–140c.

[60] G. Hoehler et al., Nucl. Phys. **B114** (1976) 505–534.

[61] S. Platchkov et al., Nucl. Phys. **A510** (1990) 740–758.

[62] V. Keiner, Z. Phys. **A354** (1996) 87.

[63] S. Mandelstam, Proc. Roy. Soc. **233** (1955) 248–266.

[64] P. Maris and C. D. Roberts, Phys. Rev. **C56** (1997) 3369.

[65] P. Maris and P. C. Tandy, Phys. Rev. **C60** (1999) 055214.

[66] E. E. Salpeter, Phys. Rev. **87** (1952) 328–343.

[67] R. G. Sachs, Phys. Rev. **126** (1962) 2256–2260.

[68] I. J. R. Aitchison and A. J. G. Hey, *Gauge Theories in Particle Physics*, Adam Hilger, Bristol, UK, 1989.

[69] M. K. Jones et al., Phys. Rev. Lett. **84** (2000) 1398–1402, *Jefferson Lab Hall A coll.*

[70] H. Haberzettl, Phys. Rev. **C56** (1997) 2041.

[71] A. N. Kvinikhidze and B. Blankleider, Phys. Rev. **C60** (1999) 044003.

[72] A. N. Kvinikhidze and B. Blankleider, Phys. Rev. **C60** (1999) 044004.

[73] B. Blankleider and A. N. Kvinikhidze, *electronic preprint*, nucl-th/9912003, 1999.

[74] F. Gross and D. O. Riska, Phys. Rev. **C36** (1987) 1928.

[75] T. D. Lee and C. N. Yang, Phys. Rev. **128** (1962) 885.

[76] K. Ohta, Phys. Rev. **C40** (1989) 1335–1346.

[77] K. Nishijima and A. H. Singh, Phys. Rev. **162** (1967) 1740–1746.

[78] J. C. R. Bloch, C. D. Roberts, S. M. Schmidt, A. Bender, and M. R. Frank, Phys. Rev. **C60** (1999) 062201.

[79] J. C. R. Bloch, C. D. Roberts, and S. M. Schmidt, Phys. Rev. **C61** (2000) 065207.

[80] I. Passchier et al., Phys. Rev. Lett. **82** (1999) 4988–4991.

[81] M. Ostrick et al., Phys. Rev. Lett. **83** (1999) 276–279.

[82] S. Kopecky, P. Riehs, J. A. Harvey, and N. W. Hill, Phys. Rev. Lett. **74** (1995) 2427–2430.

[83] N. C. Mukhopadhyay, *electronic preprint*, nucl-th/9810039, 1998.

[84] D. E. Groom et al., Eur. Phys. J. **C15** (2000) 1.

[85] T. Kitagaki et al., Phys. Rev. **D42** (1990) 1331.

[86] N. Ishii, *electronic preprint*, nucl-th/0004063, 2000.

[87] P. Maris, C. D. Roberts, and P. C. Tandy, Phys. Lett. **B420** (1998) 267.

[88] R. Delbourgo and M. D. Scadron, J. Phys. **G5** (1979) 1621.

[89] R. A. Arndt, R. L. Workman, and M. M. Pavan, Phys. Rev. **C49** (1994) 2729.

[90] J. Rahm et al., Phys. Rev. **C57** (1998) 1077.

[91] R. Machleidt, K. Holinde, and C. Elster, Phys. Rept. **149** (1987) 1.

[92] T. Meissner, Phys. Rev. **C52** (1995) 3386–3392.

[93] G. V Efimov and M. A. Ivanov, *The quark confinement model of hadrons*, IOP, Bristol, UK, 1993.

[94] M. Stingl, Z. Phys. **A353** (1996) 423.

[95] R. Oehme, Int. J. Mod. Phys. **A10** (1995) 1995–2014.

[96] K. Bleuler, Helv. Phys. Acta **23** (1950) 567.

[97] J. I. Skullerud and A. G. Williams, *electronic preprint*, hep-lat/0007028, 2000.

[98] P. Maris and C. D. Roberts, Phys. Rev. **C58** (1998) 3659.

[99] P. Maris and P. C. Tandy, *electronic preprint*, nucl-th/0005015, 2000.

[100] P. Maris and P. C. Tandy, Phys. Rev. **C61** (2000) 045202.

[101] J. S. Ball and T.-W. Chiu, Phys. Rev. **D22** (1980) 2542.

[102] D. C. Curtis and M. R. Pennington, Phys. Rev. **D42** (1990) 4165–4169.

[103] P. Markowitz et al., Phys. Rev. **C48** (1993) R5–R9.

[104] E. E. W. Bruins et al., Phys. Rev. Lett. **75** (1995) 21–24.

[105] H. Anklin et al., Phys. Lett. **B428** (1998) 248–253.

[106] A. Lung et al., Phys. Rev. Lett. **70** (1993) 718–721.

[107] M. Q. Tran et al., Phys. Lett. **B445** (1998) 20–26, *SAPHIR collaboration*.

[108] S. Ahlig, R. Alkofer, C. Fischer, M. Oettel, and H. Reinhardt, *Production Processes as a Tool to Study Parameterizations of Quark Confinement*, in preparation.

[109] R. Alkofer, S. Ahlig, C. Fischer, and M. Oettel, πN Newslett. **15** (1999) 238–241.

[110] R. Jakob, P. J. Mulders, and J. Rodrigues, Nucl. Phys. **A626** (1997) 937.

[111] G. C. Wick, Phys. Rev. **96** (1954) 1124–1134.

[112] S. Ahlig, *(In-)Konsistenz der Beschreibung relativistischer angeregter Zustände in der Bethe-Salpeter Gleichung*, Diploma Thesis, Tübingen University, 1998, (unpublished, in German).

[113] S. Ahlig and R. Alkofer, Annals Phys. **275** (1999) 113–147.

[114] J. Bijtebier, Nucl. Phys. **A623** (1997) 498.

[115] B. C. Metsch and H. R. Petry, Acta Phys. Polon. **B27** (1996) 3307–3320.

[116] P. C. Tiemeijer and J. A. Tjon, Phys. Rev. **C49** (1994) 494.

[117] V. Keiner, Phys. Rev. **C54** (1996) 3232–3239.

[118] T. Nieuwenhuis and J. A. Tjon, Phys. Rev. Lett. **77** (1996) 814–817.

[119] C. Fischer, *Assoziierte Strangeness-Produktion in einem kovarianten Diquark-Quark-Modell der Baryonen*, Diploma Thesis, Tübingen University, 1999, (unpublished, in German).

Lebenslauf

Allgemeine Informationen

Name:	**Oettel, Martin**
Anschrift:	Dorfstr. 22, 72827 Wannweil
Geburtsdatum und -ort:	14. März 1973, Jena
Staatsangehörigkeit:	deutsch
Familienstand:	ledig

Ausbildung

9/1979-8/1987	Polytechnische Oberschule in Freiberg i. S.
9/1987-6/1991	Spezialschule mathematisch-naturwissenschaftlicher Richtung in Karl-Marx-Stadt/Chemnitz
28.6.1991	Abitur, Durchschnittsnote: 1.1
10/1991-8/1993	Studium der Physik an der TU Clausthal
8/1993-5/1994	Studium der Physik an der State University of New York at Stony Brook, USA
10/1994-12/1997	Studium der Physik und der Philosophie an der Universität Tübingen
12/1996-12/1997	Diplomarbeit *Massen und Wellenfunktionen von Baryonen in einem kovarianten Diquark-Quark-Modell* unter Anleitung von Prof. Dr. Reinhardt am Institut für Theoretische Physik der Universität Tübingen
1.12.1997	Diplom in Physik, Gesamtnote *sehr gut*
1991-1997	Förderung durch die Studienstiftung des deutschen Volkes
seit 1/1998	Anfertigung der Dissertation *Baryons as Relativistic Bound States of Quark and Diquark* unter Anleitung von PD Dr. Alkofer

Anstellungen

10/1996-12/1997	Wissenschaftliche Hilfskraft an der Universität Tübingen (Philosophisches Seminar und Institut für Theoretische Physik)
seit 1/1998	Wissenschaftlicher Angestellter am Institut für Theoretische Physik der Universität Tübingen

Akademische Lehrer

Alkofer, Averin, Baake, Clement, Fritsche, Gaukler, Gradmann, Hübener, Jung, McCoy, Mertins, Mihaly, Nieuwenhuizen, Orozco, Reinhardt, Schaumann, Stumpf, Weigel

Publications

Papers in refereed journals:

1. M. Oettel, R. Alkofer and L. v. Smekal,
   Nucleon Properties in a Covariant Quark-Diquark Model
   Eur. J. Phys. **A8** (2000) 553-566.

2. M. Oettel and R. Alkofer,
   A Comparison between Relativistic and Semi-Relativistic Treatment in the Diquark-Quark Model
   Phys. Lett. **B484** (2000) 243-250.

3. M. Oettel, M. A. Pichowsky and L. v. Smekal,
   Current Conservation in the Covariant Quark-Diquark Model of the Nucleon
   Eur. J. Phys. **A8** (2000) 251-281.

4. M. Oettel, G. Hellstern, R. Alkofer and H. Reinhardt,
   Octet and Decuplet Baryons in a Covariant and Confining Diquark-Quark Model
   Phys. Rev. **C58** (1998) 2459-2477.

5. G. Hellstern, R. Alkofer, M. Oettel and H. Reinhardt,
   Nucleon Form Factors in a Covariant Diquark-Quark Model
   Nucl. Phys. **A617** (1997) 679-709.

Invited Talks:

Invited Talk at the
International Workshop on Relativistic Dynamics and Few-Body Systems, ECT Trento, Italy, November 2000
Form Factors and Kaon Photoproduction in a Confining and Covariant Diquark Model

Conference Proceedings:

1. R. Alkofer, S.Ahlig, C. Fischer and M. Oettel, *Kaon Photoproduction and Form Factors in a Covariant and Confining Diquark-Quark Model for Baryons*.
   To appear in the proceedings of the International Conference On Quark Nuclear Physics, Adelaide, Australia, February 2000.

2. M. Oettel, S. Ahlig, R. Alkofer and C. Fischer,
   Form Factors of Baryons in a Confining and Covariant Diquark-Quark Model.
   Proceedings of the Workshop on Hadron Physics – Effective Theories of Low Energy QCD, Coimbra, Portugal, September 1999. AIP Conference Proceedings 508, Melville, USA (2000), 73-82.

3. S. Ahlig, R. Alkofer, C. Fischer, M. Oettel and H. Reinhardt,
   Kaon Photoproduction and Form Factors in a Covariant and Confining Diquark Model
   Proceedings of the 21st International School of Nuclear Physics, Erice, Italy, September 1999. Prog. Part. Nucl. Phys. **44** (2000), 361-362.

4. R. Alkofer, S. Ahlig, C. Fischer and M. Oettel,
   Kaon Photoproduction in a Confining and Covariant Diquark Model.
   Proceedings of the 8th International Symposium on Meson-Nucleon Physics and the Structure of the Nucleon, Zuoz, Switzerland, August 1999. πN-Newsletter **15** (1999) 238-241.

5. R. Alkofer, S. Ahlig, C. Fischer, M. Oettel and H. Reinhardt,
   Octet and Decuplet Baryons in a Confining and Covariant Diquark-Quark Model.
   Proceedings of PANIC 99, Uppsala, Sweden, June 1999.
   Nucl. Phys. **A663,664** (2000) 683c-686c.

6. G. Hellstern, M. Oettel, R. Alkofer and H. Reinhardt,
   Baryons in a Covariant and Confining Diquark–Quark Model
   Proceedings of the Workshop on Future Directions in Quark Nuclear Physics, Adelaide, Australia, March 1998. World Scientific, Singapore (1999).

Dank

An dieser Stelle möchte ich all denen Dank aussprechen, die zum Gelingen dieser Arbeit beigetragen haben.

Zuvorderst haben die Herren Privatdozenten Reinhard Alkofer und Herbert Weigel großen Anteil an dem Abschluß dieses Dissertationsprojektes. Reinhard Alkofer stand im gesamten Zeitraum als direkter Betreuer und Ansprechpartner der Arbeit Pate und seine Anregungen und Ideen sind überall in der Dissertation zu finden. Herbert Weigel, obwohl selbst die meiste Zeit am M.I.T., ermöglichte mir durch die Förderung im Rahmen seines DFG-Projektes die weitgehend sorgenfreie Beschäftigung mit der Physik. Ich danke für die Unterstützung der Reisen nach Boston und nach Coimbra, welche sehr wertvoll für mich waren. Die beiden Angesprochenen haben durch ihre ausführlichen Anmerkungen zu den verschiedenen Rohfassungen der Schrift erheblich zu der vorliegenden Endfassung beigetragen.

Herrn Prof. Hugo Reinhardt sei hier an dieser Stelle für die stete ideelle und auch materielle Unterstützung des Diquark-Quark-Projektes gedankt. Über die letzten anderthalb Jahre hat sich weiterhin eine fruchtbare Zusammenarbeit mit Herrn Privatdozent Lorenz von Smekal aus Erlangen ergeben, vielen Dank an ihn für die zahlreichen guten Ideen und die gewährte Gastfreundschaft im Frankenland.

Bei Herrn Steven Ahlig möchte ich mich herzlich für die gute Zusammenarbeit in den letzten Jahren bedanken. Unsere Diskussionen blieben nicht bei den Diquarkkorrelationen stehen, sondern entwickelten durchaus ihr berechtigtes Eigenleben zur Teezeit. Hervorheben möchte ich seine Expertise in Sachen Heidegger und australischen Weinen, an denen ich oft partizipieren konnte. Anschließen möchte ich hier den Dank an Herrn Oliver Schröder für seine unermüdliche Bereitschaft, mit mir über Allgemeines inner- und außerhalb der Physik und im besonderen über mein Dissertationsthema zu diskutieren. Seine Kritik zu dem letzteren Punkt fand, so hoffe ich, angemessenen Niederschlag in dieser Arbeit. Weiterhin möchte ich die angenehme Büropartnerschaft mit Herrn Christian Fischer und seinen botanischen Vorlieben hervorheben. Auch er blieb von den Diquarks nicht verschont und hat durch seinen eigenen Einsatz auf diesem Feld viel zur Ausarbeitung des Diquark-Quark-Modells beigetragen. Letzteres gilt auch für Herrn Gerhard Hellstern, der in der ersten Phase meiner Promotionszeit noch am Institut weilte und nun schon seit einiger Zeit ein Leben ohne Physik genießt.

Der gesamten Arbeitsgruppe sei für die fröhliche Atmosphäre gedankt, die in Gesprächen über Physik und bei anderen Anlässen spürbar war. Insbesondere